CALCULATION OF EXTREME WAVE LOADS

ON COASTAL HIGHWAY BRIDGES

A Dissertation

by

BO MENG

Submitted to the Office of Graduate Studies of
Texas A&M University
in partial fulfillment of the requirements for the degree of

DOCTOR OF PHILOSOPHY

December 2008

Major Subject: Ocean Engineering

CALCULATION OF EXTREME WAVE LOADS ON

COASTAL HIGHWAY BRIDGES

A Dissertation

by

BO MENG

Submitted to the Office of Graduate Studies of
Texas A&M University
in partial fulfillment of the requirements for the degree of

DOCTOR OF PHILOSOPHY

Approved by:

Co-Chairs of Committee,	Jun Jin
	Jun Zhang
Committee Members,	Vijay Panchang
	H. Joseph Newton
Head of Department,	David V. Rosowsky

December 2008

Major Subject: Ocean Engineering

ABSTRACT

Calculation of Extreme Wave Loads on Coastal Highway Bridges. (December 2008)

Bo Meng, B.S.; M.S., Tianjin University, China

Co-Chairs of Advisory Committee: Dr. Jun Jin
Dr. Jun Zhang

Coastal bridges are exposed to severe wave, current and wind forces during a hurricane. Most coastal bridges are not designed to resist wave loads in such extreme situations, and there are no existing analytical methods to calculate wave loads on coastal highway bridges. This study focuses on developing a new scheme to estimate the extreme wave loads on bridges for designing purpose. In order to do this, a 2D wave velocity potential model (2D Model) is set up for the deterministic analysis of wave force on bridge decks.

2D Model is a linear wave model, which has the capability of calculating wave velocity potential components in time domain based on wave parameters such as wave height, wave period and water depth, and complex structural geometries. 2D Model has Laplace equation as general equation. The free surface boundary, incoming and outgoing wave boundary conditions are linearized, decomposed first, and then solved by the finite difference method. Maximum wave forces results calculated by the linear 2D Model are compared with results from CFD software Flow3D that is using Navier Stokes theory up to the 5th order; and 2D Model is validated by comparing results with experiment data.

A case study is conducted for calculating extreme wave forces on I-10 Bridge across Escambia Bay, Florida during Hurricane Ivan in September 2004.SWAN model is adapted to investigate the parameters of wave heights and wave periods around bridge sites. SWAN model has the capability of predicting or hindcasting significant wave heights and wave periods as long as the domain and input parameters are given. The predicted significant wave heights are compared with measurements by Buoy Station 42039 and 42040 nearest to Escambia Bay.

A new prediction equation of maximum uplift wave forces on bridge decks is developed in terms of wave height, wave period, water depth, bridge width, water clearance and over top water load. To develop the equations, the relationship is investigated between maximum uplift wave forces and wave parameters, water clearance, green water effects and bridge width. 2D Model is used for up to 1886 cases with difference parameters. Flow3D model is adopted to determine coefficients of water clearance and green water effects, which cannot be calculated by 2D Model.

ACKNOWLEDGEMENTS

I would like to express my gratitude to Dr. Jun Jin and Dr. Jun Zhang, co-chairs of my advisory committee for their continuous encouragement, guidance and support throughout my PhD study. Sincere thanks are expressed to Dr. Vijay Panchang and Dr. H. Joseph Newton for serving as my committee members.

I also appreciate the valuable instructions and suggestions received from Mr. Dongcheng Li and Changkwon Jeong during my study.

TABLE OF CONTENTS

CHAPTER Page

LIST OF FIGURES

FIGURE Page

FIGURE Page

FIGURE Page

FIGURE Page

LIST OF TABLES

CHAPTER I

INTRODUCTION

1.1 Background

Coastal bridges are exposed to severe wave, current and wind forces during a hurricane. Under normal conditions, the superstructure of a coastal highway bridge is well above water level and is only subjected to wind loads. But under extreme wave situations such as in hurricane, because the density of water is greater than the density of air, the magnitudes of wave loads are much larger than those of wind loads, and can demolish the bridge superstructure if it is not specifically designed to withstand wave loads.

In September 2004, the 2.5-mile-long I-10 twin bridges over Escambia Bay near Pensacola, Florida suffered extensive structural damage during Hurricane Ivan. There were 58 spans of the eastbound and westbound bridges knocked off the piers and there were another 66 spans misaligned. Three people, including the driver of the truck shown in Figure 1.1, died due to the bridge destruction. The bridge cost $26.4 million to repair within 24 days.

This dissertation follows the style and format of the journal of Ocean Engineering.

Figure 1.1: Damaged I-10 Bridges in Escambia Bay near Pensacola, Florida during Hurricane Ivan. (U.S. Coast Guard Photo/Andrew Kendrick, Sep. 17, 2004)

During Hurricane Katrina in August 2005, 2 bridges in Louisiana and Mississippi were damaged. The decks were lifted by the large uplift wave load and pushed off the piers by the horizontal wave load as illustrated in Figure 1.2.

Figure 1.2: Damaged I-10 Bridge over Lake Ponchartrain and US90 Bridge across Biloxi Bay and Bay St. Louis during Hurricane Katrina in August 2005

Hurricane Rita made landfall on September 24, 2005 between Sabine Pass, Texas and Johnsons Bayou, Louisiana, as a Category 3 hurricane. A bridge spanning Interstate 10 across Calcasieu River in Louisiana was damaged by a floating boat and several barges.

In September 13th, 2008, Hurricane Ike made a landfall at Galveston, TX. Pelican Island Bridge was damaged as shown in Figure 1.3. Restoring it cost $400,000, and millions more will be spent to repair all the damage caused by the storm. Texas A&M University at Galveston was closed; classes were moved to College Station until the bridge is repaired. The bridge at Rollover Pass between Gilchrist and Caplen, Texas was also damaged as shown in Figure 1.4.

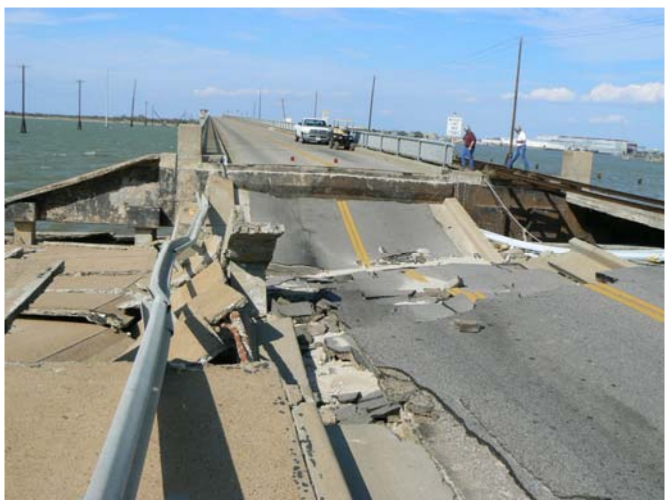

Figure 1.3: Damaged Pelican Island Bridge at Galveston, Texas by Hurricane Ike in Sep. 2008

Figure 1.4: Damaged Bridge at Rollover Pass, Texas by Hurricane Ike in Sep. 2008

There are about 23 coastal bridges located on the Hurricane evacuation route on the west Gulf of Mexico. It is possible for these bridges to experience structural failure and become impassable. The loss of one or more bridges could hamper emergency personnel re-entering the area to conduct search-and-rescue missions and other services and cause tremendous economic loss. Therefore, it is important to evaluate the possibility of structural failure of coastal bridges due to wave loads. And the magnitude of wave loads on super structure of bridge must be determined first.

1.2 Underlying Studies in Wave Load Calculations on Coastal Highway Bridges

Sheppard and Renna (2004) pointed out that the right combination of water elevation and wave height could and did produce loads that overcame the weight of the spans and their tie-downs and caused structural failure. Much research has been done in predicting the wave loads on offshore and coastal structures. It could be classified into two different approaches: (1) semi-empirical equations based on laboratory model test results; (2) analytical models by diffraction theory.

1.2.1 Semi-empirical Methods

Physical modeling is a common approach in estimating wave forces. It can be used to model many structural geometries and wave situations. By analyzing the laboratory data, the relationship between the wave forces and the important aspects is analyzed and an empirical equation could be established according to that. Many experiments have been done to look for relationship between wave parameters and wave loads on bridge decks. However, it is difficult to model all the important aspects in laboratory experiments. Also, there are very few field measurements performed at a specified site or time to capture all the important aspects that we are concerned about. It is difficult to validate the deduced equations, and to tell whether they can be applied to other situations.

1.2.2 Analytical Theory Models

Many analytical methods are applied to calculate wave loads on offshore and coastal structures. These include diffraction equation method, eigenfunction expansions method, finite element method and Morison's equation method. However, there is currently no established method for the calculation of wave loads on superstructure of bridges, the literature on this subject yields no direct results. The closest approximation is found in studies on the hydrodynamic behavior of a submerged platform breakwater which can be modeled as a thin horizontal plate in water of finite depth.

In this study, the diffraction equations method is going to be applied to set up a 2D wave velocity potential model (2D Model) to calculate the extreme wave loads on coastal highway bridges.

1.3 Objectives

Along Texas coastal line of west Gulf of Mexico, there are more than 20 bridges under threat of hurricane. Unfortunately, most are not designed to resist wave loads under hurricane situations. Recent experience has increased attention to evaluating the possibility of bridge damage by extreme wave conditions. The Texas Department of Transportation in Texas confirms the need for an accurate method of calculating extreme loads and including those calculations in bridge designs.

In this study, the objective is to develop a new scheme to estimate the maximum uplift wave force on bridges decks in terms of wave height, wave period, water depth, water clearance and structure geometry width. In order to do this, a 2D wave velocity potential model is set up for the deterministic analysis of wave pressure force on bridge decks. The 2D Model is validated by comparing results with laboratory experimental data and CFD software Flow3D.

Chapter II gives a brief description of literature search results for this study. Chapter III shows the development of the 2D wave velocity potential model and validation of this model. The wave potential diffraction theory is capable of filling the gap in which there are no reliable models for determining the maximum wave loads on bridge decks. The finite difference method will be used to calculate the wave forces on bridges. For structures with regular geometry, the grids of domain with finite difference method will be easier to work with. Chapter IV is the case study for calculation of wave loads on the I-10 Bridge across Escambia Bay near Pensacola, Florida in Hurricane Ivan in September, 2004. Chapter V is the parametric study of 2D Model results and gives a simplified equation for estimating wave loads on bridge. The maximum uplift wave forces will be investigated according to most important aspects including wave heights, wave periods, water depth, water clearance, and bridge deck width. Chapter VI is the final summary and conclusion of this study.

CHAPTER II

LITERATURE REVIEW

2.1 Semi-Empirical Methods

There is currently no established method for the calculation of extreme wave loads on coastal highway bridges. However, methods for the calculation of wave loads on similar structures were found in the literature and are summarized below.

In the design of offshore platforms, semi-empirical methods are employed for the calculation of wave loads on offshore structures. By analyzing laboratory data, the relationship between uplift wave forces and other important aspects is analyzed and an empirical equation could be established according to that.

El Ghamry (1963) and Wang (1970) found that wave-in-deck forces had two components: short duration impact pressure, and long duration lower intensity pressure. French (1970) confirmed that conclusion. Furthermore, he developed an empirical equation according to his results.

$$p = c\gamma(\eta_{\max} - Z_{deck}) \tag{2.1}$$

Where p is the pressure, γ is the unit weight of water, $\eta_{\max}$ is the wave crest elevation and Z_{deck} is the deck bottom elevation, $c \geq 1$ is an empirical coefficient.

Denson (1978, 1980) made a physical model following the U.S. 90 Bridge across St.

Louis Bay, which was damaged by Hurricane Camille in 1969. He concluded that, the bridge was mostly damaged by the wave induced moments. He also suggested having small anchorage systems on bridges to prevent this type of failure.

Tirindelli et al. (2002) and McConnell et al.(2003) also had similar conclusions:

1. the maximum uplift wave forces are sensitive to wave height and wave period;
2. uplift wave forces include a very short-duration impact pressure and a longer duration, slowly-varying pressure;

Douglass et al. (2004) gave the recommended estimating equations for the loads on elevated highway bridge decks in terms of the vertical and horizontal components as:

$$F_v = c_{v-va} F_v^* \tag{2.2}$$

$$F_h = [1 + c_r (N-1)] c_{h-va} F_h^* \tag{2.3}$$

$$F_v^* = \gamma (\Delta z_v) A_v \tag{2.4}$$

$$F_h^* = \gamma (\Delta z_h) A_h \tag{2.5}$$

Where F_v and F_h are the estimated, vertical and horizontal wave-induced loads component; F_v^* and F_h^* are the reference vertical and horizontal loads defined by Eqs. (2.4) and (2.5); c_{v-va} and c_{h-va} are the empirical coefficients for the vertical and horizontal varying loads; c_r is a reduction coefficient for reduced horizontal load on the internal girders; N is the number of girders supporting the bridge span deck; A_v,

A_h are the vertical and horizontal areas contributing to the wave loads; Δz_v, Δz_h are the differences between the elevation of the maximum crest and the elevation of the underside of the bridge deck/centroid of A_h; γ is the unit weight of water.

Bea et al. (1999) also summarized performance of platforms in the Gulf of Mexico and gave equations for buoyancy force, drag force, lift force, inertial force and slamming force.

2.2 Analytical Methods

Morison's equation is widely used in offshore and coastal engineering areas. Morison et al. (1950) proposed the equation for the total wave force as the sum of the two forces, drag and inertial. Research has been done for determining the drag and inertial force coefficients. Kaplan (1992), Kaplan et al. (1995) evaluated the forces on offshore platform decks using a modified Morison's equation and concluded that the vertical loads on decks were 8 times as large as horizontal loads. The theoretical results were within 30% of the measurements. Morison's equation is based on the fundamental assumption that the existence of structures does not affect wave kinematics. As a result, it is commonly used in force calculation on relatively thin structures, such as pipelines, columns and girders. For coastal bridges, the interaction between structures and waves cannot be neglected. The wave velocity potential model for wave forces on bridges should be a better tool for calculating such forces.

Diffraction of water waves is a phenomenon in which energy is transferred laterally along a wave crest. It is noticeable where an otherwise regular train of waves is interrupted by a barrier such as a breakwater, a small island or the oversea bridge with elevated water level during hurricane. The assumptions usually made in the development of diffraction theories are:

- Water fluid is inviscid and incompressible.
- Waves are of small amplitude and can be described by linear wave theory.
- Flow is irrotational and conforms to a potential function, which satisfies the Laplace equation.
- Depth shoreward of the structure is constant.

Putnam et al. (1948) presented experimental data verifying a method of solution proposed by Penny and Price (1944) for wave behavior after passing a single breakwater. Blue et al. (1949) dealt with the problem of wave behavior after passing through a gap, as between two breakwater arms. Wiegel (1962) used a theoretical approach to study wave diffraction around a single breakwater. Mei (1978) proposes a hybrid element method to solve the mild-slope equation by Berkhoff (1972), an approximate equation combining diffraction and refraction on a slowly varying bottom. Chen et al. (1974), Tsay et al. (1989), used the hybrid element method to solve such problems in harbor. The finite element method (Nallayarasu et al., 1994, Dermirbilek et al., 1998), the boundary element method (Rahman et al., 1992, Yueh et al., 1993) and eigenfunction expansions method (Ijima et al. 1971, Cheong et al. 1996) are also used to solve wave diffraction and refraction problems. However, the hybrid element method is more likely to be used for wave oscillation and wave kinematics analysis in harbor domain. The methods mentioned above are used in submerged or semi-submerged coastal breakwater and docks. None of them are used to calculate for coastal bridges with extreme wave conditions.

2.3 Green Water Problem and Wave-in-Deck Force

The green water problem is well-known in the maritime world for a long time. It also happens in wave loads on coastal bridge during hurricanes. During severe storm or wave conditions, waves exceed the freeboard and wet the deck of merchant vessels or FPSO. Waves can be so large that they cause damage to deck equipment, plating, structures or cargo (Nielsen, 2003). Wave overtopping on the lower decks of offshore platforms can cause severe structural damage and increased safety risks due to the high forces generated by the wave (Bea et al, 1999; Gudmestad et al., 2000).The overtopping of a shallow water coastal structure such as a breakwater can also lower the efficiency of the structures (Franco et al., 1999).

Researchers use numerical methods to simulate the green water problem. Wan et al.(1999), Fekken et al. (1999) used a Navier Stokes solver based on a volume of fluid (VOF) method. Buchner et al. (2007) used an improved volume of fluid (iVOF) method to simulate the green water problem on a TLP.

Franco et al. (1999) did hydraulic model tests on the overtopping response of various types of caisson breakwaters and drove general design formulas and graphs. Greco (2001) and Stansberg et al. (2001) conducted experimental test on green water loads on FPSOs.

Cox et al. (2002) investigated the wave free surface and velocity measurements for two cases (with and without the structure) and points out that: The effect of the structure on the free surface at the leading edge increases the total wave height by 6%; Immediately below the deck, the maximum velocity is 2.5 times greater than the corresponding velocity without the deck and 2.1 times larger than the maximum crest velocity measured without the deck; On the deck, the wave collapses into a thin bore with velocities that exceed 2.4 times the maximum crest velocity measured without the deck.

Bunchner (2002) presented experimental investigations of nonlinear relative wave motion.

Ryu et al. (2008) used a fiber optic reflectometer and bubble image velocimetry to measure the void fraction and velocity of green water. The time-averaged energy of green water measured was claimed to be much greater than predicted by the general wave energy. However, the overall green water energy was only one quarter of the incoming wave energy.

As the literature search result shows, the empiric equation from physical modeling is not accurate enough for calculating wave loads on bridges; and there is no analytical method used for the calculation of wave loads on bridges. In this study, the diffraction theory with Laplace equation is going to be used to set up the 2D model. Because of the regular geometry of a bridge superstructure, the finite difference method is well applied to obtain the solutions. It is convenient and can save computation time with conjugate gradients method proposed by Panchang et al. (1991), Panchang (2005). The Green water problem and wave-in-deck force will be considered as a modifying coefficient to the wave loads on decks.

CHAPTER III

DEVELOPMENT OF 2D WAVE VELOCITY POTENTIAL MODEL

3.1 Introduction

In this study, wave loads on bridge decks are a concern in a coastal area, which can be defined as intermediate water depth area. The wave loads include two types of loads: a very short-duration impact pressure and a longer duration, slowly-varying pressure. The very short-duration impact wave load, also called splash wave force, is sensitive to wave forms and can only be estimated from physical models in a laboratory experiment. While for the longer duration, slowly-varying wave load, the monochromatic (single frequency) regular (constant amplitude) wave theory can be well adapted to estimate the magnitude of the wave loads.

The model is solved under Airy's (1845) linear wave theory. It is easy to apply and gives a reasonable approximation of wave characteristics for a wide range of wave parameters.

In the 2D Model, the characteristic body dimension a is quite large relative to wave height H. As a result, scatter parameter $ka > \vartheta(1)$ and wave scattering is significant; Keulegan-Carpenter number $H/a << 1$ and effects of flow separation are insignificant; inertial forces are larger than drag forces. Therefore, the diffraction theory is well adopted in the 2D Model.

3.2 Governing Equations

A 2D cartesian coordinates system is defined such that the x-axis is coincident with the still water level (SWL) and the z-axis points upward. Assuming water is incompressible, inviscid and flow is irrotational, the governing velocity potential satisfies the 2-D time harmonic Laplace Equation:

$$\nabla^2 \phi(x, z, t) = 0 \tag{3.1}$$

When water depth is uniform, then the bottom boundary condition for the potential is

$$\frac{\partial \phi}{\partial z} = 0 \quad \text{at } z = 0 \tag{3.2}$$

Neglecting wind blow forces and surface tension, the dynamic and kinematic boundary conditions of the surface boundary condition are given in linear form as:

$$\frac{\partial \eta^{(1)}}{\partial t} - \frac{\partial \phi^{(1)}}{\partial z} = 0 \quad \text{on} \quad z = 0 \tag{3.3}$$

$$\frac{\partial \phi^{(1)}}{\partial t} + g\eta^{(1)} = 0 \quad \text{on} \quad z = 0 \tag{3.4}$$

where $\eta = -\frac{1}{g}\frac{\partial \phi}{\partial t}$ is the wave surface elevation.

However, in this study, the bridge is located in the intermediate water depth and the wave height is relatively high due to the strong wind velocity during a hurricane. The second order or even the third order can not be neglected. The second and higher orders are still neglected because a general approximation of the wave loads is expected and linear approximation can satisfy the objectives. The nonlinear terms including the second or higher order are much more complicated and will be left for further research.

Since we are seeking a solution corresponding to a periodic wave propagating in the x-direction without change in form, the solution should contain x and t in the form of $\theta = x - ct$, where c is the wave speed.

3.3 Conversion to Complex Velocity Potential Equations

According to the variables separation method, the ϕ can be transformed as

$$\phi(x,z,t) = \phi_1(x,z)\cos(\sigma t) + \phi_2(x,z)\sin(\sigma t) \tag{3.5}$$

Let $$\Phi = \phi_1 + i\phi_2 \tag{3.6}$$

then $$\phi(x,z,t) = \mathrm{Re}\left[\Phi e^{-i\omega t}\right] \tag{3.7}$$

Substitute Eq. 3.6 into governing Eqs. 3.1-3.4,

$$\nabla^2\Phi = 0 \quad \text{in fluid} \tag{3.8}$$

$$\frac{\partial\Phi}{\partial n} = 0 \quad \text{on seabed and interaction surface} \tag{3.9}$$

$$\frac{\sigma^2}{g}\Phi - \frac{\partial\Phi}{\partial z} = 0 \quad \text{free surface boundary condition} \tag{3.10}$$

The wave boundary condition comes to two parts: one is the incoming wave boundary condition; the other is the outgoing wave boundary condition. In the incoming wave domain $\phi = \phi_i - \phi_s$, in which ϕ_s is scattered potential; while in the outgoing wave domain, ϕ is the ϕ_s.

ϕ_i, incident wave potential, is the incoming wave without any disturbance.

ϕ_s, scattered wave potential, represents the disturbance of the incident waves due to the presence of the body. It corresponds to the wave field that is scattered by the body which is fixed in space.

Assuming

$$\phi = A\sin(kx - \sigma t) \tag{3.11}$$

From Eq. 3.11, $\phi = A\sin kx\cos\sigma t - A\cos kx\sin\sigma t$

$$= \phi_1\cos\sigma t + \phi_2\sin\sigma t \tag{3.12}$$

where $\phi_1 = A\sin(kx)$, $\phi_2 = A\cos(kx)$ (3.13)

then, $\dfrac{\partial\phi_1}{\partial x} = -k\phi_2$, $i\dfrac{\partial\phi_2}{\partial x} = ik\phi_1$

$$\frac{\partial\phi}{\partial x} = k(-\phi_2\cos\sigma t + \phi_1\sin\sigma t) \tag{3.14}$$

$$\frac{\partial \Phi}{\partial x} = k(-\phi_2 + i\phi_1) = ik(\phi_1 + i\phi_2) = ik\Phi \qquad (3.15)$$

along the incoming boundary:

$$\frac{\partial \Phi}{\partial x} = ik[2\Phi_i - \Phi] \qquad (3.16)$$

The velocity potential

$$\phi(x, y, z, t) = \mathrm{Re}(\Phi e^{-i\sigma t}) \qquad (3.17)$$

Wave elevation

$$\eta = -\frac{1}{g}\frac{\partial \phi}{\partial t} = \frac{\sigma}{g}(\phi_1 \sin \sigma t - \phi_2 \cos \sigma t) \qquad (3.18)$$

Water pressure

$$p = -\rho g z + \rho \frac{\partial \phi}{\partial t} = -\rho g z + (-\rho \sigma \phi_1) \sin \sigma t + (\rho \sigma \phi_2) \cos \sigma t \qquad (3.19)$$

3.4 Solution by the Finite Difference Method

The finite difference method is used to discretize the governing equations of Laplace equation and boundary conditions. According to the calculation domain and its grids, take Figure 3.1 as an example,

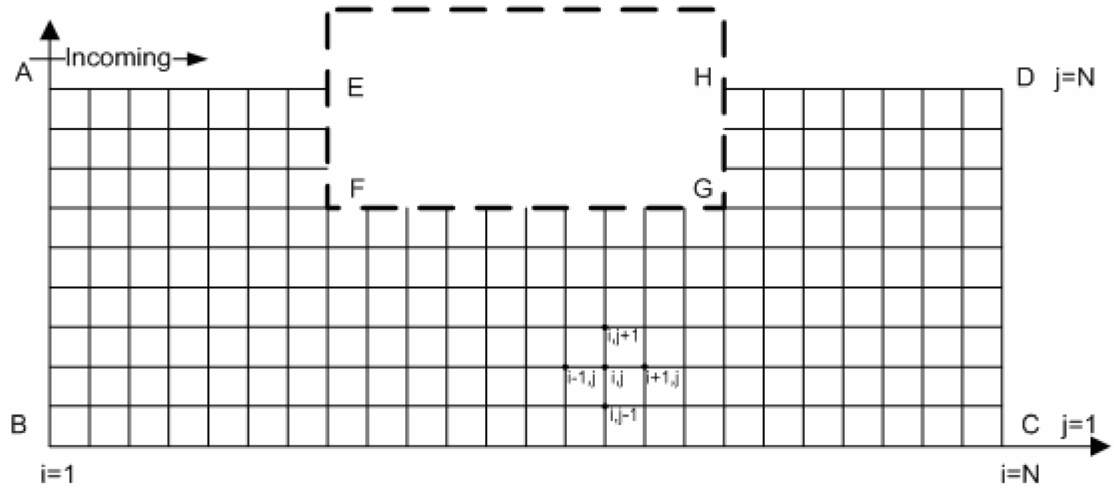

Figure 3.1: Calculation domain and grids

The general equations are discretized by finite difference method as follows.

In fluid domain, the central difference scheme is used and the general equation is

$$\phi_{i,j} = \frac{1}{4}(\phi_{i,j+1} + \phi_{i,j-1} + \phi_{i+1,j} + \phi_{i-1,j}) \tag{3.20}$$

Along bottom seabed boundary BC and interaction surface boundary EF, FG and GH, the boundary condition equations are given as:

$$\phi_{i,m+1} = \phi_{i,m}\,,\quad \phi_{n+1,j} = \phi_{n,j} \tag{3.21}$$

where *m*, *n* are integral numbers

Along the free wave surface AE and HD, the surface boundary condition equations are:

$$\phi_{i,1}(2 - \frac{\omega^2}{g}\Delta y) + \phi_{i,2}(-2 - \frac{\omega^2}{g}\Delta y) = 0 \tag{3.22}$$

Along boundary AB, the incoming wave boundary condition equation is:

$$\phi_{1,j}(-2+ik\Delta x)+\phi_{2,j}(2+ik\Delta x)=4ik\Delta x\frac{\cosh k(h+z)}{\cosh kh} \qquad (3.23)$$

Along boundary CD, the outgoing wave boundary condition equation is:

$$\phi_{I,j}=\frac{1}{1-ik\Delta x}\phi_{I-1,j} \qquad (3.24)$$

Then, the above equations can be expressed in matrix form as

$$[A][\phi]=[B] \qquad (3.25)$$

where [*A*] is the system matrix, $[\phi]$ is the unknown velocity potential vector, and [*B*] is the vector that contains information from the discretized boundary condition.

The solution of the matrix mentioned above could be a time-consuming process. Gaussian elimination method is the default way to solve the matrix equations as Eq. 3.25 above. But it requires the storage of matrix [*A*] and vector [*B*]. It is quite an inefficient method for large domain grids, taking our model for example, of 61×291 nodes.

According to the method of conjugate gradients proposed by Panchang (1991, 2005), there is no need to store all of matrix [*A*], assuming that for the matrix equation $[A][x]=[B]$, matrix [*A*] is a positive definite, symmetric matrix. As a result, the transformation of the matrix equations should be focused on how to make [*A*] a symmetric and positive definite matrix.

In such case, the governing equations around the corners of the structures have to be modified. Take Figure 3.2 for example,

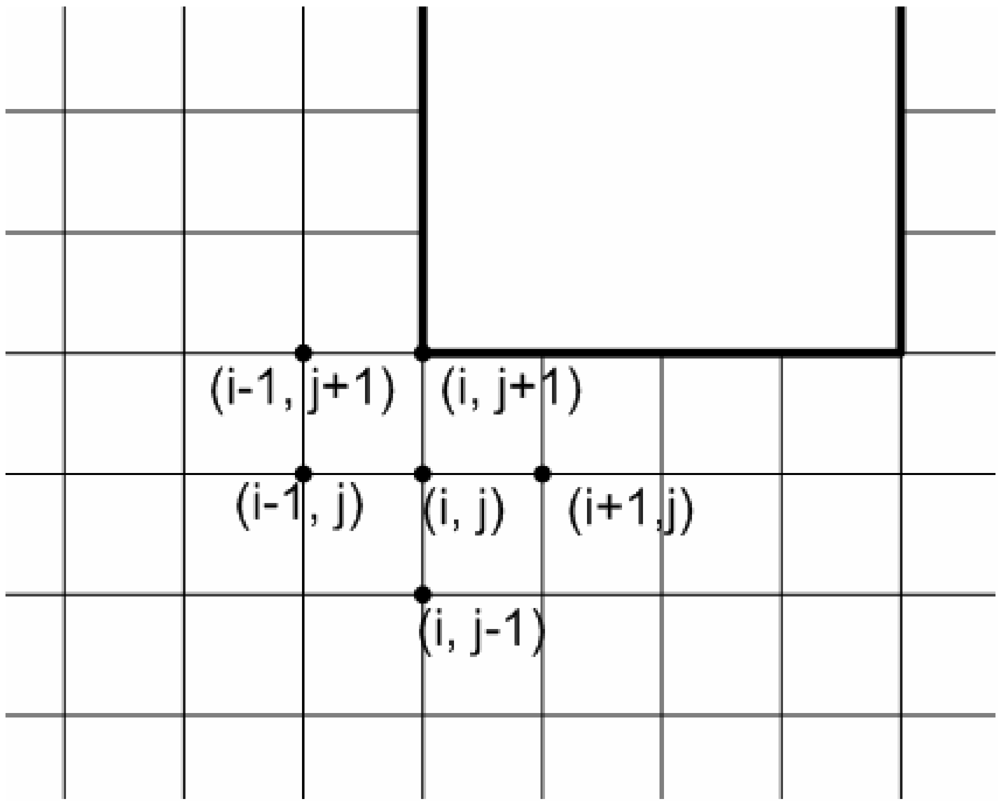

Figure 3.2: Calculation domain grids around a corner of structure

the Eq. 3.20 is modified as:

$$\phi_{i,j} = \frac{1}{4}(\phi_{i-1,j+1} + \phi_{i,j-1} + \phi_{i+1,j} + \phi_{i-1,j}) \tag{3.26}$$

As matrix [A] becomes symmetric, a remedy (Panchang et al., 1991) of Gauss transformation is used to make the matrix positive-definite. The equation is multiplied by $[A^*]$, the complex conjugate transpose of $[A]$.

$$\left[A^*\right][A][\phi] = \left[A^*\right][B] \tag{3.27}$$

$[A^*][A]$ is a symmetric and positive-definite. Solutions by iteration, which are the complex velocity potential of each node in the domain, will converge to the final solution with the preferred error. Figure 3.3 shows a flow chart of the numerical calculation scheme as proposed by Panchang et al. (1991).

Once the real velocity potential and the water pressure in the domain are determined, the uplift wave force on the structure deck is also determined by integral forces caused by the pressure on the interface surface.

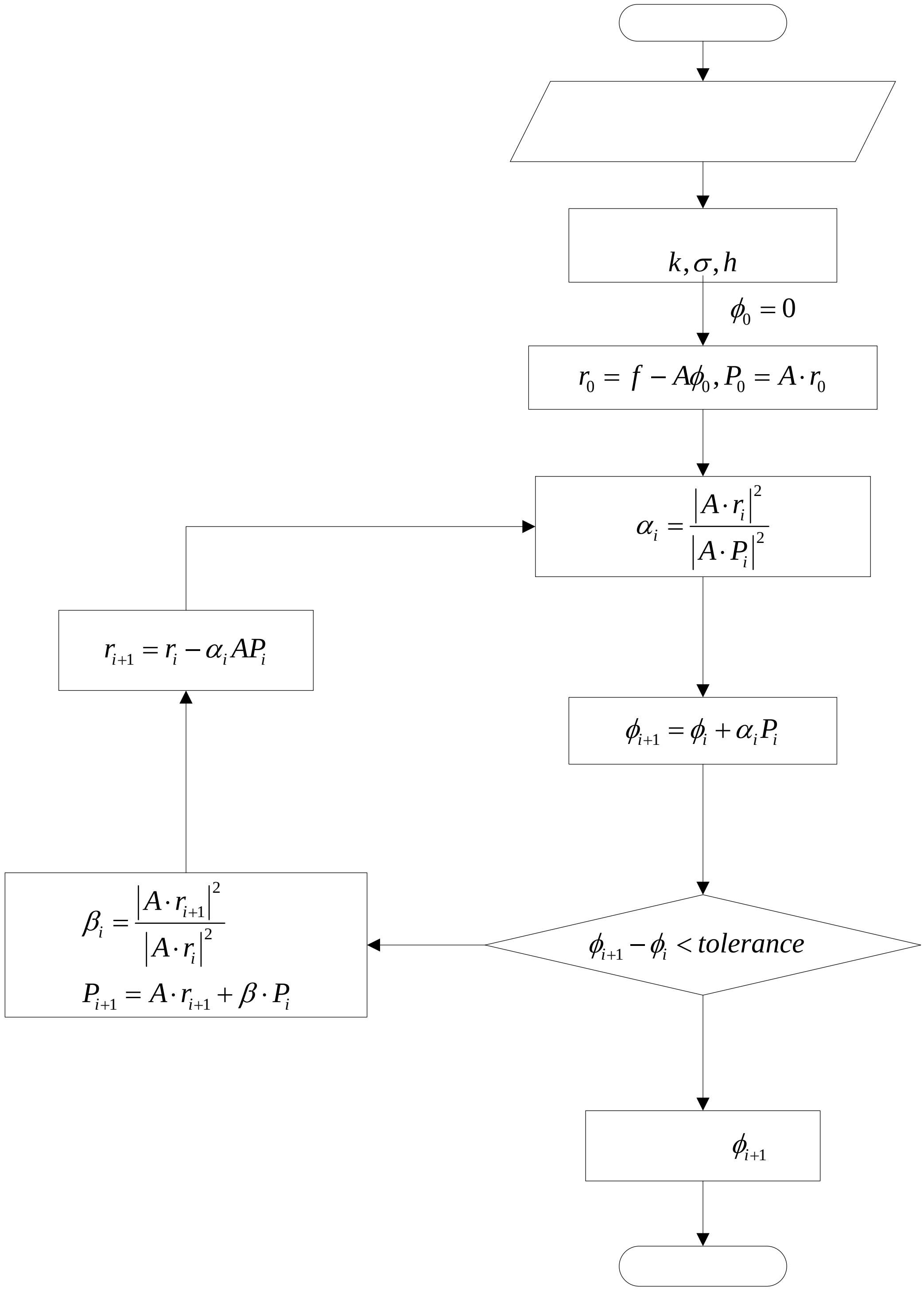

Figure 3.3: Flow chart of wave velocity potential calculation (Panchang et al., 1991)

3.5 Validation of 2D Model by a CFD Model Flow 3D

3.5.1 Introduction

Flow3D is a CFD software developed by the Flow Science Company and was first released in 1985. It can handle all kinds of problems related to current, fluid with viscosity, turbulence, transient flow, heat transfer analysis and so on. Flow3D is capable of solving hydraulic problems using Navier Stokes theories up to 5^{th} order. The Volume of Fluid (VOF) method enables the free surface modeling and can define and generate the liquid/gas interface. Flow3D can also handle fluid with viscosity and bottom shear stress. The multi-block grids and structured grids can also improve the efficiency of the calculation.

Since the 2D Model is a potential flow linear approximation of Navier Stokes equations, a validation of the 2D Model is performed by comparing it with Flow3D.The 2D Model can only do calculations within the calculation domain in water, it cannot handle all cases. A Flow3D model is also used for the calculation of the phenomenon such as: the green water load problem and the wave loads with water clearance in later sections.

However, it consumes much more computation time with Flow3D than with the 2D Model. To generate the new estimating equations, thousands of cases need to be calculated to investigate the relationship between wave loads and all kinds of parameters. In such a case, the 2D Model is a better approximation of the wave loads but need to be validated by a full Navier Stokes model of Flow3D. The Flow3D model will only be used in some special cases that the 2D Model cannot handle.

In this section, a simple model with one regular fixed box placed in the SWL is going to be set up for both: Flow3D using Navier Stokes 5th order theory and 2D Model using linear wave theory. The results will be analyzed to address the differences and gaps between Flow3D and 2D Model. Furthermore, based on the results from Flow3D, the green water effects will be modified in the 2D Model which cannot deal with the problem directly.

In this simple model, a rectangular fixed box is placed at the surface of the water. The wave form is regarded as ideal for the regular wave form with no viscosity and no shear stress on the bottom. Results are going to be analyzed to find out the correlation between the two models.

3.5.2 Validation of Flow3D Hydraulic Wave Model

To begin using Flow3D, it is necessary to validate its applicability to the hydraulic problem. For a CFD model, boundary conditions are most important. Unlike the boundary conditions of a 2D Model, the boundary is defined as wave particle velocities directly in Flow3D for the incoming and outgoing boundary. A simple simulation, with waves only, is set up for the validation.

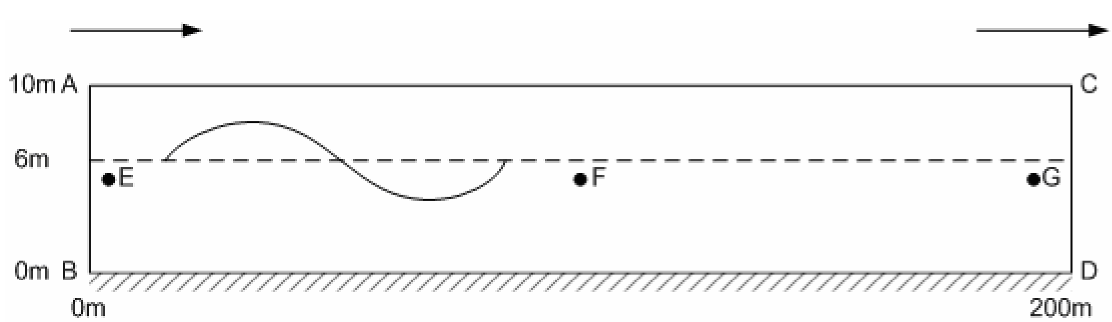

Figure 3.4: Flow3D domain and particle source points

The Flow3D model domain is a 2-D domain of $200m \times 10m$. The domain is meshed by 1000×50 grids which size is 0.2m in both x and z directions.

The initial fluid is sea water at $20^{\circ}C$ which the density is $1.032\,kg/m^3$. As shown in Figure 3.4, the wave is coming from AB to CD. Point E, F and G are particles which are examined for the particle routes and velocities under water. AB boundary condition is defined as incoming wave boundary with parameters of wave height 2m, wave period 6s and water depth 6m. CD boundary condition is defined as outflow boundary condition.

The outflow boundary condition in Flow3D is still under improvement. Since all the calculations in Flow3D are done in the calculation domain, all the fluid parameters are well determined except for those out of the calculation domain. As a result, the CD outflow boundary condition can only determine how much fluid goes out from the fluid domain and there will be no fluid coming into the domain from out of the CD boundary. Thus, the outflow boundary condition can definitely affect the refraction and diffraction of the whole domain.

In this section, three characteristics are going to be analyzed, the fluid volume in the domain, the underwater particles routes and velocities.

3.5.2.1 Fluid volume

Fluid domain volume is an important criterion for the validation of the model. The volume of fluid must not change much. Otherwise, it can be regarded as a failure of the boundary condition definition.

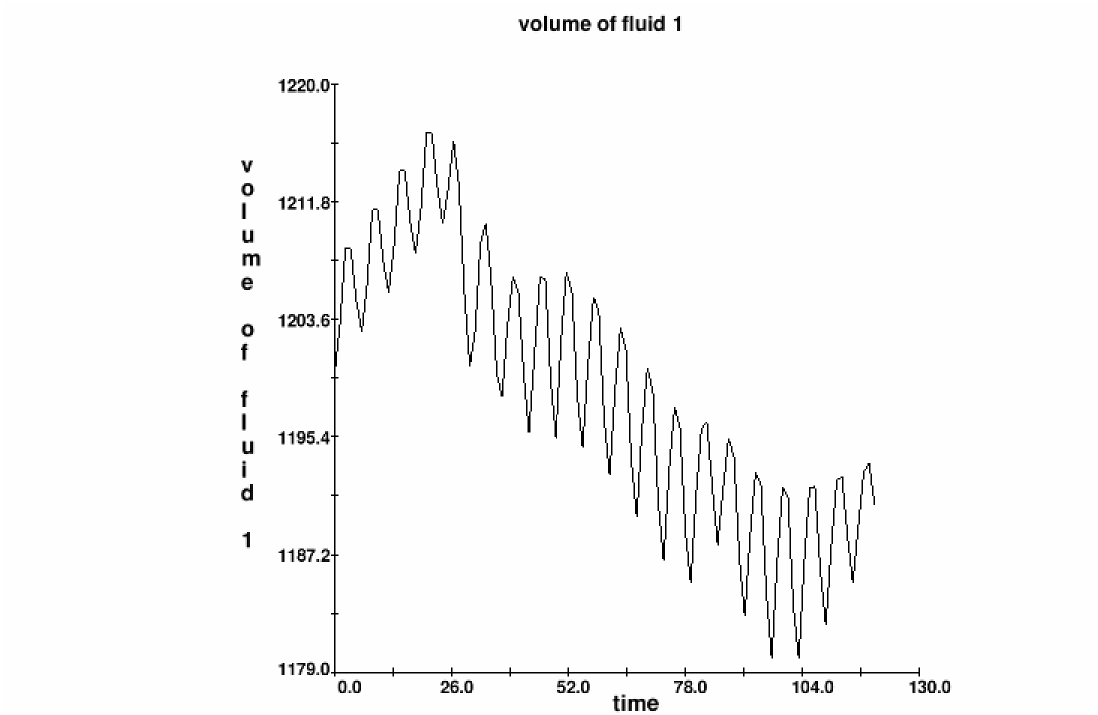

Figure 3.5: Fluid domain volumes according to simulation time

In Figure 3.5, the biggest error is around 3%. From view of the fluid domain, the model is acceptable for application.

3.5.2.2 Particles paths and velocities

Under the linear wave theory assumption, water particles generally move in elliptical paths in shallow or transitional depth water and in circular paths in deep water. The particles horizontal and vertical velocity will be the sinusoidal form:

$$u = \frac{H}{2}\frac{gT}{L}\frac{\cosh\left[2\pi\left(z+d\right)/L\right]}{\cosh\left(2\pi d/L\right)}\cos\theta \tag{3.28}$$

$$v = \frac{H}{2}\frac{gT}{L}\frac{\sinh\left[2\pi\left(z+d\right)/L\right]}{\cosh\left(2\pi d/L\right)}\cos\theta \tag{3.29}$$

where $\theta = \frac{2\pi}{T}t - x$

H = wave height,

T = wave period,

d = water depth,

L = wave length

Under Stokes finite-amplitude wave theory assumption, the higher order terms in the displacement of water particles make particles move forward in spiral paths and velocity curves become steeper.

In this model, 3 fixed particle sources E, F and G in Figure 3.4 are defined in the calculation domain. The particle sources will release 10 particles per second. The particles moving path and the particle velocity in the three points are examined to see whether they obey the linear or nonlinear theory assumption.

Figure 3.6 is a 1000×50 grid calculation domain and the 3 particles movement paths. It can be concluded that the particles' paths obey the Stokes nonlinear wave theory. Particles' paths and velocities are zoomed out and analyzed around E, F and G particles sources in Figure 3.7-3.9.

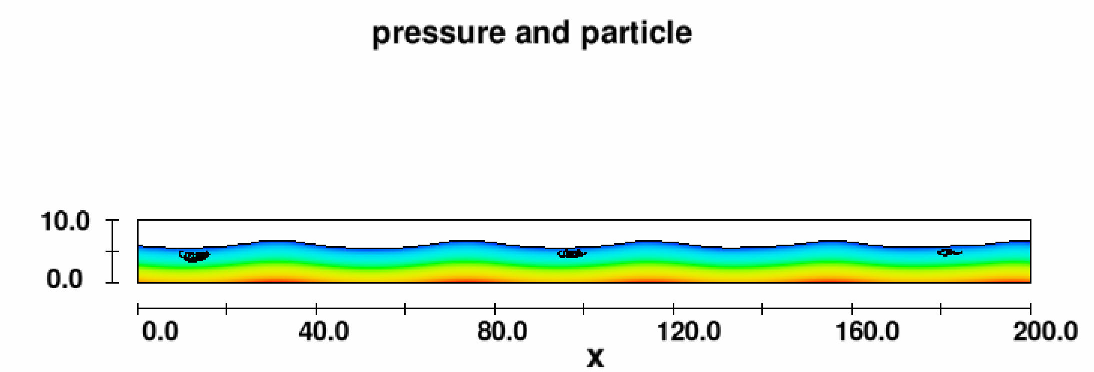

Figure 3.6: The calculation domain and particles moving paths

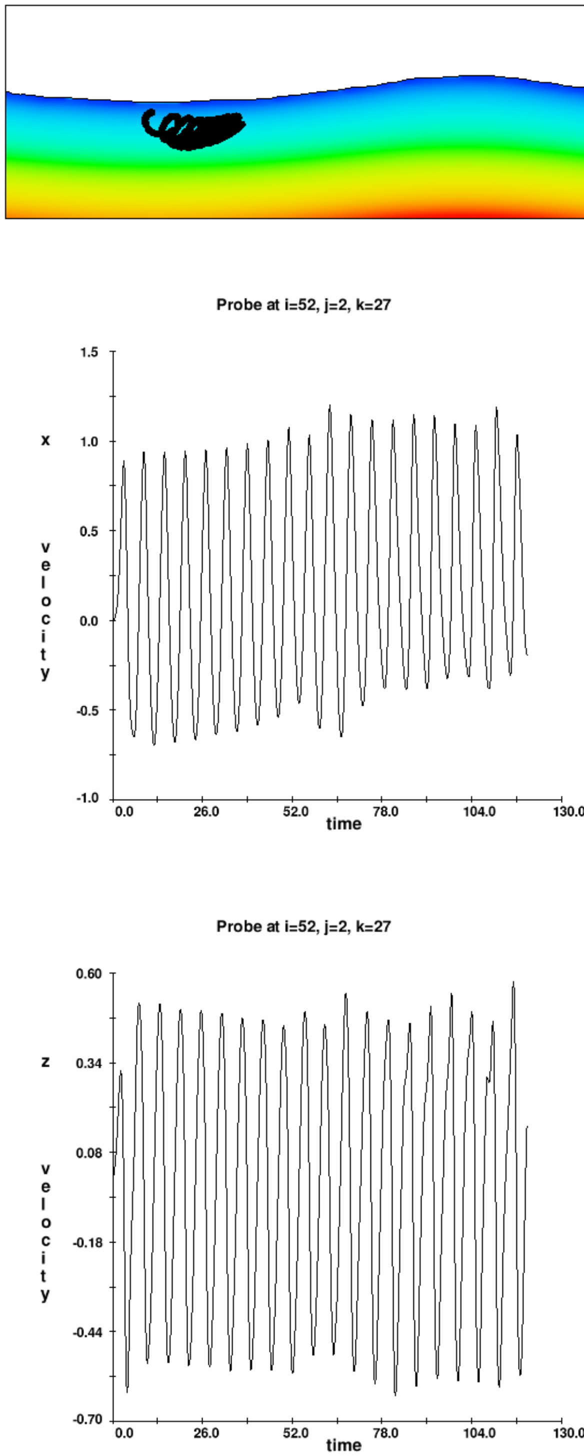

Figure 3.7: Point E particle path and velocities in *x* and *z* directions

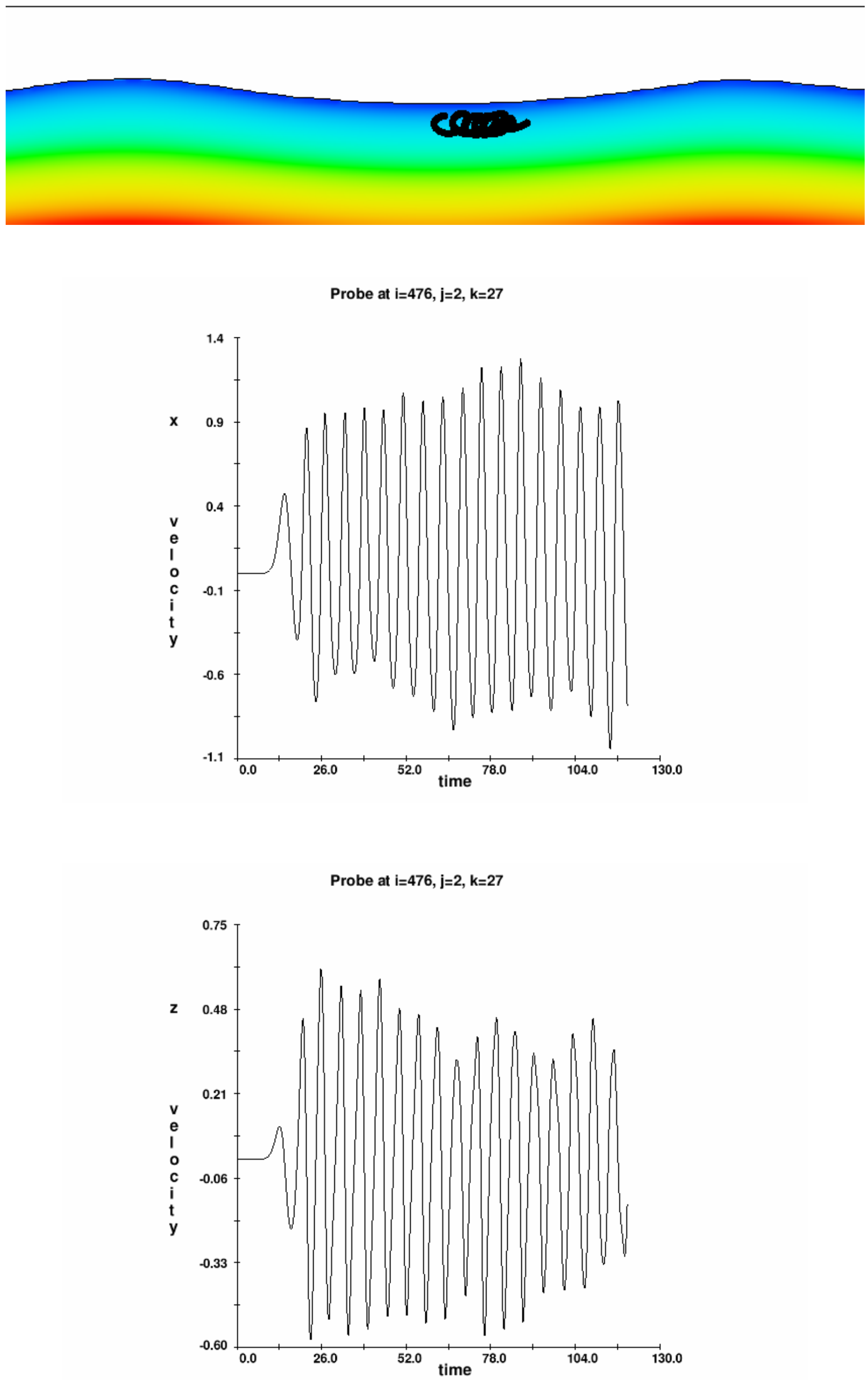

Figure 3.8: Point F particle path and velocities in *x* and *z* directions

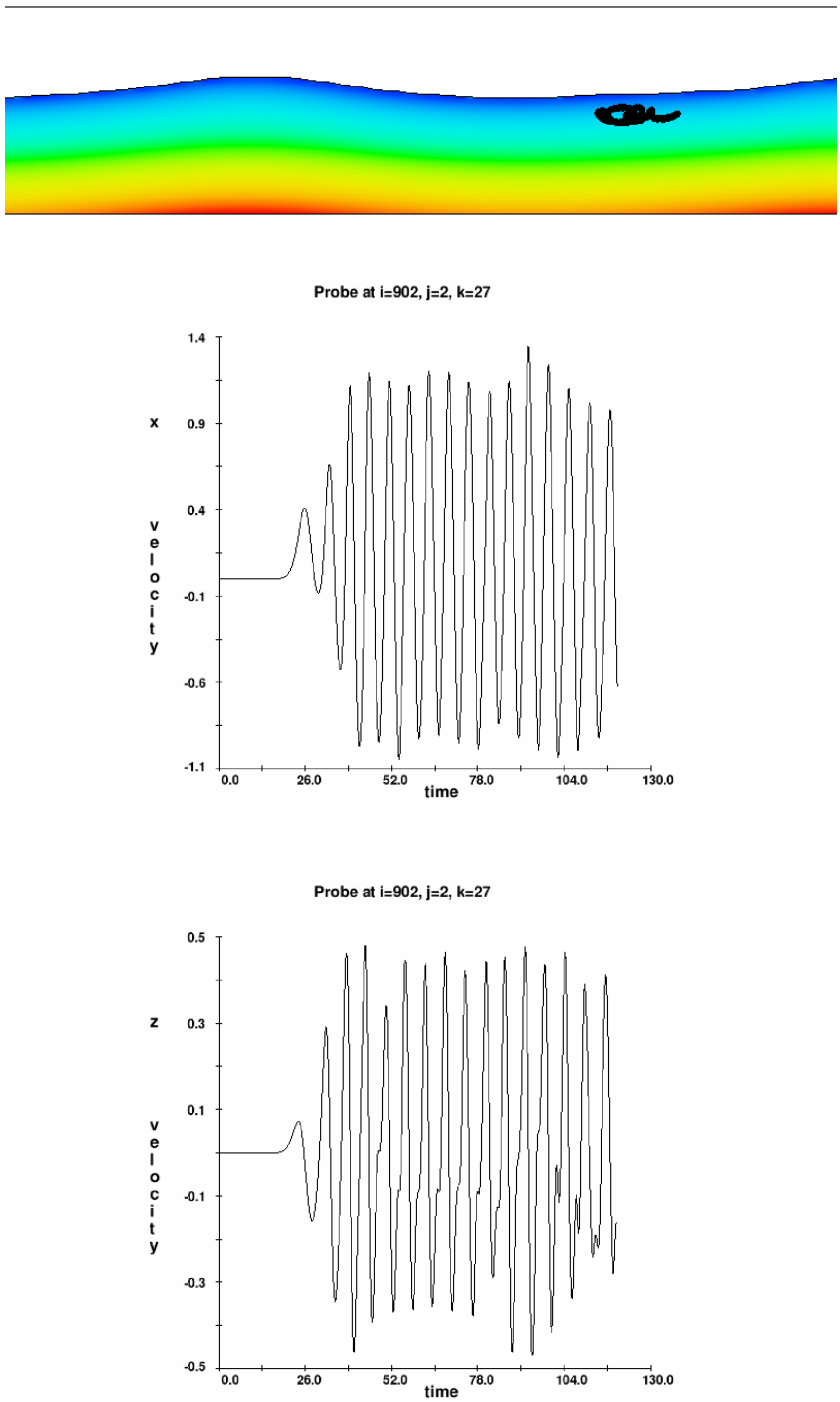

Figure 3.9: Point G particle path and velocities in *x* and *z* directions

The particles paths and velocities are all well formed and similar to the analytical solutions; the overall domain fluid volume is also conservative. It can be concluded that the Flow3D wave model can generate applicable waves for further analysis. Then a simple model with one fixed rectangular box will be setup to compare the results from Flow3D and those from 2D Model.

3.5.3 Comparison between Flow3D and 2D Model

3.5.3.1 Model description

In this section, a model is setup for comparison of results from Flow3D and those from 2D Model. In the model shown in Figure 3.10, a fixed rectangular box is placed in water. The still water level is 6m high and the bottom of box is placed 5m high to the water bottom.

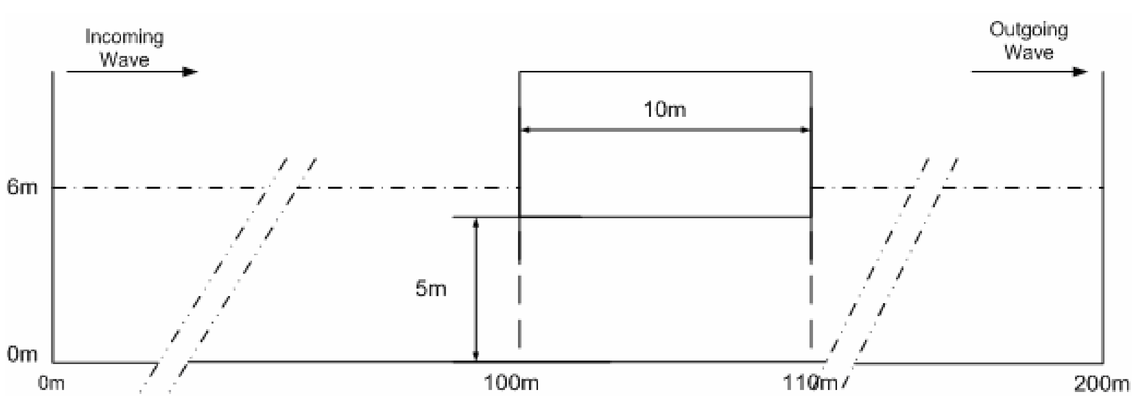

Figure 3.10: Model descriptions for comparison between Flow3D and 2D Model

The incoming wave parameters for the model are 2m wave height, 6s wave period and 6m water depth.

3.5.3.2 Flow3D model results

The calculation domain is setup as $10m \times 200m$, with 50×1000 grids of size 0.2m. Figure 3.11 shows the final simulation results.

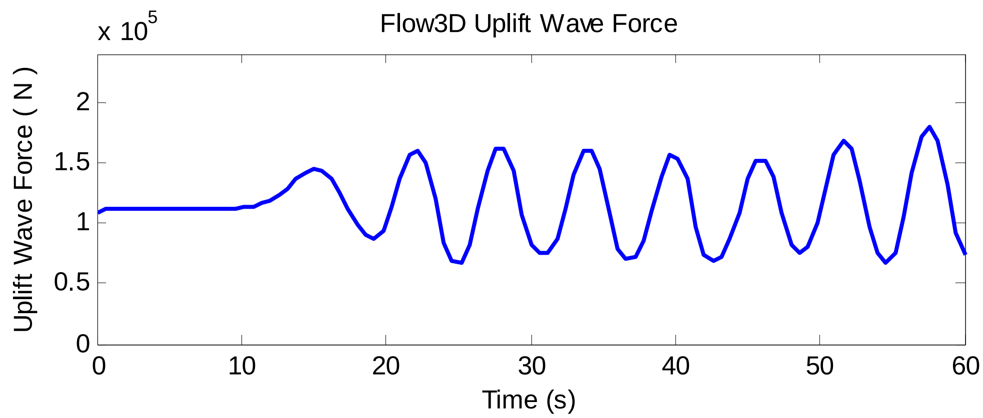

Figure 3.11: Flow3D uplift wave force over simulation time

The results are cut at time 60 sec. Because of the improper outflow boundary condition in Flow3D, there is an obvious increase of fluid volume after 60 seconds. Before that, the fluid volume remains stable. When the incoming wave goes by the obstacle and reaches the outflow boundary, part of it is reflected and thus causes an increase in fluid volume. The reflected wave also affects the wave form around the obstacle and the wave force as well. As a result, the simulation results are cut at 60 sec.

3.5.3.3 2D Model results

The calculation domain is setup as $6m \times 200m$, with 30×1000 grids of size 0.2m.

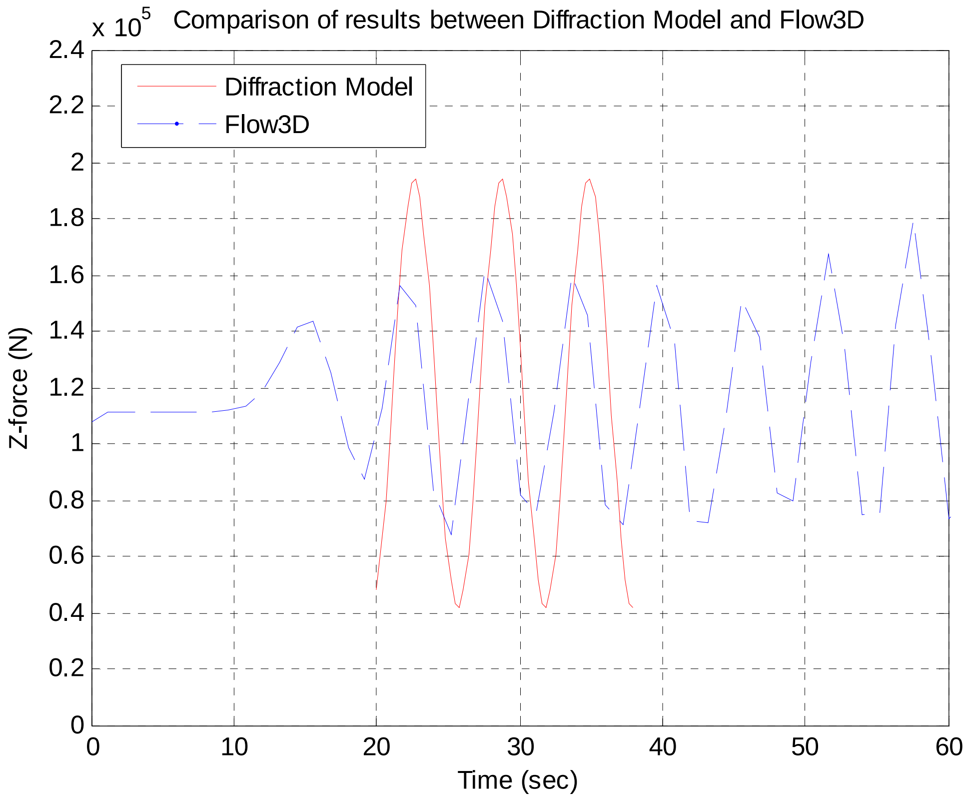

Figure 3.12: Comparison of uplift wave force results between Flow3D and 2D Model

Figure 3.12 shows the 2D Model uplift wave forces results comparison with Flow3D. The maximum uplift wave force error between them is around 10%. Similarly, Figure 3.13 shows the horizontal wave forces results compared with the Flow3D Model.

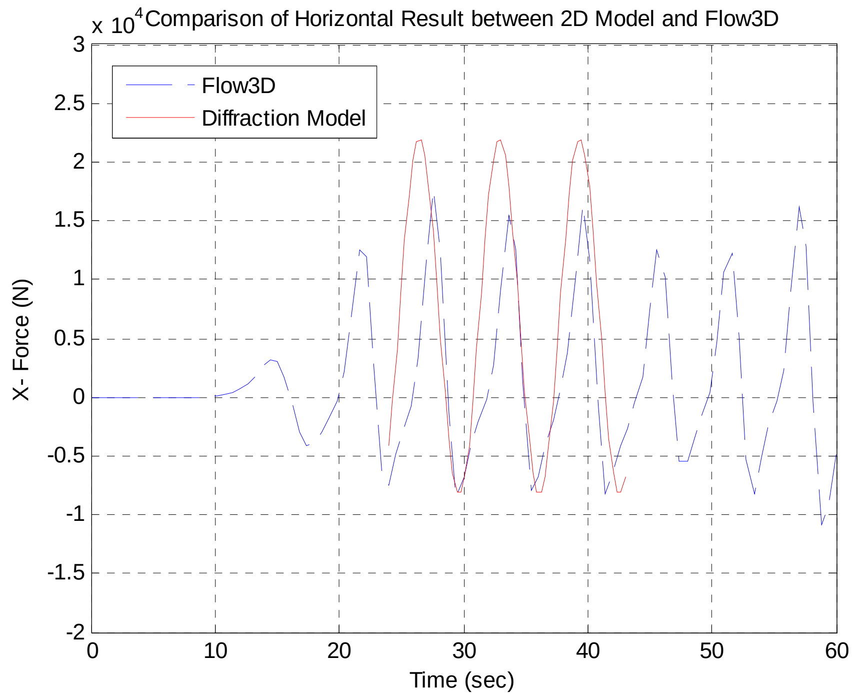

Figure 3.13: Comparison of horizontal wave force results between Flow3D and 2D Model

3.6 Validation of 2D Model by Experiment Data (Tirindelli et al., 2002)

3.6.1 Physical Model Description

In this section, a physical model setup by Tirindelli et al. (2002) is studied and used as a comparison with the results from 2D (x-z plane) wave velocity potential model. Tirindelli made a model of a jetty structure located at HR Wallingford. A series of tests were conducted in a wave flume to study inconsistencies and gaps in some existing methods for evaluating wave loading. He made comparisons with Kaplan's (1992, 1995, 1997) method on vertical wave forces on horizontal elements based on an extension of Morison's equations (1950); as well as with Shih & Anastasiou's (1992) empirical equations.

As shown in Figure 3.14, the frame of the model jetty was bolted to the flume floor. A partially absorbing slope with 1:5 slope covered with absorbing matting and rocks was installed to reduce reflections. Three wave gauges (number 0, 1 and 2) in Figure 3.14 were used to correlate wave heights and loads on the deck.

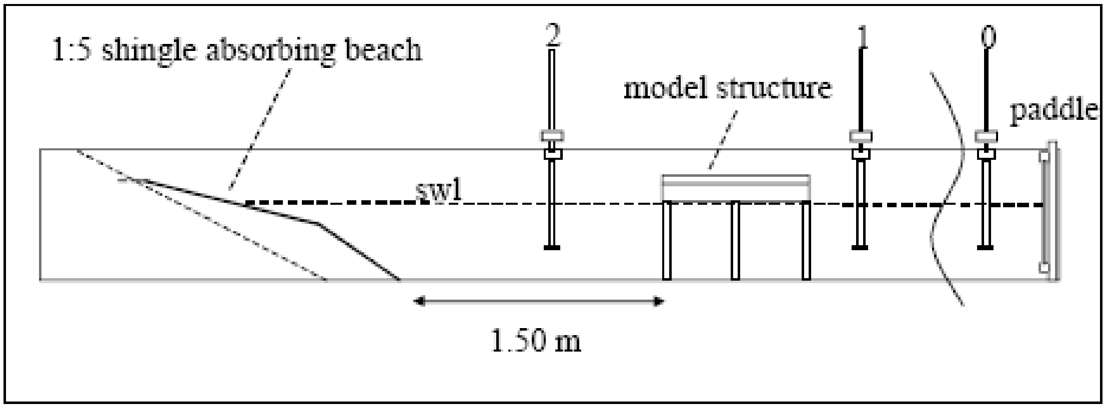

Figure 3.14: Experimental set-up in the wave absorbing flume by Tirindelli et al. (2002)

Model structure is shown in Figure 3.15:

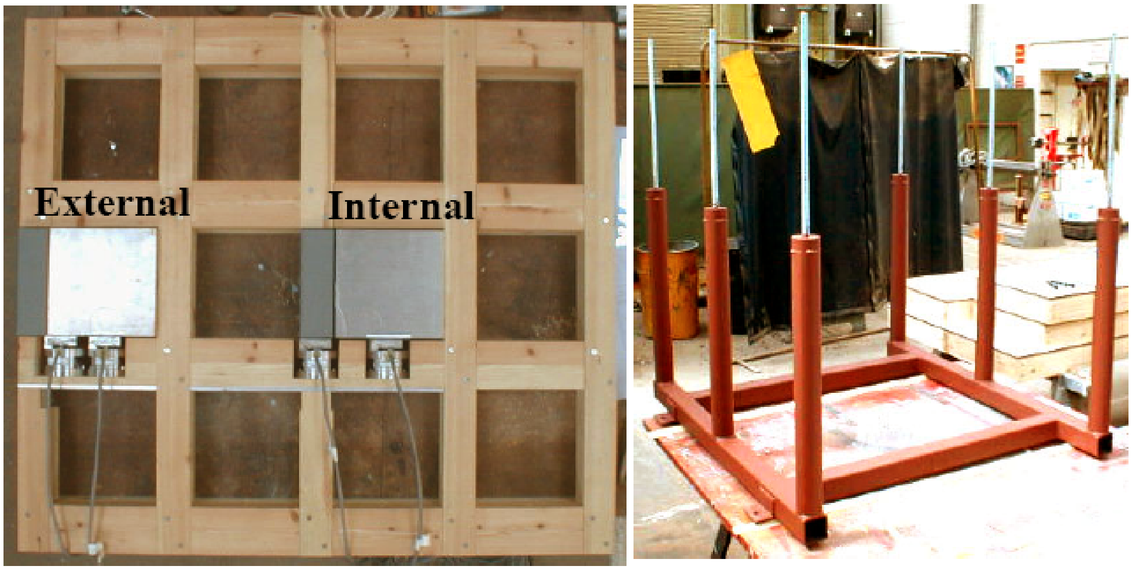

Figure 3.15: Down-standing frame of beams with testing elements and support pile structure (Tirindelli et al., 2002)

The wave parameters matrix is listed in Table 3.1:

Table 3.1: Wave parameters in 2D Model

Hs(m) & T(s)	1.00	1.20	1.25	1.50	1.75	2.00	2.25	2.50	2.75	3.00
0.10	X		X	X	X	X	X	X		
0.14		X	X	X	X	X	X	X	X	X
0.18			X	X	X	X	X	X	X	X
0.22				X	X	X	X	X		

3.6.2 Experiment Results and Conclusions

The experiment results and comparisons with Kaplan’s predictions are shown in Figures 3.16.

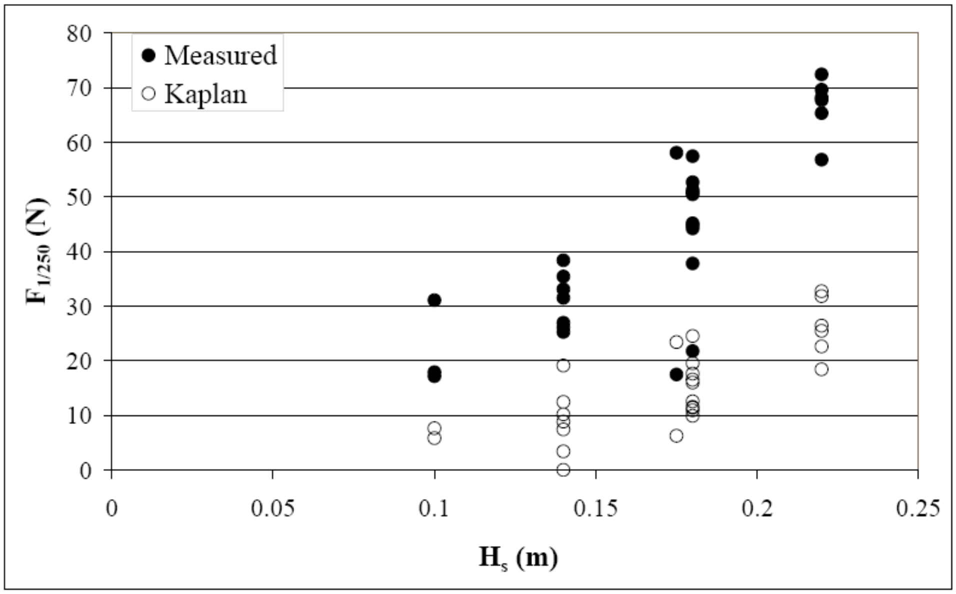

Figure 3.16: Measured uplift wave forces on external deck and Kaplan's predictions (Tirindelli et al., 2002)

In Figure 3.16, Tirindelli compares the measurement results with Kaplan's predictions and concludes that Kaplan under-estimates the wave uplift load on decks. $F_{1/250}$ is used for the uplift wave loads, which means the average value of highest 1/250 wave heights for random waves.

3.6.3 2D Wave Velocity Potential Model

3.6.3.1 Model description

Following the experiment physical model by Terindelli, the wave potential model is set up as shown in Figure 3.17. In Tirindelli's experiment, two water depths, 0.75m and 0.60m are considered. Since the data for water depth of 0.60m shown in his study is not as adequate as those for water depth of 0.75m, the wave forces in the 2D Model is calculated only for water depth of 0.75m. And the maximum uplift wave force will be compared only in the external deck area as shown in Figure 3.17 as External Plate Sensor area.

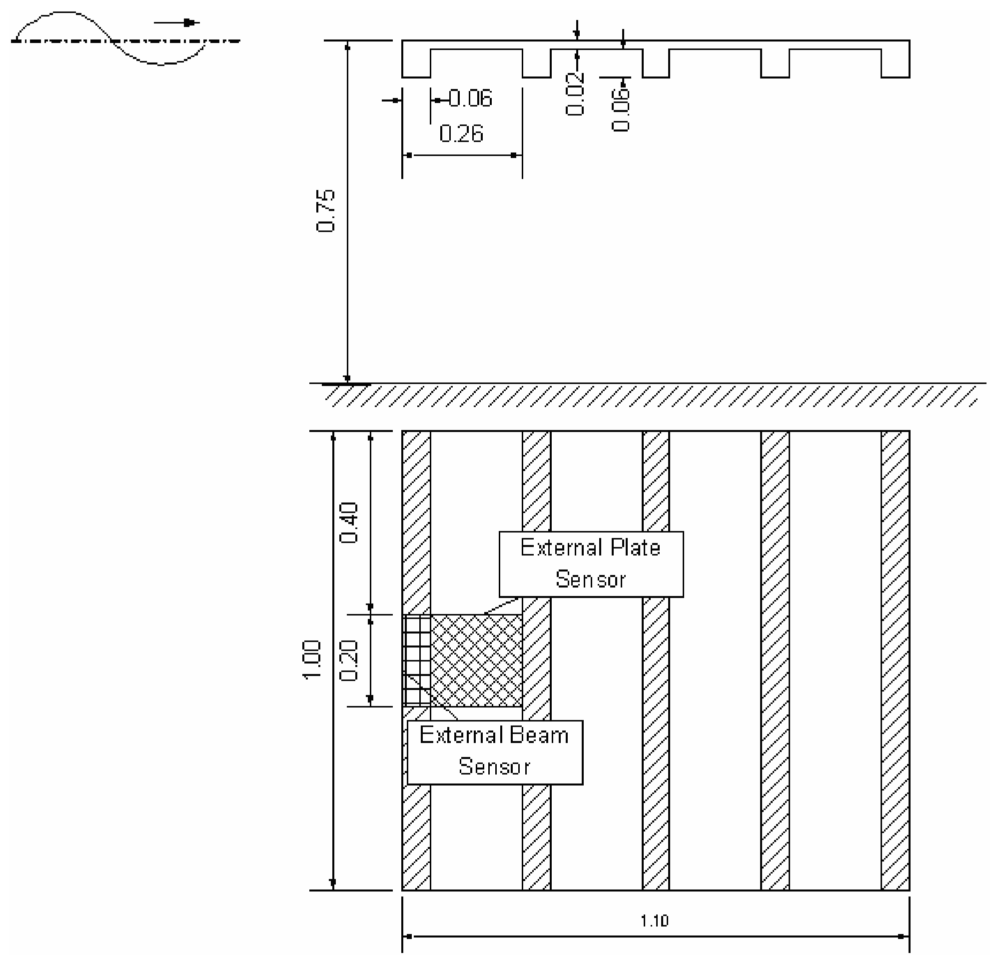

Figure 3.17: 2D wave velocity potential model (metric unit)

3.6.3.2 Wave parameters

Table 3.1 shows the wave parameters of significant wave heights and wave periods that will be calculated in the 2D Model. The significant wave heights and wave periods follow Tirindelli's experiments.

3.6.3.3 Statistic analysis of wave height distribution in real random waves

The 2D Model and calculation is conducted based on the monochromic regular wave theory assumption. While in a real sea state, waves are random and irregular, and can be treated as a superposition by waves with different wave heights and periods.

Assuming wave heights follow Rayleigh distribution,

$$H_s = H_{1/3} = 1.416 H_{rms} \tag{3.30}$$

$$H_{1/250} = 2.547 H_{rms} = 1.798 H_s \tag{3.31}$$

According to the wave parameters in Table 3.1, the wave parameters applied in the 2D Model are listed in Table 3.2:

Table 3.2: Wave parameters of $H_{1/250}$ and T (s) in 2D Model

$H_{1/250}$ (m) & T (s)	1.00	1.20	1.25	1.50	1.75	2.00	2.25	2.50	2.75	3.00
0.18	X		X	X	X	X	X	X		
0.25		X	X	X	X	X	X	X	X	X
0.32			X	X	X	X	X	X	X	X
0.40				X	X	X	X	X		

3.6.3.4 Simulation Results

In the 2D Model, the incoming wave is a monochromic sinusoidal wave with no clearance. Under the monochromic sinusoidal wave assumption, the numerical simulation results are listed in Table 3.3:

Table 3.3: Calculation results from 2D Model

Wave Periods (s)	Wave Heights (m)	Force_1st_plate (N)
1.00	0.18	34.24
1.25	0.18	40.03
1.50	0.18	43.56
1.75	0.18	45.39
2.00	0.18	46.24
2.25	0.18	46.53
2.50	0.18	46.57
1.20	0.25	49.78
1.25	0.25	51.13
1.50	0.25	56.04
1.75	0.25	58.58
2.00	0.25	59.76
2.25	0.25	60.16
2.50	0.25	60.22
2.75	0.25	60.09
3.00	0.25	59.84
1.25	0.32	62.23
1.50	0.32	68.52
1.75	0.32	71.77
2.00	0.32	73.28
2.25	0.32	73.79
2.50	0.32	73.86
2.75	0.32	73.70
3.00	0.32	73.39
1.50	0.40	82.78
1.75	0.40	86.84
2.00	0.40	88.73
2.25	0.40	89.37
2.50	0.40	89.46

where

Force_1st_plate = the maximum uplift wave force on the external plate area shown in Figure 3.17.

The wave periods and wave heights in Table 3.3 are input variables to 2D Model, and *Force_1*st*_plate* is the result from 2D Model.

3.6.3.5 Modification according to the water clearance

The analysis and simulation above is all based on the reference example with clearance $cl = 0$. In most real cases, there is always some clearance greater than 0 and it plays a role in uplift wave forces. In this part, the effects and modification according to clearance is analyzed.

Figure 3.18 is a sketch of the sinusoidal incoming wave. The assumption of modification due to clearance is that the overall maximum uplift wave force is linearly dependent on the interaction area of the bridge deck and the waves.

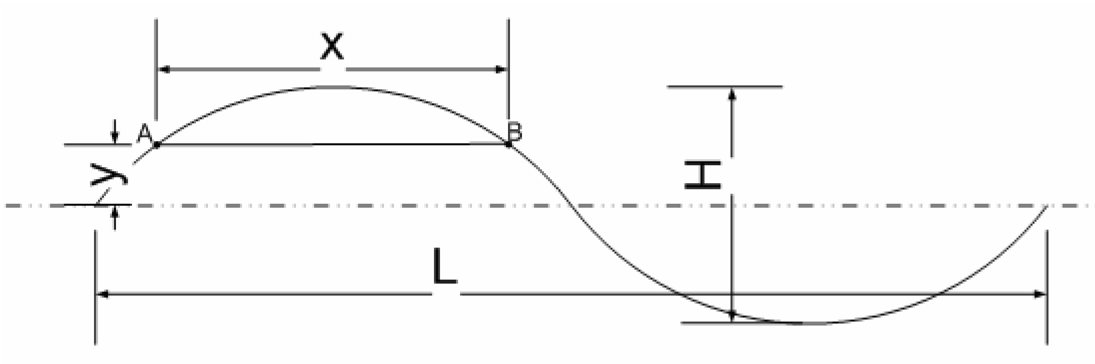

Figure 3.18: Sketch of incoming sinusoidal wave and clearance

The Figure 3.18 shows that as the clearance increase, the interaction area decreases. If the clearance $cl = 0$, the waves forces coincide with the results shown in above parts; if the clearance is equal or above half of wave height, that is, $cl > \frac{H}{2}$, the wave may not reach the bottom of the bridge deck and in this case, the uplift wave force is 0.

Problem: Find out the modification coefficient according to the clearance

Known: wave height H, clearance cl, maximum uplift wave force $F_{cl=0}$

Desired: F_{cl}

Solution:

The equation to describe the sinusoidal wave surface curve is:

$$y = \frac{H}{2}\sin(\frac{x}{L} \cdot 2\pi) \tag{3.32}$$

at $cl = y = 0$,

$$x = x_B - x_A = L/2, \quad F_v = F_{cl=0}$$

at $cl = y = \frac{H}{2}$,

$$x = x_B - x_A = 0, \quad F_v = F_{cl=0} \cdot a$$

$$\text{Where} \quad a = \frac{\text{girder section area}}{\text{deck section area}}$$

at $cl = y$, $0 < y \le \frac{H}{2}$

$$
\begin{aligned}
x &= x_B - x_A \\
&= \frac{L}{2\pi}\left[(\pi - \arcsin\frac{2y}{H}) - \arcsin\frac{2y}{H}\right] \\
&= \frac{L}{2\pi}(\pi - 2\arcsin\frac{2y}{H}) \\
&= \frac{L}{2}(1 - \frac{2\arcsin\frac{2y}{H}}{\pi})
\end{aligned}
$$

then $$F_{cl=y} = F_{cl=0}\left[1 - \frac{2\arcsin\frac{2y}{H}}{\pi}(1-a)\right]$$

As a result, let

$$A_{cl} = 1 - \frac{2\arcsin\frac{2cl}{H}}{\pi}(1-a) \tag{3.33}$$

Then $$F_{cl=y} = F_{cl=0} \cdot A_{cl} \tag{3.34}$$

Where $$a = \frac{\text{girder section area}}{\text{deck section area}} \tag{3.35}$$

3.6.3.6 Water clearance coefficient validation by Flow3D

The 2D Model cannot do the calculation out of the calculation domain, and thus cannot do the calculation if there is a water clearance. A Flow3D model is set up to investigate the relationship between wave load and water clearance and to validate the wave clearance coefficient assumption.

A reference Flow3D model is setup following the Bridge I-10 across Escambia Bay near Pensacola, Florida as shown in Figure 3.19. More detailed information will be explained in later section 4.3.

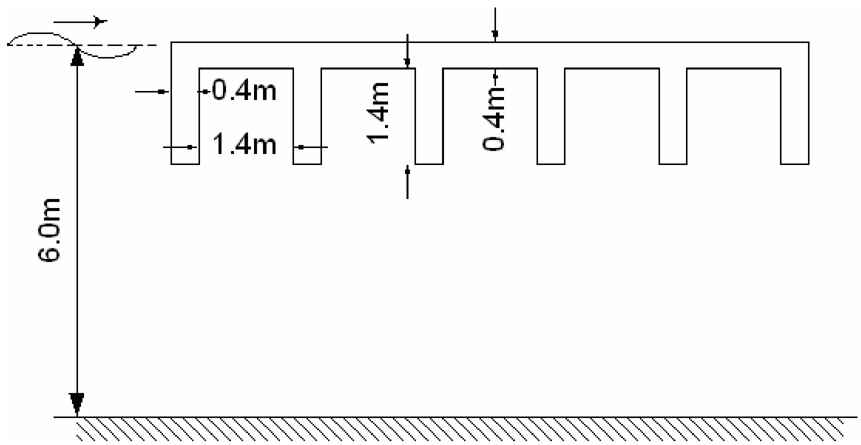

Figure 3.19: Geometry of the bridge deck and girders of reference model

In the Flow3D model shown in Figure 3.19, wave height is 2 meters, wave period is 6 seconds and water depth is 6 meters. The components and meshes are set up as shown in Figure 3.20. The calculation domain is 10×60 meters in $Z \times X$ direction, and one unit meter in Y direction. The mesh grid count is $100 \times 600 \times 1$. The left side is defined as incoming wave boundary condition and the right side is defined as flow out boundary condition.

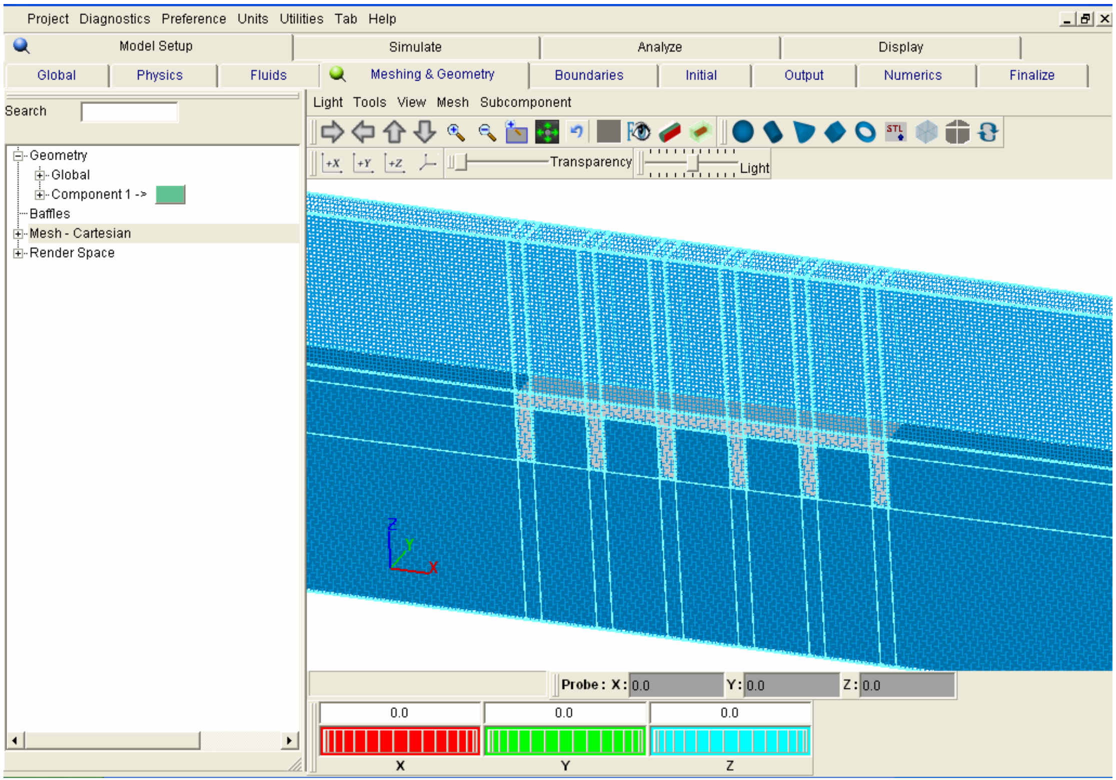

Figures 3.20: Flow3D model component and mesh blocks

The water clearance is chosen as 0, 0.2, 0.4, 0.6, 0.8, 1.0, 1.2 meters. The case with water clearance of 0 meters is taken as an example first here.

The simulation time is set to 120 seconds and the results are taken from 1-80 seconds. Figure 3.21 shows the simulation results lasting for 2 wave periods from 36 sec to 48 sec.

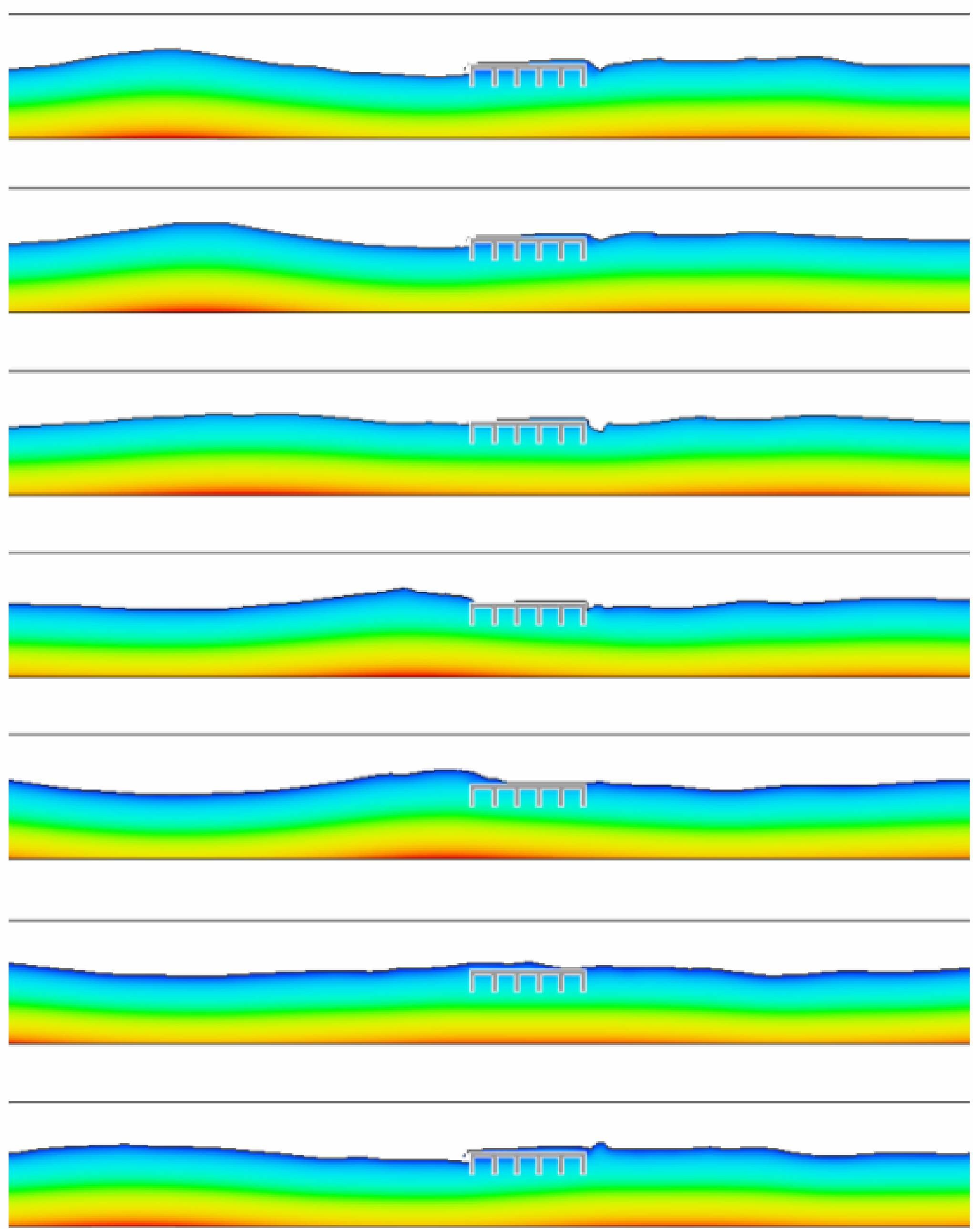

Figure 3.21: Simulation results lasting for 2 wave periods from 36 sec to 48 sec

The contour in Figure 3.21 is defined as hydraulic pressure. And from the figure, it shows that: The incoming wave is partially reflected back by the bridge superstructure and partially transmits through the bridge; The incoming wave height is larger than the transmitted wave height and a transmission coefficient can be obtained from the ratio of the wave heights in front of and behind the bridge; As wave crest goes by the bridge, the waves go on top of the bridge, which is called the green water problem; As wave crest passes by the bridge, the hydraulic pressure under the bridge becomes the largest.

In Flow3D model, other force windows can also be defined to examine the overall uplift wave forces and downward wave forces.

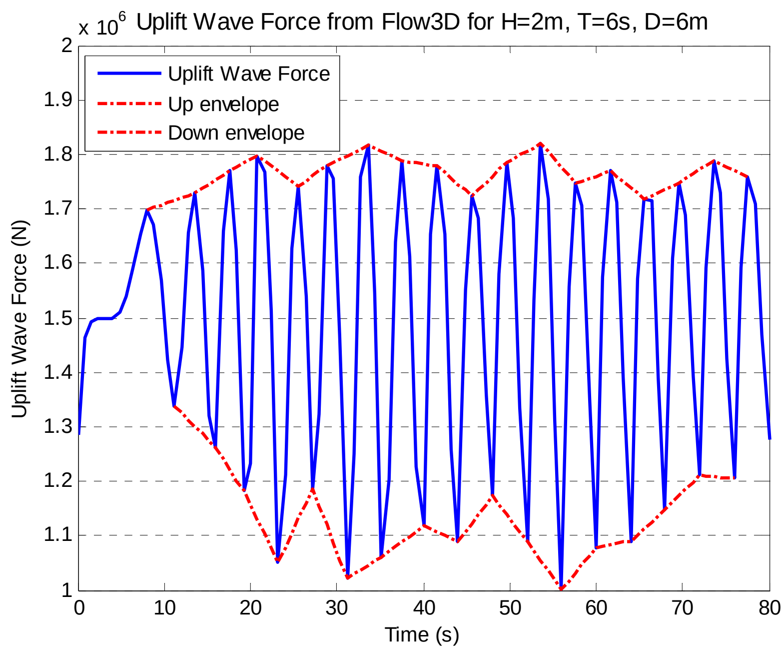

Figure 3.22: Uplift wave forces from Flow3D model for H=2m, T=6s, D=6m

The maximum uplift wave force of the example case shown in Figure 5.22 is 1.82×10^{6} N.

Following the same steps of calculation above, the maximum uplift wave forces for water clearance of 0.2 to 1.2 are listed below in Figure 5.23-5.28:

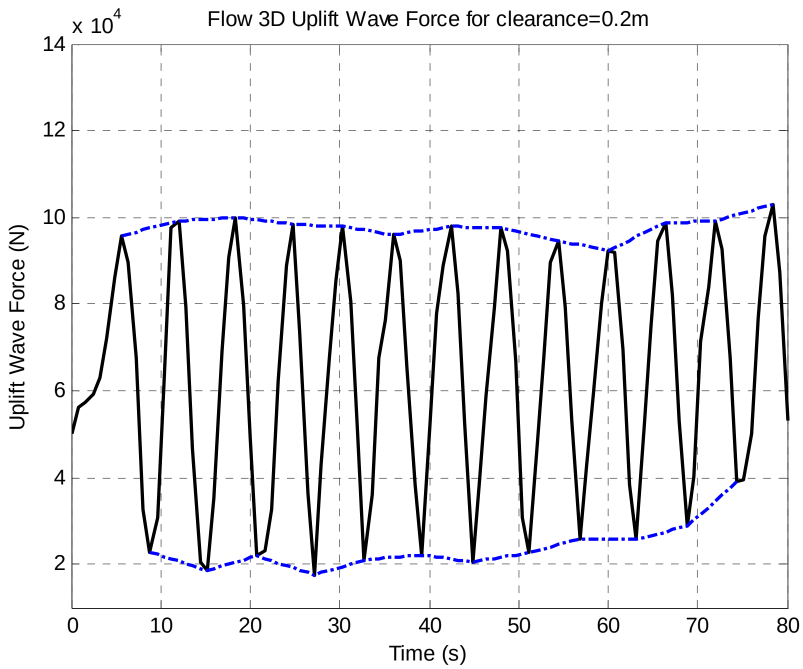

Figure 3.23: Flow3D uplift wave force for H=2m, T=6s, D=6m at clearance=0.2m

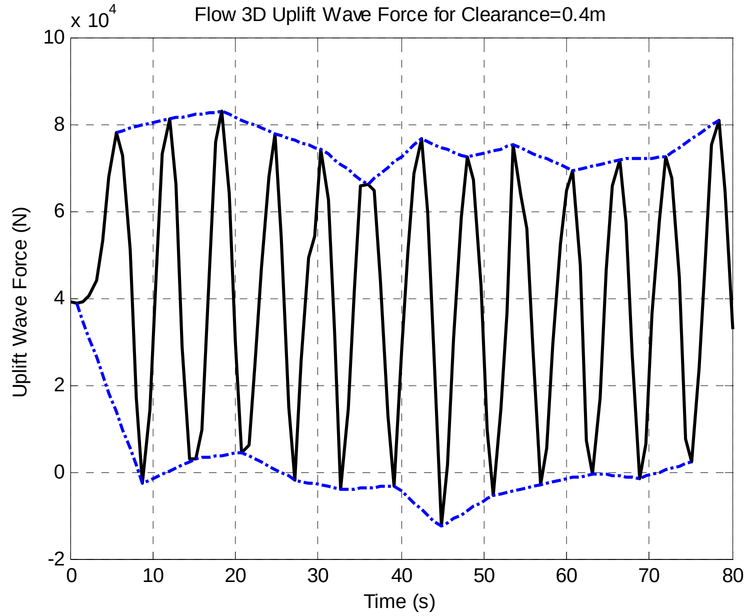

Figure 3.24: Flow3D uplift wave force for H=2m, T=6s, D=6m at clearance=0.4m

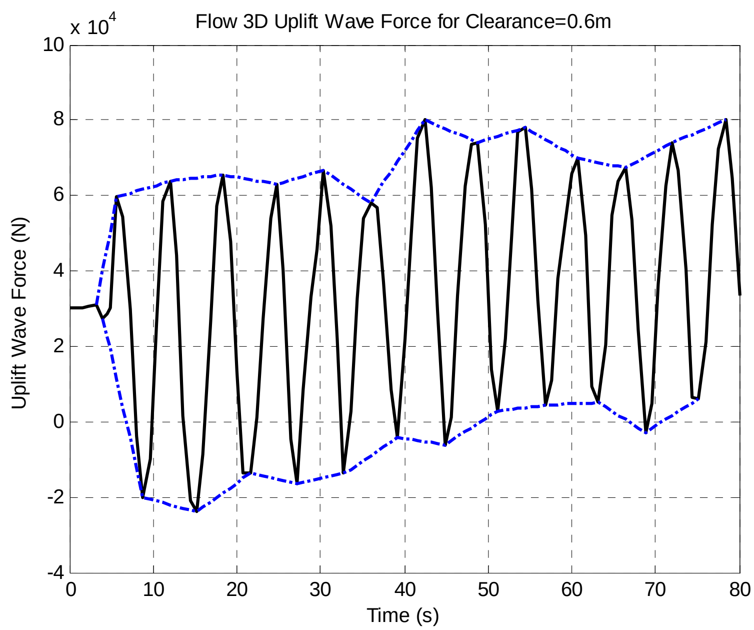

Figure 3.25: Flow3D uplift wave force for H=2m, T=6s, D=6m at clearance=0.6m

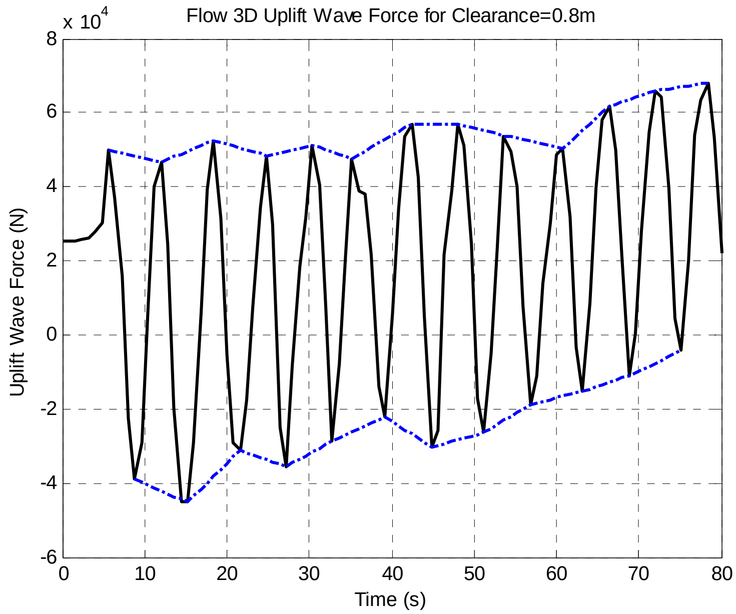

Figure 3.26: Flow3D uplift wave force for H=2m, T=6s, D=6m at clearance=0.8m

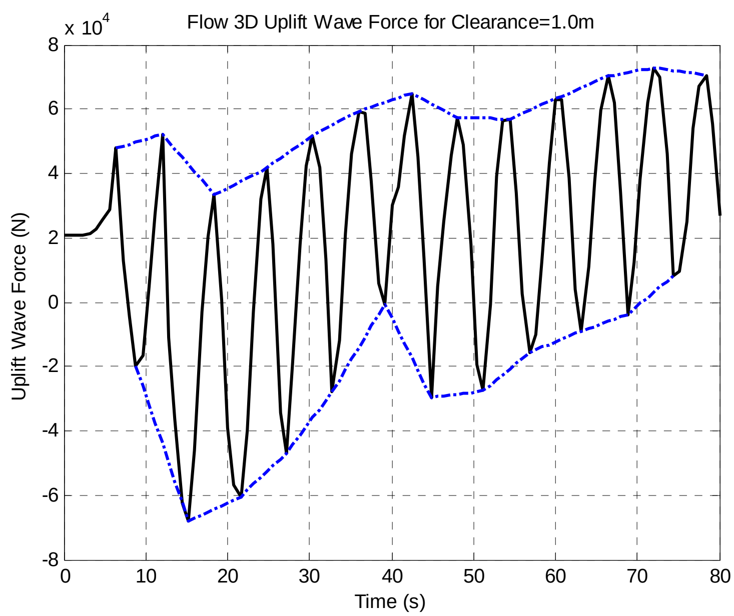

Figure 3.27: Flow3D uplift wave force for H=2m, T=6s, D=6m at clearance=1.0m

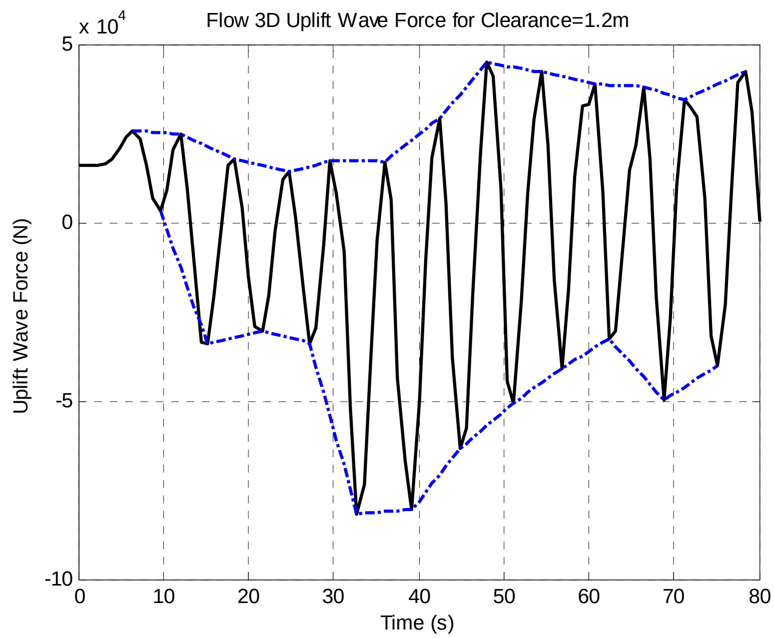

Figure 3.28: Flow3D uplift wave force for H=2m, T=6s, D=6m at clearance=1.2m

Taking the maximum and average values for the upper limit of uplift wave forces , we have the maximum uplift wave forces according to the clearances for wave model of H=2m, T=6s and D=6m.

The results are shown in Figure 3.29. The y axis stands for the coefficients of water clearance which are the uplift wave loads divided by the maximum uplift wave force at clearance=0; the x axis is water clearance index which are the values of water clearances divided by wave amplitude also know as half wave height. Water clearance coefficients from Eqs. 3.33 and 3.34 fit the results, in which coefficient $a = \dfrac{\text{girder section area}}{\text{deck section area}} = 0.26$ according to Eq. 3.35.

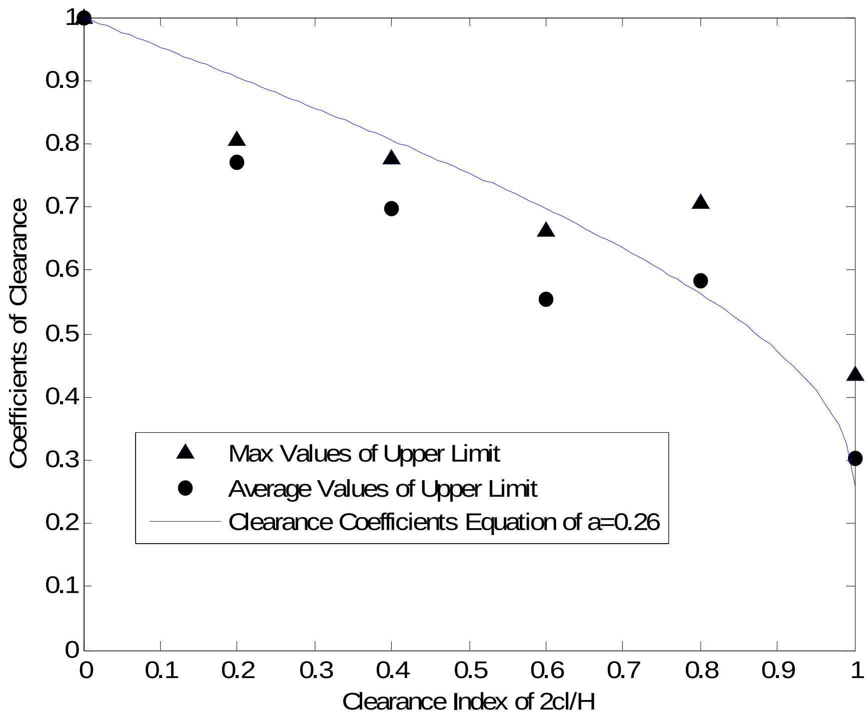

Figure 3.29 Flow3D model maximum uplift wave forces and water clearance coefficients equations and estimate equations

3.6.3.7 Water clearance application in the 2D Model results

When applying the clearance coefficient from equation 3.33 and 3.34, in which $a = \frac{\text{girder section area}}{\text{deck section area}} = 0.273$, the results from Table 3.3 will be modified as shown in Table 3.4:

Table 3.4: Maximum uplift wave force modified by clearance coefficient

T (s)	H_s (m)	$H_{1/250}$ (m)	$F_{1/250}$ (N)	
			$clearance = 0$	$clearance = 0.06$
1.00	0.10	0.18	34.24	19.84
1.25	0.10	0.18	40.03	23.20
1.50	0.10	0.18	43.56	25.25
1.75	0.10	0.18	45.39	26.31
2.00	0.10	0.18	46.24	26.80
2.25	0.10	0.18	46.53	26.97
2.50	0.10	0.18	46.57	26.99
1.20	0.14	0.25	49.78	34.70
1.25	0.14	0.25	51.13	35.64
1.50	0.14	0.25	56.04	39.06
1.75	0.14	0.25	58.58	40.83
2.00	0.14	0.25	59.76	41.65
2.25	0.14	0.25	60.16	41.93
2.50	0.14	0.25	60.22	41.97
2.75	0.14	0.25	60.09	41.88
3.00	0.14	0.25	59.84	41.71
1.25	0.18	0.32	62.23	47.38
1.50	0.18	0.32	68.52	52.17
1.75	0.18	0.32	71.77	54.64
2.00	0.18	0.32	73.28	55.79
2.25	0.18	0.32	73.79	56.18
2.50	0.18	0.32	73.86	56.24
2.75	0.18	0.32	73.70	56.11
3.00	0.18	0.32	73.39	55.87
1.50	0.22	0.40	82.78	66.84
1.75	0.22	0.40	86.84	70.12
2.00	0.22	0.40	88.73	71.65
2.25	0.22	0.40	89.37	72.17
2.50	0.22	0.40	89.46	72.24

In Table 3.4, $F_{1/250}$ for clearance of 0.06m will be compared with the Tirindelli's laboratory data of Figure 3.16 and the comparison is plotted in Figure 3.30:

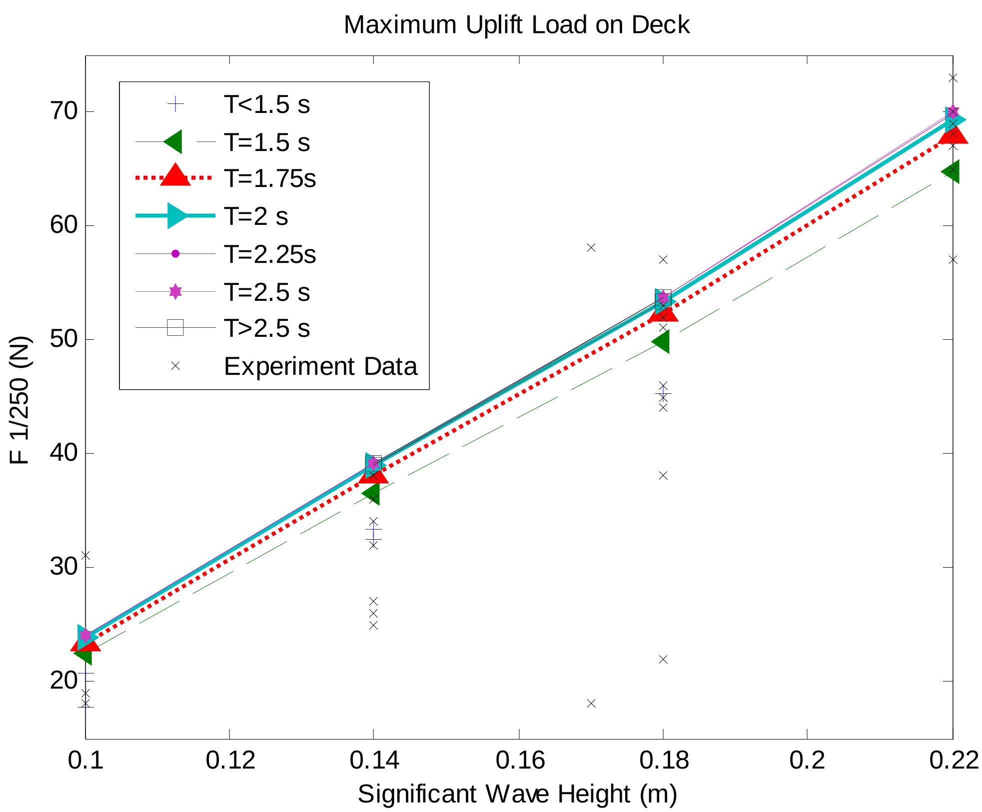

Figure 3.30: Comparison of results from 2D Model and laboratory data from Tirindelli's experiment for the deck

The 2D Model numerical simulation results well coincides with Tirindelli's laboratory data in Figure 3.16, and this proves the assumption and applicability of 2D wave velocity potential model. According to Tirindelli's results in Figure 3.16, the present results perform better than Kaplan's prediction.

3.7 Conclusion

Flow3D is popular in many areas for computational fluid dynamic simulation. But for hydraulic wave problem, its boundary condition definition still needs improvement. However, its solution can still provide reference for further analysis. To avoid its shortcoming at boundary conditions, simulation results should be taken just for the first few periods in case that the improperly reflected waves affect the calculation results. The comparison in Figure 3.12 and 3.13 shows that the results from the two models coincide with each other. Even being applied on nonlinear problems, the wave potential model can also make a good calculation under the linear wave theory assumption.

Tirindelli (2002) made a study on other empirical equations and those equations' applicability. His research is based on laboratory experiment in a flume tank using random incoming waves. The wave potential model's results coincide with his laboratory data. This can prove the validation of the model and the clearance coefficient assumption.

Horizontal wave forces on the model plate can also be obtained by integrating hydraulic pressure around vertical surface. However, the model is such a thin plate that the hydraulic pressure around the edge may change rapidly. For this case, the calculation results may have much error as well as Tirindelli's measurement and the comparison is omitted.

CHAPTER IV

CASE STUDY: EXTREME WAVE LOADS ON I-10 BRIDGE ACROSS ESCAMBIA BAY DURING HURRICANE IVAN

4.1 Introduction

In this chapter, the 2D wave velocity potential model is applied in wave force calculation on the I-10 Bridge across the Escambia Bay near Pensacola, Florida, which was destroyed during Hurricane Ivan in September, 2004. Figure 4.1 shows the tracking route and strength of Hurricane Ivan in Sep, 2004.

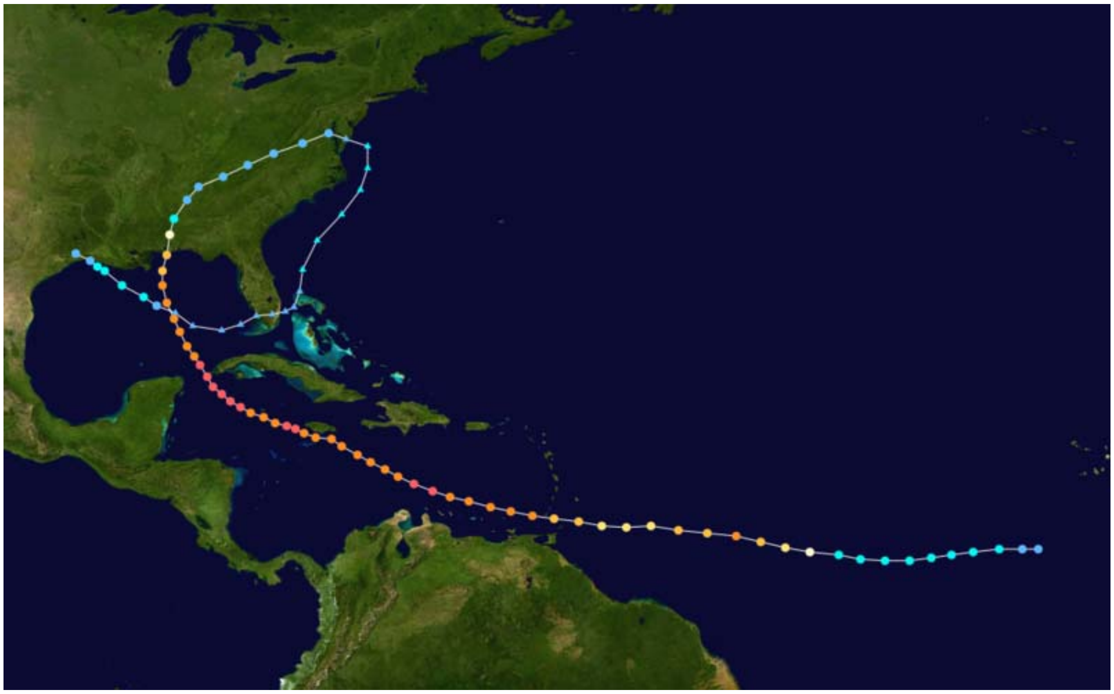

Figure 4.1: Hurricane Ivan Track (The background image is from NASA, tracking data is from the National Hurricane Center)

Sheppard and Renna (2004) point out that because Hurricane Ivan's track is perpendicular to the coast and immediately west of Pensacola, the strongest winds, storm surge, and waves drive the storms surge and waves directly into Escambia Bay. There is an approximate water depth of 25ft, wind speed of 145 mph, wave height of 13ft, and wave period of 6.5sec. The maximum uplift force is estimated to be 900,000 lb per span with weight of span being only 220,000 lb. Because of that, 58 spans of the eastbound and westbound bridges are knocked off piers and another 66 spans are misaligned as shown in Figure 4.2.

Figure 4.2: I-10 Bridge destroyed by Hurricane Ivan across Escambia Bay in Sep, 2004

In Sheppard's report, there is no mention about how he makes the calculation. Before applying 2D wave potential model in calculating maximum uplift wave forces on the I-10 Bridge, the next step is acquiring wave parameters around the bridge's location at the time the hurricane made landfall. SWAN model is used to hindcast wave parameters around Escambia Bay in Sep, 2004.

4.2 SWAN Model and Wave Parameters Hindcasting

4.2.1 Introduction

The SWAN model is used to estimate the realistic wave parameters, given the wind and bottom condition in coastal or lake areas. It is impossible to inspect the wave parameters in a specific location and in a certain time period. But the wind and bottom parameters are available all the time. In such a case, SWAN is a suitable and good model based on the wave action balance equation considering sources and sinks.

The SWAN model was developed by Delft University of Technology in the Netherlands as a third generation numerical model for computing spectral wave energy within the near shore environment. SWAN can be applied to: near shore wave modeling for harbor and offshore installation design; coastal development, management, and wave hindcasting. Li et al. (2005) has setup an online coastal wave prediction system using the SWAN model. Panchang et al. (1990) and Panchang et al. (2008) also applied the SWAN model in coastal wave climatology analysis.

In this study, SWAN model will be used to determine the wave parameters during a hurricane considering the following physics: refraction due to bottom, shoaling, blocking and reflections, wave generation by wind, depth induced wave breaking, bottom friction and non-linear wave-wave interactions. However, SWAN also has many limitations. It does not calculate wave-induced currents, and the simulation of standing-wave patterns may lead to inaccurate results. The calculation approximation for triad wave-wave interactions and quadruplet wave-wave interactions all depend on the frequency resolution. All more details can be found in the SWAN user manual.

4.2.2 Governing Equations

In SWAN the waves are described with the two-dimensional wave action density spectrum, even when nonlinear phenomena dominate. The rationale for using the spectrum in such highly nonlinear conditions is that, even in such conditions it seems possible to predict with reasonable accuracy this spectral distribution of the second order moment of the waves (although it may not be sufficient to fully describe the waves statistically). The spectrum that is considered in SWAN is the action density spectrum $N(\sigma,\theta)$ rather than the energy density spectrum $E(\sigma,\theta)$ since in the presence of currents, action density is conserved whereas energy density is not. The independent variables are the relative frequency σ (as observed in a frame of reference moving with current velocity) and the wave direction θ (the direction normal to the wave crest of each spectral component). The action density is equal to the energy density divided by the relative frequency: $N(\sigma,\theta) = E(\sigma,\theta)/\sigma$. In SWAN this spectrum may vary with time and space.

The governing equation in SWAN is the spectral action balance equation which describes the evolution of the wave spectrum in terms of Cartesian co-ordinates.

$$\frac{\partial}{\partial t}N + \frac{\partial}{\partial x}C_x N + \frac{\partial}{\partial y}C_y N + \frac{\partial}{\partial \sigma}C_\sigma N + \frac{\partial}{\partial \theta}C_\theta N = \frac{S}{\sigma} \tag{4.1}$$

In the Action balance equation, the first term in the left-hand side of this equation represents the local rate of change of action density in time, the second and third term represent propagation of action in geographical space (with propagation velocities C_x and C_y in x and y space, respectively). The fourth term represents shifting of the relative frequency due to variations in depths and currents (with propagation velocity C_σ in σ space). The fifth term represents depth-induced and current-induced refraction (with propagation velocity C_θ in θ space). More details are given in the SWAN user manual.

4.2.3 Application Procedure

4.2.3.1 Choose the general domain

The source data is from NOAA (National Oceanic & Atmosphere Administration). NOAA is a scientific agency within the United States Department of Commerce focused on the conditions of the oceans and the atmosphere. NOAA warns of dangerous weather, charts seas and skies, guides the use and protection of ocean and coastal resources, and conducts research to improve understanding and stewardship of the environment. From NOAA data base, (ftp://polar.ncep.noaa.gov/pub/history/waves/), there are three general domains as shown in Table 4.1

Table 4.1: NOAA general domains description

nww3	global 1x1.25 degree model
Akw	Alaskan Waters 0.25x0.5 degree mode
Wna	Western North Atlantic 0.25 degree model

For each domain, the data base includes the historic wave and wind parameters from 2003, such as wind speed U and V components, significant wave height, peak wave period and peak wave direction.

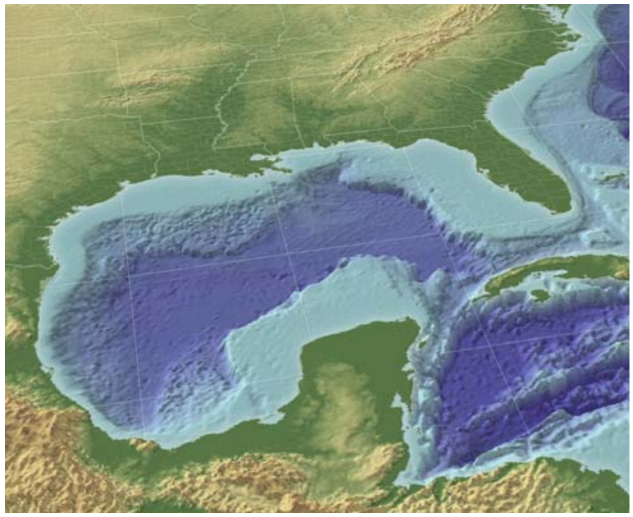

Figure 4.3: A 3D bottom map of Gulf of Mexico from

(http://commons.wikimedia.org/wiki/Image:GulfofMexico3D.png)

Escambia Bay is within the Gulf of Mexico, shown in Figure 4.3, which is located in the general domain of Western North Atlantic (wna). The size of wna domain from NOAA is listed in Table 4.2:

Table 4.2: WNA domain size description

WNA domain	From	To
Longitude:	98.25 West	29.75 West
Latitude:	0.25 South	50.25 North

4.2.3.2 Intermediate domain

The general domain of Western North Atlantic is too large for the hindcasting calculation of Escambia Bay. An intermediate domain should be generated which is large enough to consider all the complicated land geometry around the site of interest. All the information such as bottom depth, wind speed, direction, and et al. are generated based on parameter data in the general domain. However, due to the computation limitation, the size of intermediate domain cannot be too large. As a result, the intermediate domain is defined in Table 4.3:

Table 4.3: Intermediate domain size description

Intermediate Domain	From	To
Longitude:	94.00 West	81.00 West
Latitude:	26.00 North	31.00 North

4.2.3.3 Sub-domain

Locate the sub-domain around Escambia Bay. The sub-domain is the domain around the concerned area. One intermediate domain can have several sub-domains that are of interest. In this study, only one sub-domain is considered as listed in Table 4.4:

Table 4.4: Sub domain size description

Sub Domain	From	To
Longitude:	87.50 West	86.50 West
Latitude:	30.00 North	30.75 North

The intermediate domain and the sub domain are shown in Figure 4.4, in which the color contour is defined as bottom depth. The blue line in Escambia Bay represents the location of I-10Bridge.

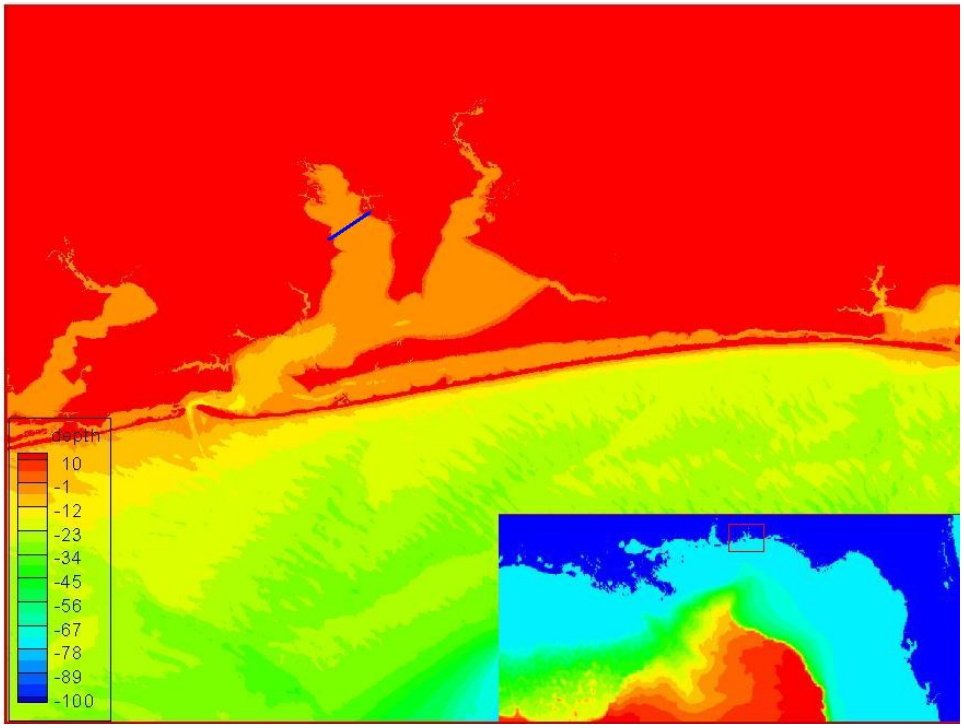

Figure 4.4: Intermediate domain and sub domain, the color contour is defined as water depth

The Grid Database option is the US Coastal Relief Model Grids and the Grid Cell Size is 2 minutes for intermediate domain and 15 seconds for sub-domain of Escambia Bay. As a result, grids of 391×151 for intermediate domain and 241×181 for sub-domain are generated. The value for each grid node stands for water depth in metric units.

4.2.3.4 Running the wave parameters hindcasting code for Escambia Bay

The hindcasting code mainly includes the following steps:

Step 1: Prepare the input files of the SWAN model. The downloaded data from NOAA site of wind speed, significant wave height, peak wave period and direction, is coded in **.grb* format. It needs to be unpacked and transformed to **.DAT* format for further application.

Step2: Generate a boundary condition file for intermediate domain.

Step3: Extract the data from the prepared data file exactly according to the intermediate domain and define the grid size of output results.

Step4: Run the SWAN program. The output will be the wind speed, significant wave height, peak wave period and direction according to the grid size determined by step 2 for intermediate domain. Also, another boundary condition file for sub-domain is generated.

Step5: Repeat the step 3 and 4 for sub-domain, and output the results of wind speed, significant wave height, peak wave period and direction for sub-domain.

4.2.3.5 Locate the I-10 Bridge in the local domain

Longitude: $87^{\circ}09'42.67''W$ to $87^{\circ}07'45.02''W$

Latitude: $30^{\circ}30'24.60''N$ to $30^{\circ}31'48.40''N$

Extract the results of wave parameters around the I-10 Bridge.

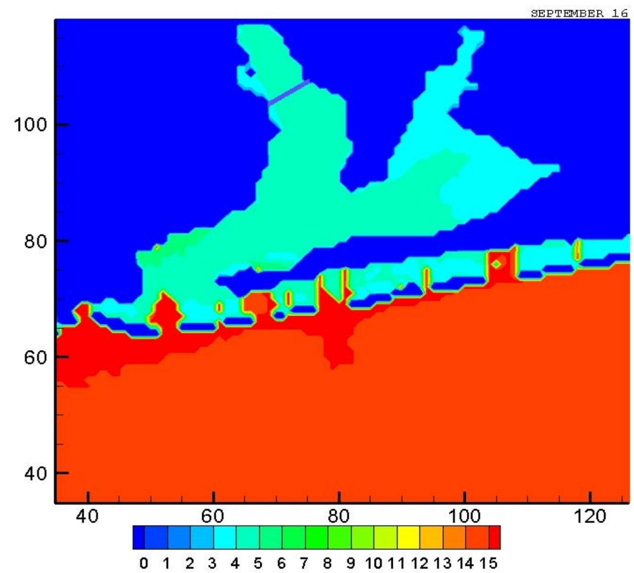

Figure 4.5: Significant wave heights on Sep 16th, 2004; the color contour is defined for significant wave heights in metric units

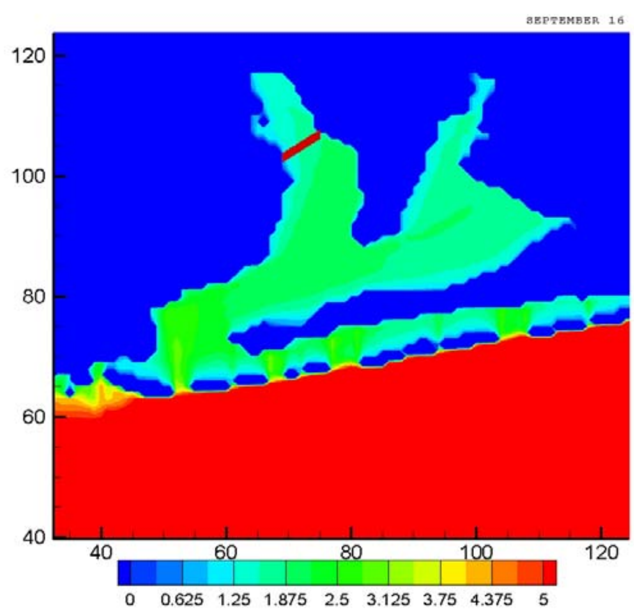

Figure 4.6: Wave period on Sep 16th, 2004; the color contour is defined for wave periods in seconds

Figure 4.5 and 4.6 show the final results of significant wave height and peak wave period on Sep 16th, 2004. At the site of I-10 Bridge, which is marked as the blue line, the max significant wave height is 1.78 meters and the peak wave period is 4.45 seconds.

4.2.4 Validation of SWAN Model

There are no probes for detecting wave or wind parameters around the I-10 Bridge in Escambia Bay. The SWAN model results are validated by comparing the predicted results with observation by Buoy Station of 42039 (29.18 N 88.21 W) and 42040(28.79 N 86.02 W), which are shown in Figure 4.7. The hindcasting results match those of the observation from the Buoy station very well in Figure 4.8 and 4.9. The satisfactory agreement proves the applicability of SWAN model.

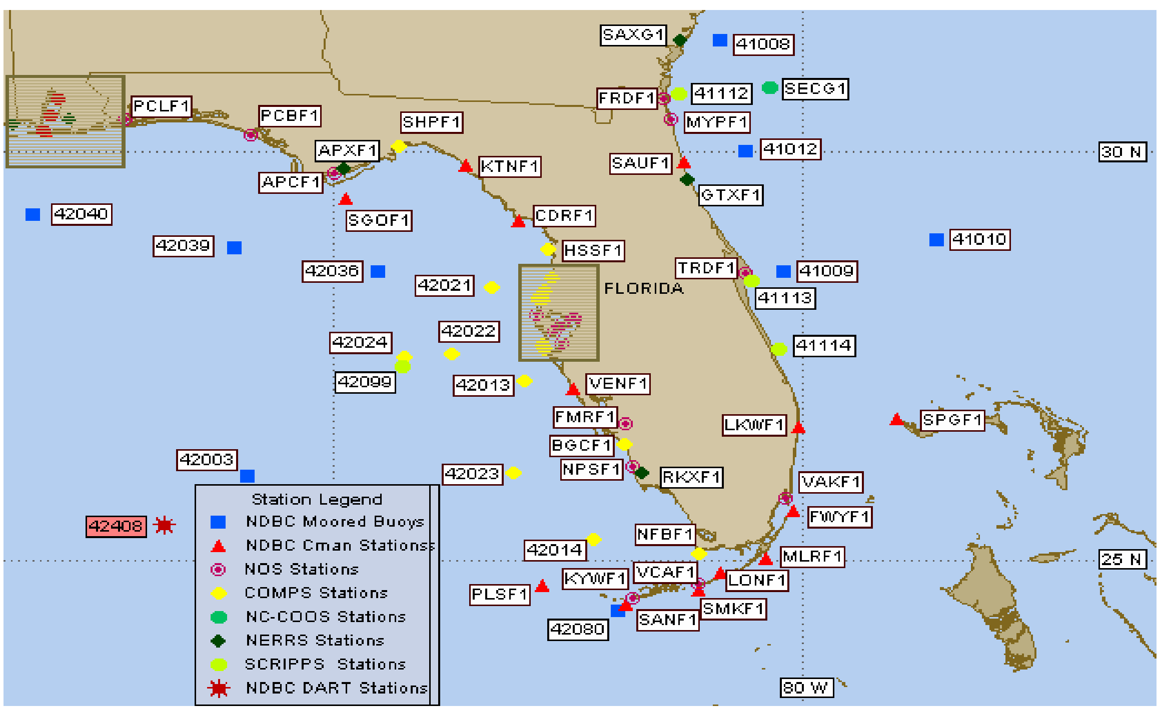

Figure 4.7: Buoy Stations 42039 and 42040 location map from NOAA

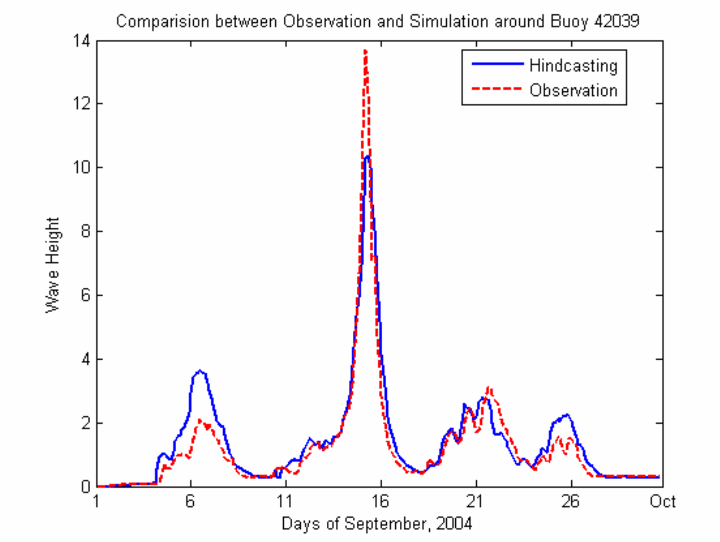

Figure 4.8: Comparison between observation and simulation results around Buoy Station 42039

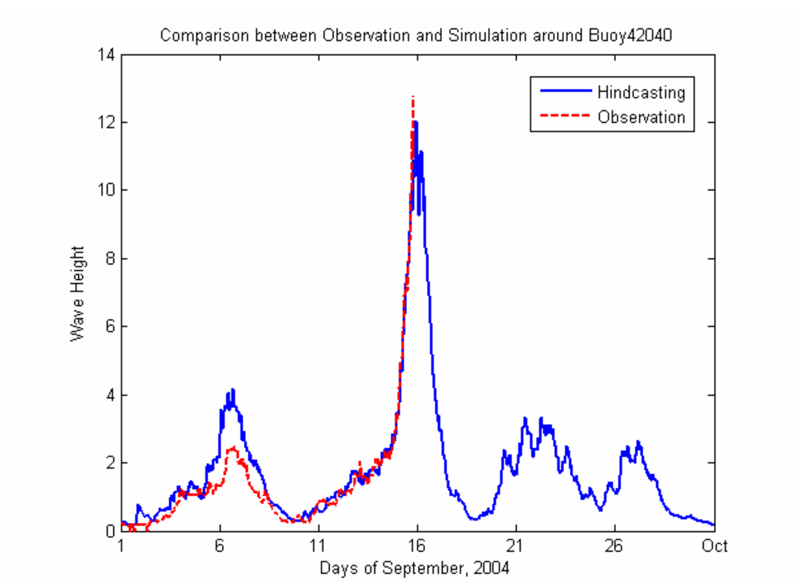

Figure 4.9: Comparison between observation and simulation results around Buoy Station 42040, the observation data is lost after destroyed by Hurricane Evan.

4.3 2D Model Calculation

4.3.1 Model Description

Figure 4.10 and Figure 4.11 are the 3D and 2D scheme of structural geometry and dimensions of I-10 Bridge over Escambia Bay. Along the *x* direction, the bridge deck plate is 9.4 meters wide with six girders evenly separated under the deck. Along the *z* direction in Figure 4.12, the bridge is 19.2 meters long. The superstructures, including bridge decks, fenders and girders, are placed and moderately fixed with bolts on the lower structures which are mainly composed with piles. And the lower structures are separated 19.2 meters with each other along the *z* direction.

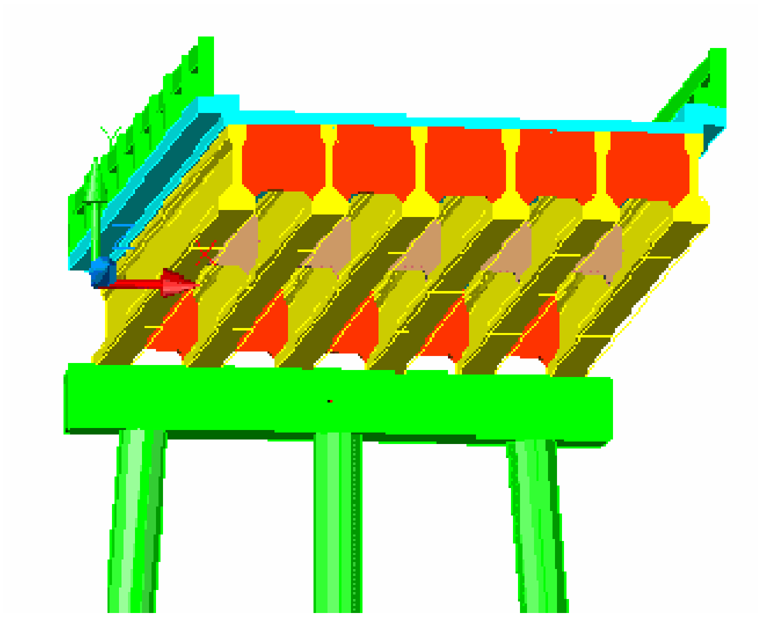

Figure 4.10: Structural geometry of I-10 Bridge over Escambia Bay

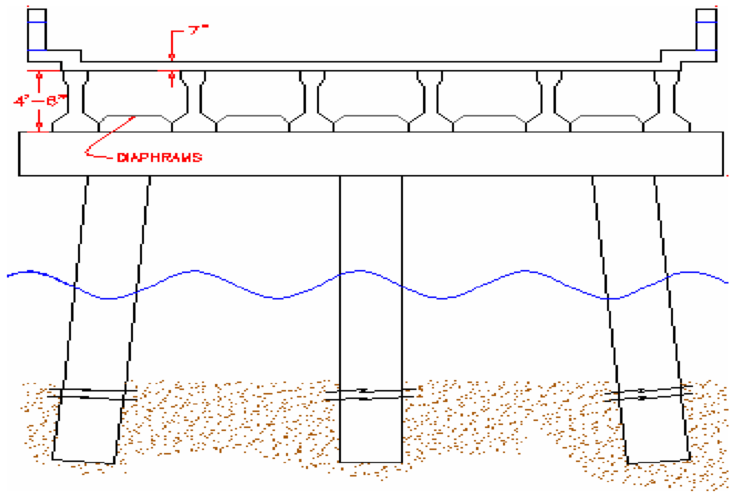

Figure 4.11: 2-D structural dimensions of I-10 Bridge over Escambia Bay

In the 2D Model with structural dimensions as shown in Figure 4.11, the lower structures and fenders are neglected. The lower structures are separated 19.2 meters away from each other and have very little effect on the maximum uplift wave forces on superstructures. The fenders are all above the still water level which is out of the calculation domain. Therefore, the structure model is simplified as shown in Figure 4.12.

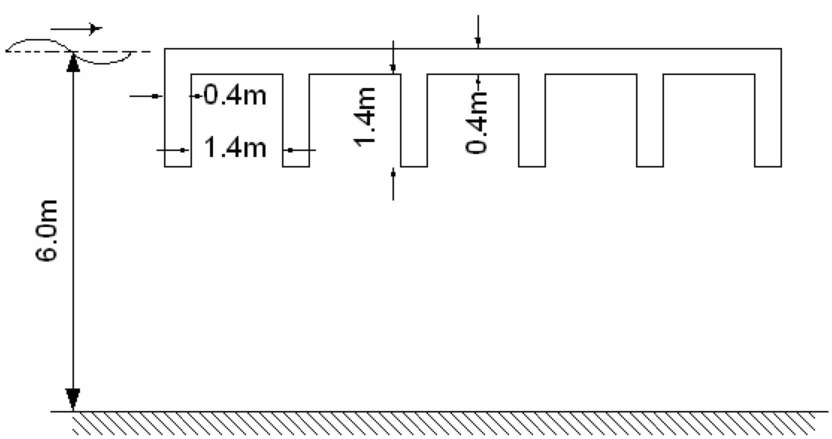

Figure 4.12: Geometry of the bridge deck and girders of reference model

In Figure 4.12, the bridge has one bridge deck of $9.4 \times 19.2 \times 0.4$ meters, and 6 bridge girders of $0.4 \times 19.2 \times 1.4$ meters supporting under the deck. The girders are separated evenly 1.4 meters away from each other along x direction. The water depth is 6.0 meters; the wave height is 1.78 meters and the wave period is 4.45 seconds. There is no water clearance in this case. The water clearance here means the distance between the still water level and the upper surface of the bridge deck.

The calculation domain is defined as 6×29.4 m, with 10 m distance between the incoming wave boundary and the left side of bridge, and 10 m distance between the outgoing wave boundary and the right side of bridge. The domain is meshed by 61×295 grids with grid size of $dx = dz = 0.1m$. The grids of calculation domain are shown by Figure 4.13.

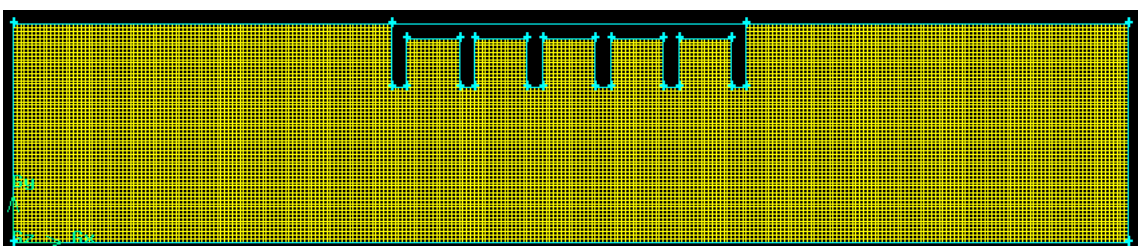

Figure 4.13: Calculation domain and meshing grids of 2D Model

The grids of the calculation domain will not be changed for different wave heights and wave periods. But they will be changed in accordance with changes of water depth and bridge geometry length which mainly means the width of the bridge deck. The calculation domain and grids will not be mentioned again in the following sections.

The general equation, incoming wave equation, outgoing wave boundary condition equation, bottom boundary condition equation, and free surface boundary condition equations are all the same as mentioned in Chapter III. For the wave-structure interaction boundary condition, all the surfaces of bridge in water, including the three surfaces of girders in water, should be included and specified.

4.3.2. Maximum Extreme Wave Force

The 2D Model is developed based on the wave velocity potential diffraction theory using finite difference method. Wave parameters, structure geometry dimensions and calculation domain grids are all inputs to the 2D Model. After the iteration mentioned in Chapter III with iteration error of 1×10^{-20}, the output results are the matrix of wave potential components ϕ_1 and ϕ_2 of every grid node for every time step. According to the pressure equation,

$$p = -\rho g z + \rho \frac{\partial \phi}{\partial t} = -\rho g z + (-\rho\sigma\phi_1)\sin\sigma t + (\rho\sigma\phi_2)\cos\sigma t \qquad (4.2)$$

The pressure for every grid node is determined for every time step. And the length of time step can be chosen according to the need for efficiency and accuracy.

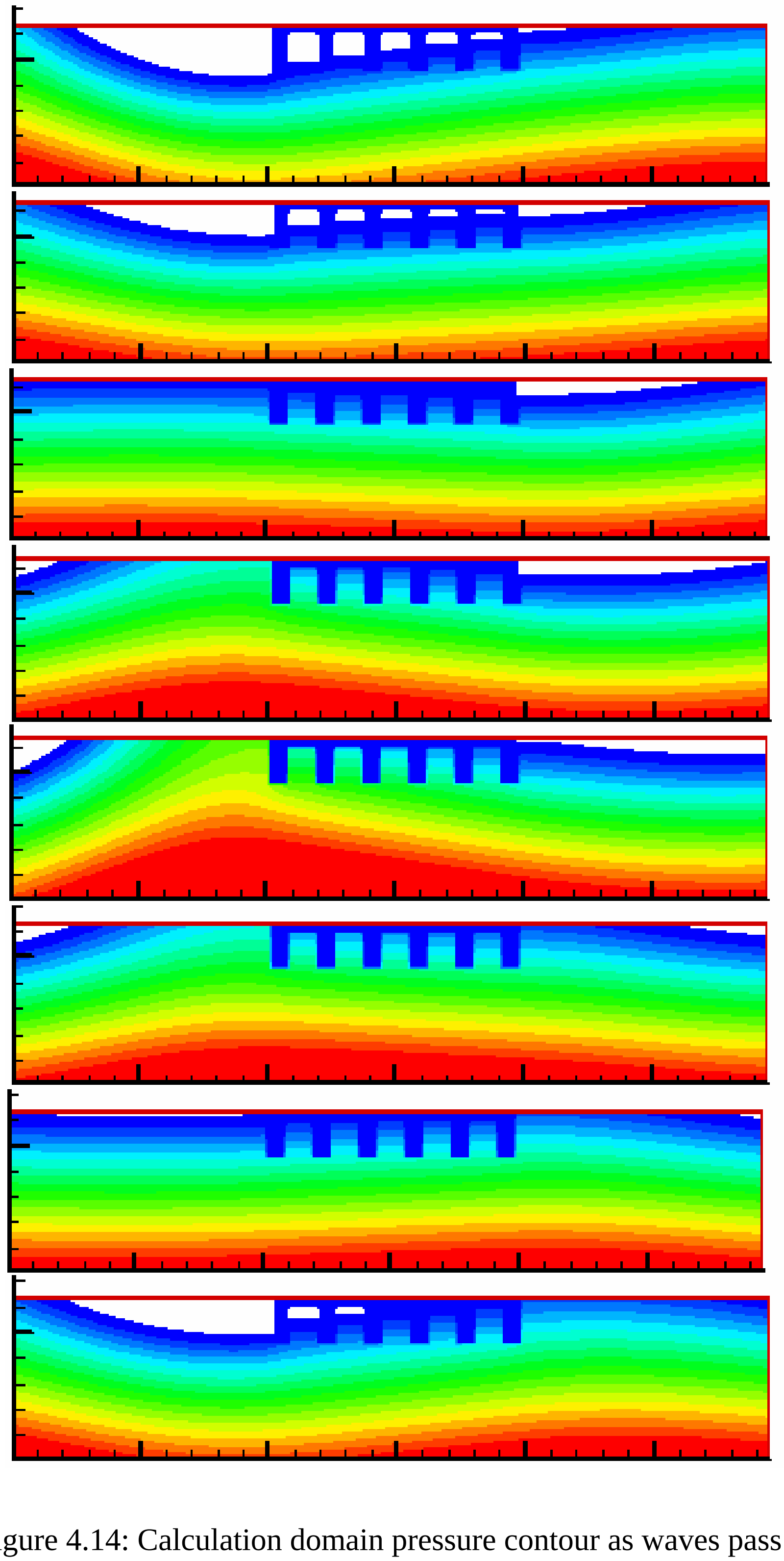

Figure 4.14: Calculation domain pressure contour as waves pass by

Figure 4.14 shows the pressure contour of the calculation domain at each time step. It shows that as a wave comes from left to right, the hydraulic pressure under the superstructure of bridge becomes greater when the crest arrives at the bridge. Not only the hydraulic pressure, but also the wave elevation, water particle velocity, direction and acceleration can be determined by the results of potential components ϕ_1 and ϕ_2.

By integrating the hydraulic pressure within the under surface of the superstructure, the overall uplift wave force of that time step is determined. By further integrated and multiplied by the distance of force, force moment can also be obtained. Take an example of the 2D model with wave height of 1.78 meters and wave period of 4.45 seconds. The uplift wave force is shown in Figure 4.15.

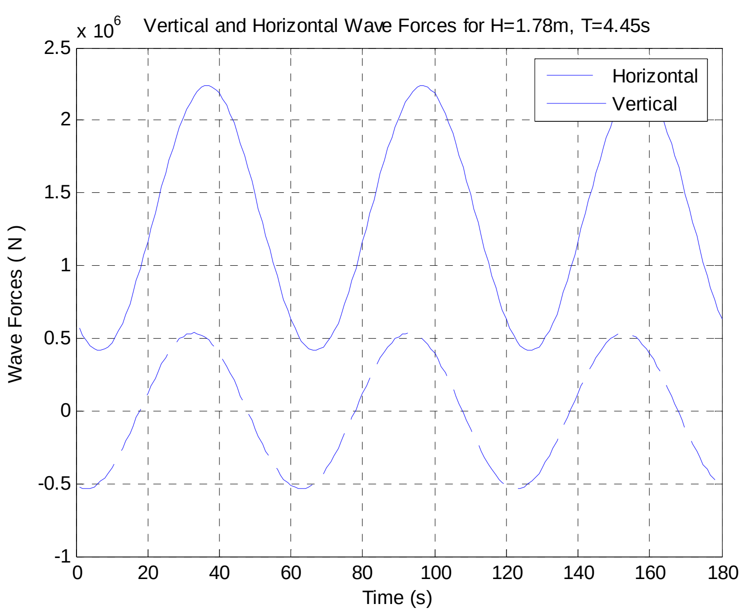

Figure 4.15: Wave force on bridge in reference model with H =1.78m, T=4.45s

Maximum uplift wave force is the max value of uplift wave force shown in Figure 4.15, which in the example case is $2.238\times10^{6}N$. Similarly, maximum horizontal wave force is $0.537\times10^{6}N$.

4.3.3 Random Maximum Wave Forces

The results show that, when a regular wave with 1.78m wave height and 4.45s wave period comes to the bridge which is 250ton weight, the maximum uplift wave force is $2.238\times10^{6}N$ and horizontal wave force is $0.537\times10^{6}N$. However, in reality we have to determine the random wave forces on bridge.

Similar to section 3.7.3, with statistic analysis, it is assumed that random wave heights obey Rayleigh distribution. Then, for random waves of $H_s = 1.78m$, $T_s = 4.45s$, the results will be

$$F_{1/3}^{V} = 2.238\times10^{6}N\,,\quad F_{1/3}^{H} = 0.537\times10^{6}N$$

$$F_{1/250}^{V} = 2.965\times10^{6}N\,, F_{1/250}^{H} = 0.96\times10^{6}N$$

where F^{V} means the vertical wave force and F^{H} means the horizontal wave force.

As a result, for one plate of 250ton weight, or $2.45\times10^{6}N$ gravity, the bridge decks can not withstand the wave force.

CHAPTER V

PARAMETRIC STUDY OF EXTREME WAVE FORCES

5.1 Introduction

The wave load on coastal bridges depends on the following major factors: wave parameters, water depth, geometry of bridge structure, water clearance, and green water downward force. It is time consuming to do the calculations for each case with different parameters. It is also very inconvenient for the bridge designer to estimate the wave loads on different bridges at different locations. In this chapter, parametric study is conducted for these different factors and an estimation equation is going to be proposed for wave loads on coastal highway bridges according to these factors.

The most critical design wave parameter is the wave height, because the wave energy is proportional to the square of wave height. Other wave parameters, such as wave period, wave direction and spectral shape are also design concerns. In this section, models are set up for different wave heights and wave periods. Because this is a 2D Model for regular waves, wave direction and spectral shape are omitted here.

Water depth is an important parameter which is critical to the basic assumption of different theories. It is affected by astronomical tides, storm surge and wave setup. All coastal bridges are located in intermediate water level, and water depth for different locations may not change a lot.

Geometry of the structure in 2D Model mainly refers to the width of bridge deck. A series of cases with bridge decks of different width are investigated.

Water clearance is very important to wave loads on coastal bridges. Wave surge caused by hurricane decreases the water clearance and makes bridge superstructure suffer rapidly increasing wave forces. Coefficients equation of water clearance is proposed and validated in Chapter III.

2D Model is not capable to calculate downward wave force for semi-submerged bridge superstructure. Flow3D models are developed to find out the solution.

5.2 Maximum Uplift Wave Forces According to Wave Parameters

5.2.1 Breaking Wave Height

Wave height and wave period are most important parameters to determine the wave form and wave mechanics. In this section, a group of wave heights and wave periods are going be chosen around the reference wave height of 2 meters and the reference wave period of 6 seconds. The maximum uplift wave forces are calculated according to wave heights of 0.1-4.6 meters and wave periods of 2.0-10.0 seconds.

However, wave height is limited by both water depth and wave period. For a given water depth and wave period, there is always an upper limit wave height, which is called breaking wave height. In deep water, this breaking wave height is a function of wave period; in transitional or shallow water, this breaking wave height is a function of water depth and wave period.

Early studies of breaking wave height were conducted on solitary waves using breaker depth index. McCowan (1891) determined the breaker depth index as $\gamma_b = 0.78$, which is still being used in industry area.

For monochromatic breaking wave height, Weggel (1972) derived the breaker depth index equations from laboratory experiment as follows:

$$\gamma_b = \frac{H_b}{d_b} \tag{5.1}$$

where γ_b = Breaking index

H_b = Breaking wave height

d_b = Water depth

$$\gamma_b = \frac{H_b}{d_b} = b - a\frac{H_b}{gT^2} \tag{5.2}$$

for $\tan\beta \leq 0.1$ and $H_0/L_0 \leq 0.06$

Where $$a = 43.8(1 - e^{-19\tan\beta}) \tag{5.3}$$

$$b = \frac{1.56}{(1 + e^{-19.5\tan\beta})} \tag{5.4}$$

$$\tan\beta \ = \text{slope of bottom} \tag{5.5}$$

Figure 5.1 shows the above equations.

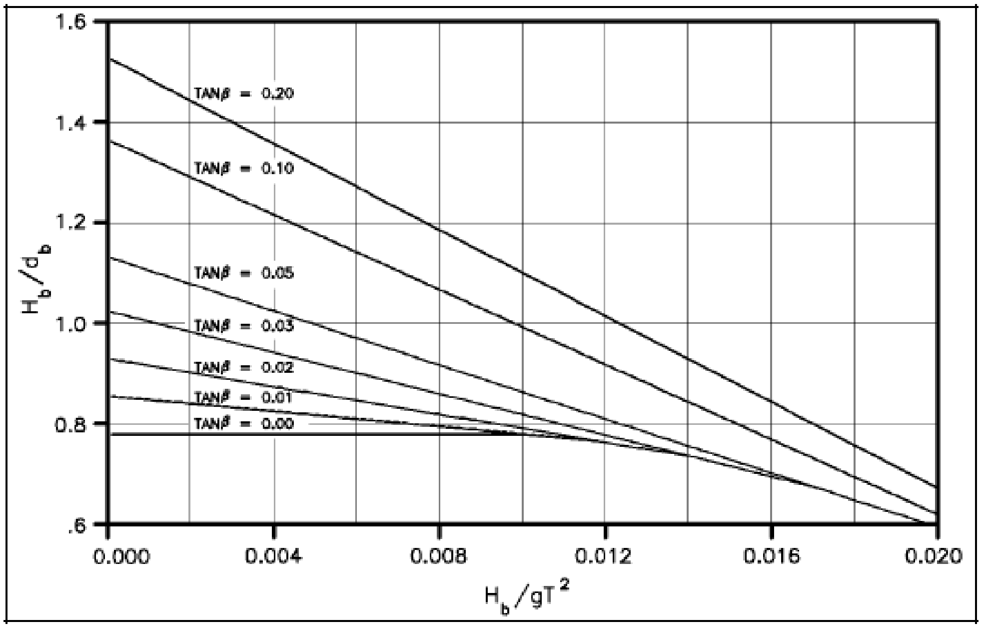

Figure 5.1: Breaker depth index (Weggel 1972)

In the reference model, the bottom slope $\tan\beta=0$, water depth=6m. Figure 5.2 shows the breaking wave height according to wave periods for water depth of 6m.

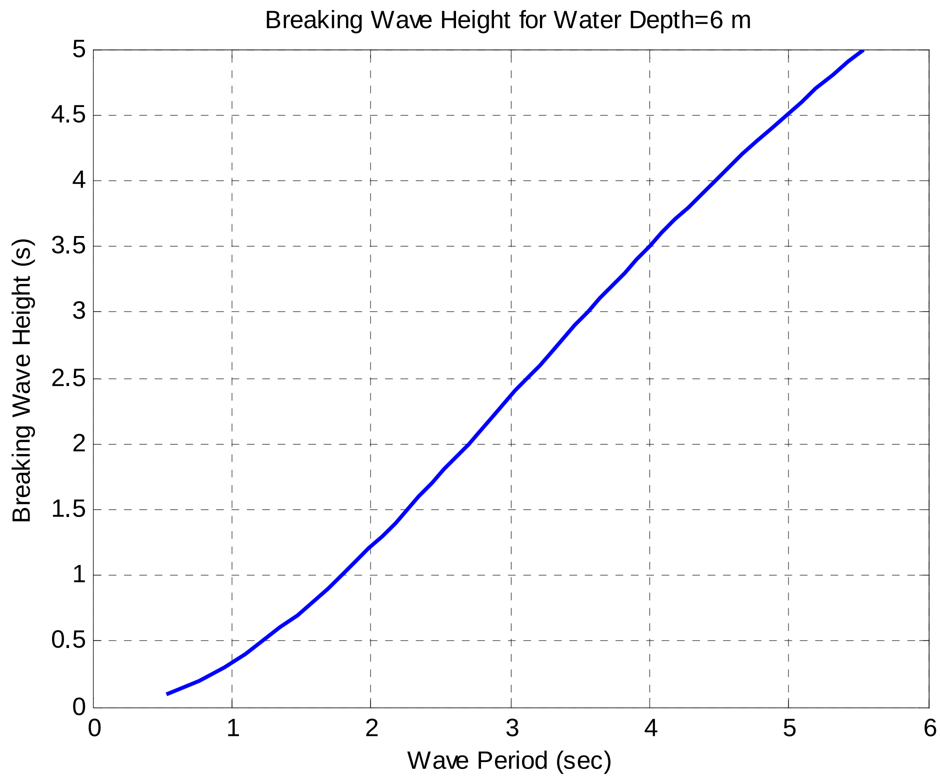

Figure 5.2: Breaking wave height according to wave periods for water depth of 6m

According to the breaking wave height limit from Figure 5.2, the wave parameters selected for calculation are wave heights 0.1-4.6 meters and wave periods 2-10 seconds, excluding those below the breaking wave curve in Figure 5.2.

5.2.2 Calculation Results According to Wave Heights and Wave Periods

The calculation results according to the wave parameters listed in 5.2.1 are given in the Table 5.1 – 5.4 for the reference model. The first column variables are the wave heights of 0.1-4.6 meters and the first row variables are the wave periods of 2.0-10.0 seconds. The content of the table is the maximum overall uplift wave forces in the situation of the different wave heights and wave periods.

Table 5.1: Maximum overall uplift forces (N) due to different wave heights (0.1-2.3m) and wave period (2-5s)

	2	2.2	2.4	2.6	2.8	3	3.2	3.4	3.6	3.8	4	4.2	4.4	4.6	4.8	5
0.1	1332200	1335300	1339000	1343000	1347200	1351500	1355700	1359900	1363800	1367500	1370900	1374000	1376900	1379400	1381700	1383900
0.2	1338100	1344300	1351700	1359700	1368000	1376600	1385100	1393400	1401300	1408700	1415500	1421700	1427500	1432600	1437200	1441500
0.3	x	1353300	1364300	1376300	1388900	1401800	1414500	1427000	1438800	1449900	1460000	1469400	1478000	1485700	1492600	1499000
0.4	x	1362300	1377000	1393000	1409700	1426900	1443900	1460500	1476300	1491100	1504600	1517100	1528600	1538800	1548000	1556600
0.5	x	1371300	1389700	1409700	1430600	1452000	1473300	1494100	1513800	1532300	1549200	1564800	1579200	1591900	1603400	1614200
0.6	x	x	1402300	1426400	1451400	1477200	1502700	1527600	1551300	1573500	1593700	1612500	1629700	1645100	1658900	1671800
0.7	x	x	1415000	1443000	1472300	1502300	1532100	1561200	1588800	1614800	1638300	1660300	1680300	1698200	1714300	1729300
0.8	x	x	1427700	1459700	1493100	1527500	1561500	1594800	1626300	1656000	1682900	1708000	1730900	1751300	1769700	1786900
0.9	x	x	x	1476400	1514000	1552600	1590900	1628300	1663800	1697200	1727400	1755700	1781400	1804400	1825100	1844500
1	x	x	x	1493100	1534900	1577800	1620300	1661900	1701300	1738400	1772000	1803400	1832000	1857600	1880600	1902100
1.1	x	x	x	1509700	1555700	1602900	1649700	1695400	1738800	1779600	1816600	1851100	1882600	1910700	1936000	1959600
1.2	x	x	x	x	1576600	1628100	1679100	1729000	1776300	1820800	1861100	1898800	1933100	1963800	1991400	2017200
1.3	x	x	x	x	1597400	1653200	1708500	1762500	1813800	1862000	1905700	1946500	1983700	2016900	2046800	2074800
1.4	x	x	x	x	1618300	1678400	1737900	1796100	1851300	1903200	1950300	1994200	2034300	2070000	2102300	2132400
1.5	x	x	x	x	1639100	1703500	1767300	1829600	1888800	1944400	1994900	2041900	2084900	2123200	2157700	2189900
1.6	x	x	x	x	x	1728700	1796700	1863200	1926300	1985600	2039400	2089600	2135400	2176300	2213100	2247500
1.7	x	x	x	x	x	1753800	1826100	1896800	1963800	2026800	2084000	2137300	2186000	2229400	2268500	2305100
1.8	x	x	x	x	x	1778900	1855500	1930300	2001300	2068000	2128600	2185000	2236600	2282500	2324000	2362700
1.9	x	x	x	x	x	x	1884900	1963900	2038800	2109200	2173100	2232700	2287100	2335700	2379400	2420200
2	x	x	x	x	x	x	1914300	1997400	2076300	2150400	2217700	2280400	2337700	2388800	2434800	2477800
2.1	x	x	x	x	x	x	1943600	2031000	2113800	2191600	2262300	2328100	2388300	2441900	2490200	2535400
2.2	x	x	x	x	x	x	x	2064500	2151300	2232800	2306800	2375800	2438800	2495000	2545700	2593000
2.3	x	x	x	x	x	x	x	2098100	2188800	2274000	2351400	2423500	2489400	2548200	2601100	2650500

Table 5.2: Maximum overall uplift forces (N) due to different wave heights (2.4-4.6m) and wave period (2-5s)

	2	2.2	2.4	2.6	2.8	3	3.2	3.4	3.6	3.8	4	4.2	4.4	4.6	4.8	5
2.4	x	x	x	x	x	x	x	2131600	2226300	2315200	2396000	2471200	2540000	2601300	2656500	2708100
2.5	x	x	x	x	x	x	x	2165200	2263800	2356500	2440500	2519000	2590500	2654400	2711900	2765700
2.6	x	x	x	x	x	x	x	x	2301300	2397700	2485100	2566700	2641100	2707500	2767400	2823300
2.7	x	x	x	x	x	x	x	x	2338800	2438900	2529700	2614400	2691700	2760700	2822800	2880800
2.8	x	x	x	x	x	x	x	x	2376300	2480100	2574300	2662100	2742200	2813800	2878200	2938400
2.9	x	x	x	x	x	x	x	x	x	2521300	2618800	2709800	2792800	2866900	2933600	2996000
3	x	x	x	x	x	x	x	x	x	2562500	2663400	2757500	2843400	2920000	2989100	3053600
3.1	x	x	x	x	x	x	x	x	x	2603700	2708000	2805200	2894000	2973200	3044500	3111100
3.2	x	x	x	x	x	x	x	x	x	2644900	2752500	2852900	2944500	3026300	3099900	3168700
3.3	x	x	x	x	x	x	x	x	x	x	2797100	2900600	2995100	3079400	3155300	3226300
3.4	x	x	x	x	x	x	x	x	x	x	2841700	2948300	3045700	3132500	3210800	3283800
3.5	x	x	x	x	x	x	x	x	x	x	2886200	2996000	3096200	3185600	3266200	3341400
3.6	x	x	x	x	x	x	x	x	x	x	x	3043700	3146800	3238800	3321600	3399000
3.7	x	x	x	x	x	x	x	x	x	x	x	3091400	3197400	3291900	3377100	3456600
3.8	x	x	x	x	x	x	x	x	x	x	x	3139100	3247900	3345000	3432500	3514100
3.9	x	x	x	x	x	x	x	x	x	x	x	3186800	3298500	3398100	3487900	3571700
4	x	x	x	x	x	x	x	x	x	x	x	x	3349100	3451300	3543300	3629300
4.1	x	x	x	x	x	x	x	x	x	x	x	x	3399600	3504400	3598800	3686900
4.2	x	x	x	x	x	x	x	x	x	x	x	x	3450200	3557500	3654200	3744400
4.3	x	x	x	x	x	x	x	x	x	x	x	x	3500800	3610600	3709600	3802000
4.4	x	x	x	x	x	x	x	x	x	x	x	x	x	3663800	3765000	3859600
4.5	x	x	x	x	x	x	x	x	x	x	x	x	x	3716900	3820500	3917200
4.6	x	x	x	x	x	x	x	x	x	x	x	x	x	3770000	3875900	3974700

Table 5.3: Maximum overall uplift forces (N) due to different wave heights (0.1-2.3m) and wave period (5-8.2s)

	5	5.2	5.4	5.6	5.8	6	6.2	6.4	6.6	6.8	7	7.2	7.4	7.6	7.8	8	8.2
0.1	1383900	1385800	1387600	1389300	1390700	1392100	1393400	1394400	1395600	1396500	1397400	1398200	1399000	1399800	1400400	1401000	1401600
0.2	1441500	1445300	1448900	1452200	1455200	1457800	1460400	1462500	1464800	1466600	1468600	1470200	1471700	1473200	1474500	1475700	1477000
0.3	1499000	1504800	1510200	1515200	1519600	1523500	1527500	1530700	1534100	1536700	1539700	1542100	1544400	1546700	1548600	1550400	1552300
0.4	1556600	1564300	1571500	1578200	1584000	1589300	1594500	1598800	1603300	1606900	1610800	1614100	1617000	1620100	1622700	1625000	1627600
0.5	1614200	1623800	1632800	1641100	1648500	1655000	1661600	1666900	1672600	1677000	1681900	1686000	1689700	1693600	1696800	1699700	1703000
0.6	1671800	1683300	1694100	1704100	1712900	1720700	1728600	1735000	1741800	1747200	1753000	1757900	1762400	1767100	1770900	1774400	1778300
0.7	1729300	1742800	1755400	1767000	1777300	1786500	1795700	1803100	1811100	1817300	1824200	1829900	1835100	1840500	1845000	1849100	1853600
0.8	1786900	1802300	1816700	1830000	1841800	1852200	1862700	1871200	1880300	1887500	1895300	1901800	1907800	1914000	1919100	1923800	1928900
0.9	1844500	1861800	1878000	1893000	1906200	1917900	1929800	1939300	1949600	1957600	1966400	1973700	1980500	1987400	1993100	1998500	2004300
1	1902100	1921300	1939400	1955900	1970600	1983700	1996800	2007400	2018800	2027800	2037500	2045700	2053100	2060900	2067200	2073100	2079600
1.1	1959600	1980800	2000700	2018900	2035100	2049400	2063900	2075600	2088100	2097900	2108700	2117600	2125800	2134300	2141300	2147800	2154900
1.2	2017200	2040300	2062000	2081800	2099500	2115100	2130900	2143700	2157300	2168000	2179800	2189500	2198500	2207800	2215400	2222500	2230200
1.3	2074800	2099800	2123300	2144800	2163900	2180900	2198000	2211800	2226600	2238200	2250900	2261500	2271200	2281300	2289500	2297200	2305600
1.4	2132400	2159300	2184600	2207800	2228400	2246600	2265000	2279900	2295800	2308300	2322000	2333400	2343900	2354700	2363600	2371900	2380900
1.5	2189900	2218800	2245900	2270700	2292800	2312400	2332100	2348000	2365100	2378500	2393200	2405300	2416600	2428200	2437700	2446600	2456200
1.6	2247500	2278300	2307200	2333700	2357200	2378100	2399100	2416100	2434300	2448600	2464300	2477300	2489200	2501600	2511800	2521200	2531500
1.7	2305100	2337800	2368500	2396600	2421700	2443800	2466200	2484200	2503600	2518800	2535400	2549200	2561900	2575100	2585900	2595900	2606900
1.8	2362700	2397300	2429800	2459600	2486100	2509600	2533200	2552300	2572800	2588900	2606500	2621100	2634600	2648500	2660000	2670600	2682200
1.9	2420200	2456800	2491100	2522600	2550500	2575300	2600300	2620500	2642100	2659100	2677600	2693100	2707300	2722000	2734100	2745300	2757500
2	2477800	2516300	2552400	2585500	2615000	2641000	2667300	2688600	2711300	2729200	2748800	2765000	2780000	2795500	2808200	2820000	2832900
2.1	2535400	2575800	2613700	2648500	2679400	2706800	2734400	2756700	2780600	2799300	2819900	2836900	2852700	2868900	2882300	2894600	2908200
2.2	2593000	2635300	2675000	2711500	2743800	2772500	2801400	2824800	2849900	2869500	2891000	2908900	2925300	2942400	2956400	2969300	2983500
2.3	2650500	2694800	2736300	2774400	2808300	2838200	2868500	2892900	2919100	2939600	2962100	2980800	2998000	3015800	3030400	3044000	3058800

Table 5.4: Maximum overall uplift forces (N) due to different wave heights (2.4-4.6m) and wave period (5-8.2s)

	5	5.2	5.4	5.6	5.8	6	6.2	6.4	6.6	6.8	7	7.2	7.4	7.6	7.8	8	8.2
2.4	2708100	2754300	2797600	2837400	2872700	2904000	2935500	2961000	2988400	3009800	3033300	3052700	3070700	3089300	3104500	3118700	3134200
2.5	2765700	2813800	2858900	2900300	2937100	2969700	3002600	3029100	3057600	3079900	3104400	3124700	3143400	3162700	3178600	3193400	3209500
2.6	2823300	2873300	2920200	2963300	3001600	3035500	3069600	3097200	3126900	3150100	3175500	3196600	3216100	3236200	3252700	3268100	3284800
2.7	2880800	2932800	2981500	3026300	3066000	3101200	3136700	3165400	3196100	3220200	3246600	3268500	3288800	3309700	3326800	3342700	3360100
2.8	2938400	2992300	3042800	3089200	3130400	3166900	3203700	3233500	3265400	3290300	3317700	3340500	3361400	3383100	3400900	3417400	3435500
2.9	2996000	3051800	3104100	3152200	3194900	3232700	3270700	3301600	3334600	3360500	3388900	3412400	3434100	3456600	3475000	3492100	3510800
3	3053600	3111300	3165400	3215100	3259300	3298400	3337800	3369700	3403900	3430600	3460000	3484300	3506800	3530000	3549100	3566800	3586100
3.1	3111100	3170800	3226700	3278100	3323700	3364100	3404800	3437800	3473100	3500800	3531100	3556300	3579500	3603500	3623200	3641500	3661500
3.2	3168700	3230300	3288000	3341100	3388200	3429900	3471900	3505900	3542400	3570900	3602200	3628200	3652200	3676900	3697300	3716200	3736800
3.3	3226300	3289800	3349300	3404000	3452600	3495600	3538900	3574000	3611600	3641100	3673400	3700200	3724900	3750400	3771400	3790800	3812100
3.4	3283800	3349300	3410600	3467000	3517000	3561300	3606000	3642200	3680900	3711200	3744500	3772100	3797500	3823800	3845500	3865500	3887400
3.5	3341400	3408800	3471900	3529900	3581500	3627100	3673000	3710300	3750100	3781400	3815600	3844000	3870200	3897300	3919600	3940200	3962800
3.6	3399000	3468300	3533200	3592900	3645900	3692800	3740100	3778400	3819400	3851500	3886700	3916000	3942900	3970800	3993700	4014900	4038100
3.7	3456600	3527800	3594500	3655900	3710300	3758600	3807100	3846500	3888600	3921600	3957800	3987900	4015600	4044200	4067700	4089600	4113400
3.8	3514100	3587300	3655900	3718800	3774800	3824300	3874200	3914600	3957900	3991800	4029000	4059800	4088300	4117700	4141800	4164200	4188700
3.9	3571700	3646800	3717200	3781800	3839200	3890000	3941200	3982700	4027100	4061900	4100100	4131800	4161000	4191100	4215900	4238900	4264100
4	3629300	3706300	3778500	3844700	3903600	3955800	4008300	4050800	4096400	4132100	4171200	4203700	4233600	4264600	4290000	4313600	4339400
4.1	3686900	3765800	3839800	3907700	3968100	4021500	4075300	4118900	4165600	4202200	4242300	4275600	4306300	4338000	4364100	4388300	4414700
4.2	3744400	3825300	3901100	3970700	4032500	4087200	4142400	4187100	4234900	4272400	4313500	4347600	4379000	4411500	4438200	4463000	4490100
4.3	3802000	3884800	3962400	4033600	4096900	4153000	4209400	4255200	4304100	4342500	4384600	4419500	4451700	4485000	4512300	4537700	4565400
4.4	3859600	3944300	4023700	4096600	4161400	4218700	4276500	4323300	4373400	4412700	4455700	4491400	4524400	4558400	4586400	4612300	4640700
4.5	3917200	4003800	4085000	4159500	4225800	4284400	4343500	4391400	4442600	4482800	4526800	4563400	4597100	4631900	4660500	4687000	4716000
4.6	3974700	4063300	4146300	4222500	4290200	4350200	4410600	4459500	4511900	4552900	4597900	4635300	4669700	4705300	4734600	4761700	4791400

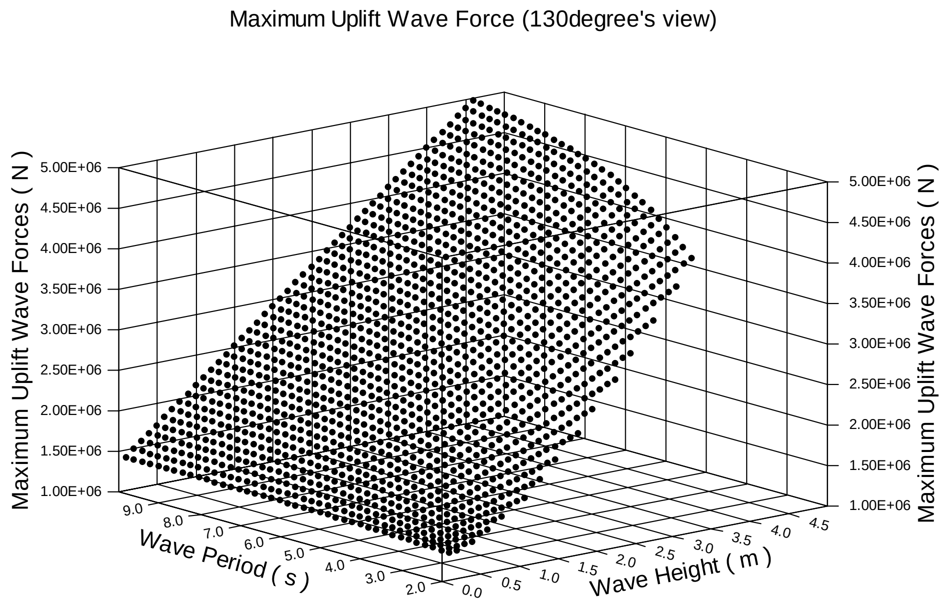

Figure 5.3: 3-D plot of maximum overall uplift wave force (210° degree direction)

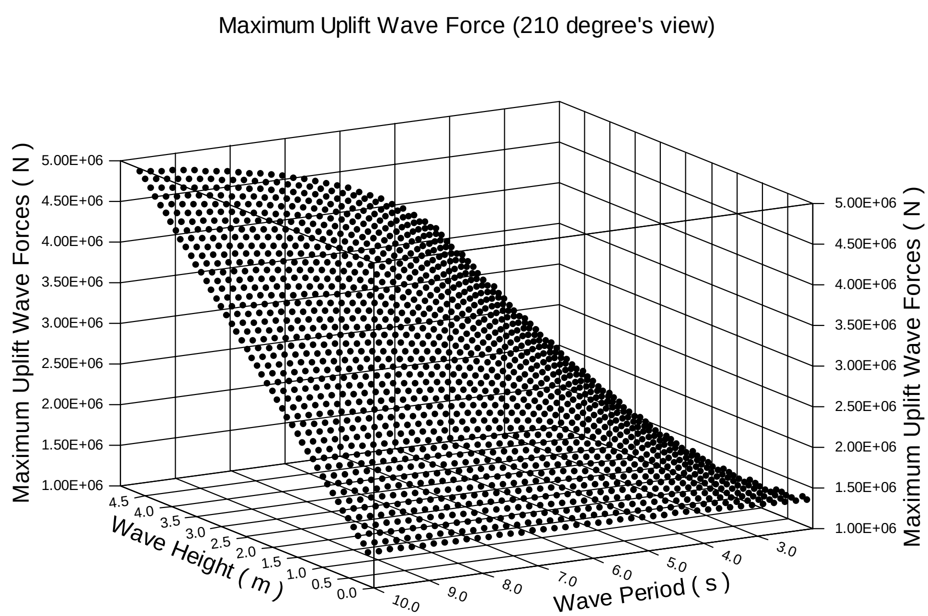

Figure 5.4: 3-D plot of maximum overall uplift wave force (30° degree direction)

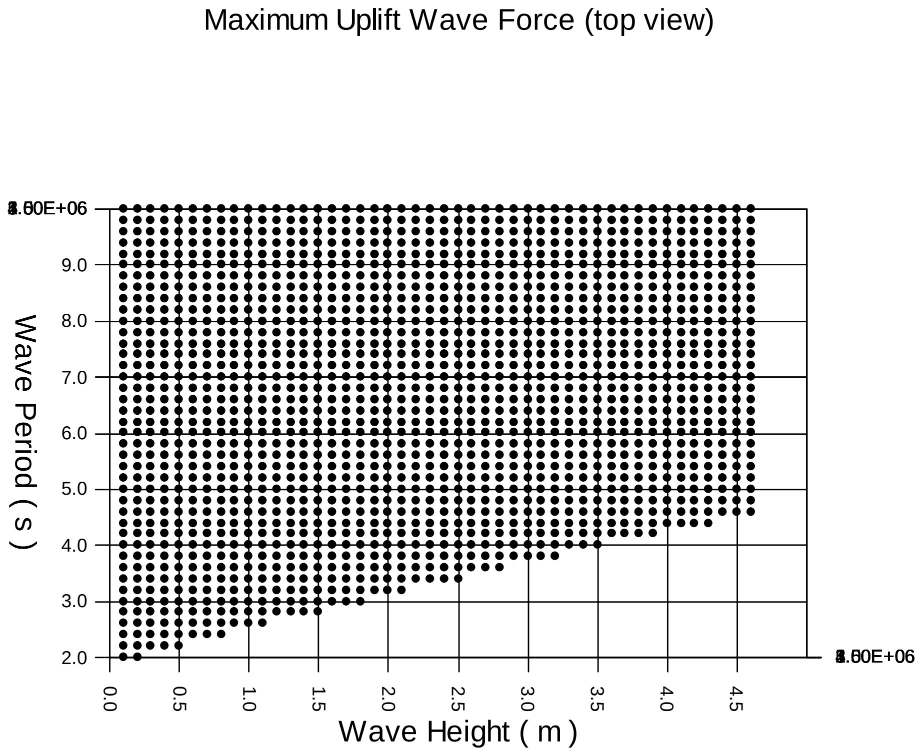

Figure 5.5: 3-D plot of maximum overall uplift wave force (top view)

The relationship of the maximum overall uplift forces with the wave periods and wave heights is plotted in Figure 5.3, 5.4 and Figure 5.5.

5.3 Calculation Results According to Water Clearance

According to section 3.7.3, a Flow3D model is set up with different water clearances. The results from the Flow3D model show the non-linear relationship between uplift wave load and water clearance. The coefficient of water clearance is given in Eq. 3.33

$$A_{cl} = 1 - \frac{2\arcsin\frac{2cl}{H}}{\pi}(1-a)$$

where $$a = \frac{\text{girder section area}}{\text{deck section area}}$$

5.4 Downward Wave Forces due to Green Water

As stated from the above conclusions, wave force induced by green water can cause severe damage to those structures which can be calculated by Morison's equation. Damage due to horizontal forces is much larger than that due to vertical forces. However, comparing with the uplift wave forces, the horizontal forces caused by waves or green water are relatively small. Although there is much overtopping wave on bridge decks, the horizontal wave force caused by it is not the main reason of destruction of bridges during hurricanes. Thus in this section, a model is going to be set up for investigating the downward wave force induced by overtopping waves and its relationship with wave heights.

To analyze the relationship between the downward wave force and wave heights, a set of model wave parameters is chosen in Table 5.5:

Table 5.5: Wave parameters for water depth=6m and no clearance

Wave Height (m)	Wave Period (s)
1	6
2	6
3	6
4	6
4.5	6

The simulation results are shown in Figure 5. 6-5.10

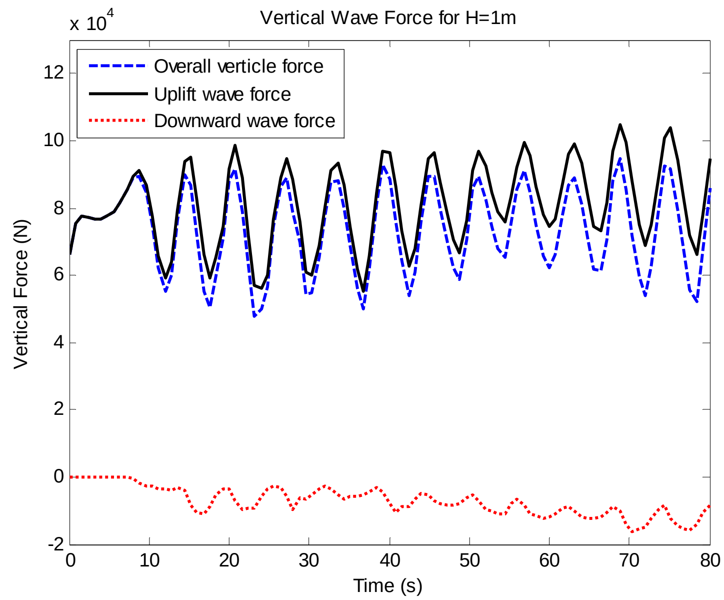

Figure 5.6: Vertical wave forces for H=1m

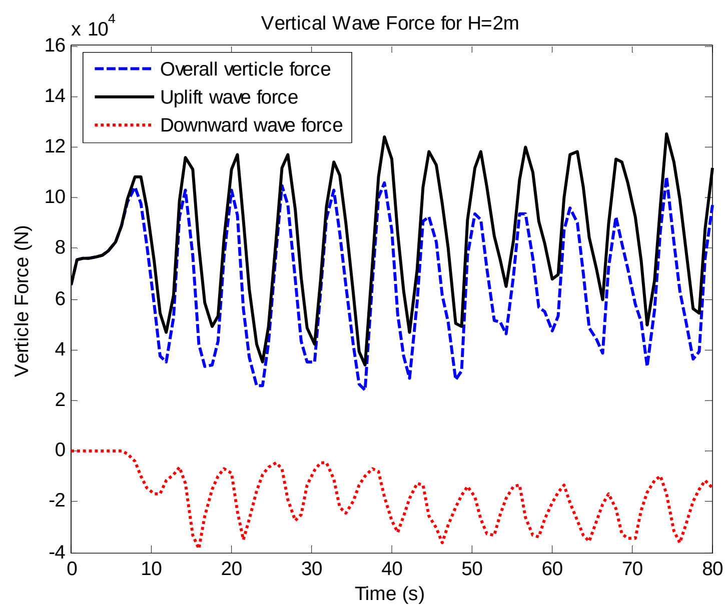

Figure 5.7: Vertical wave forces for H=2m

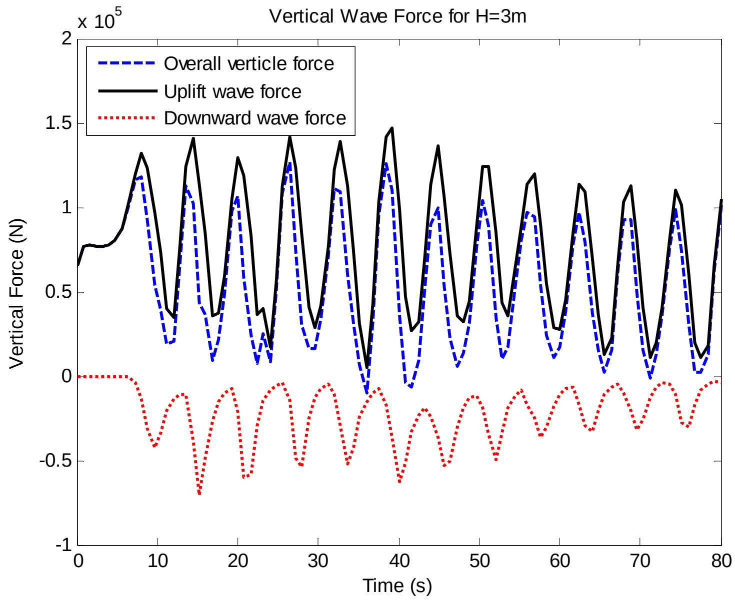

Figure 5.8: Vertical wave forces for H=3m

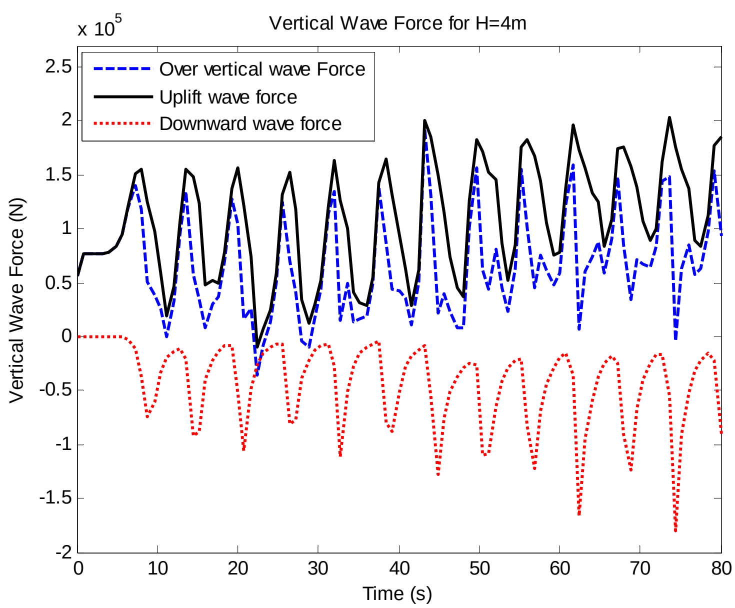

Figure 5.9: Vertical wave forces for H=4m

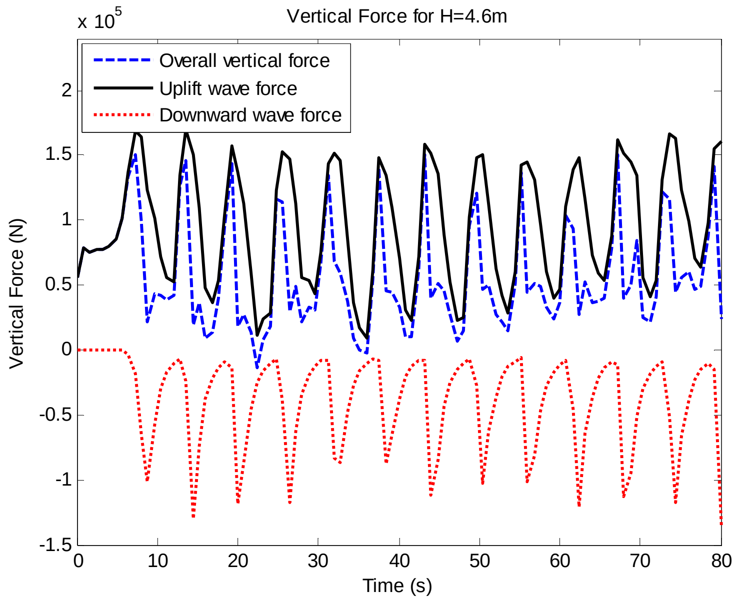

Figure 5.10: Vertical wave forces for H=4.6m

As wave heights increase, more waves can go over the bridge edge and cause more downward green water load. From Figure 5.6-5.10, it shows that:

- Green water loads on bridges increase as the wave heights increase from 1m to 4.6 m, which is shown in Figure 5.11. As wave heights increase much higher to 4.6 m, the green water load can account for over 35% of the uplift wave force, but it does not mean that the bridge is safer.

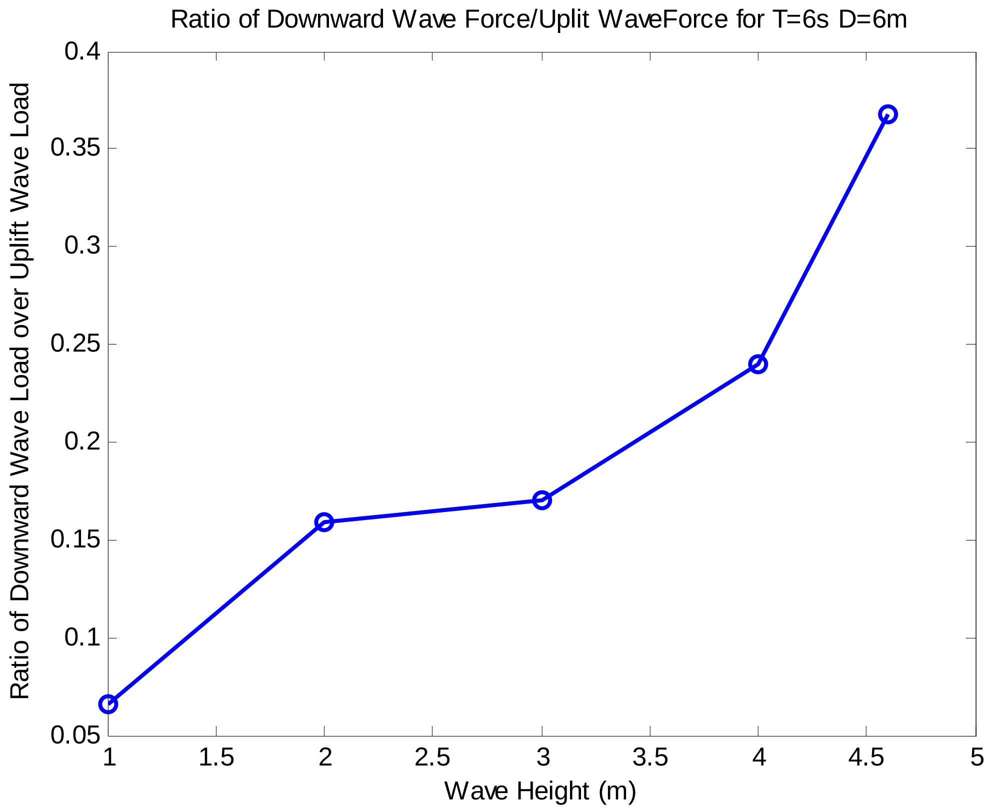

Figure 5.11: Green water load ratio to uplift wave force according to wave heights in the reference model of wave period 6s and water depth 6m.

- For small wave heights, like 1m and 2m, the green water does help to reduce the over vertical forces. For wave height of 1m, it is decreased by 7% and for 2 m, it is decreased by 15%.

- Although green water force is equal to a large fraction of the uplift wave force for large wave heights, which are from 3m to breaking wave height of 4.6m, there is always a little different phase between green water force and uplift wave force. Sometimes, the overtopping water load does help to reduce the uplift wave force; but some times it does not. Take Figure 5.10 for example, among the 11 periods of wave loads there are 4 periods in which the overall uplift wave force is almost the same as uplift wave force.

As a result, for designing of oversea bridges, it is a conservative way not to count in the green water load deduction for the overall vertical wave force.

5.5 Bridge Geometry Effects on Maximum Uplift Wave Force

For a given wave height, wave period and water depth, the maximum uplift wave force on bridge decks will also change due to the width of the bridge. To understand how the force changes with different bridge geometry length; a 2D Model is set up for given wave height of 2 meters, wave period of 6 seconds and water depth of 6 meters. The 6 girders supporting the deck have a width of 0.4 meters but they separate from each other a range of distances as listed in Figure 5.12 and Tables 5.6.

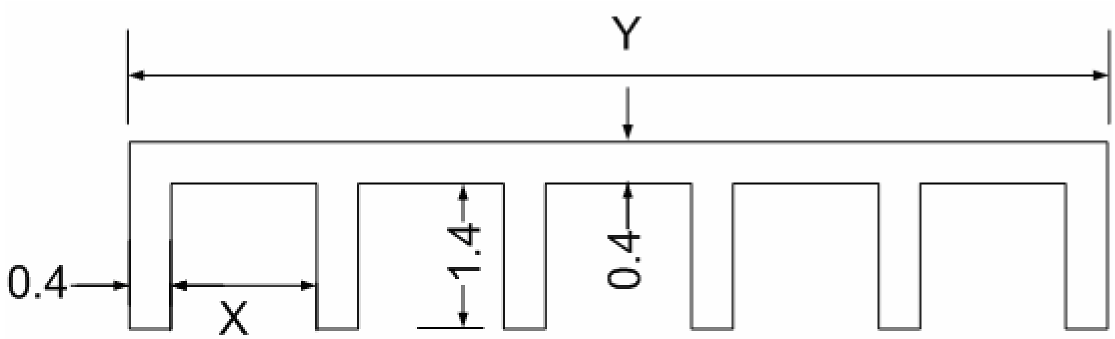

Figure 5.12: Structure component geometry in metric units, x is defined as the distance between the girders and y is defined as the overall width of the bridge deck cross section

Table 5.6: Wave parameters and model geometry lengths for water depth of 6 meters, * means parameters for the reference model

Wave Heights (m)	Wave Periods (s)	Distance between the six girders X (m)	Overall Bridge Cross Sections Width Y (m)
2	6	1.3	6.9
2	6	1.4	7.4
2	6	1.5	7.9
2	6	1.6	8.4
2	6	1.7	8.9
2*	6*	1.8*	9.4*
2	6	1.9	9.9
2	6	2	10.4
2	6	2.1	10.9
2	6	2.2	11.4
2	6	2.3	11.9

The final calculation results of maximum uplift wave forces according to the parameters in Table 5.6 are shown in Figure 5.13.

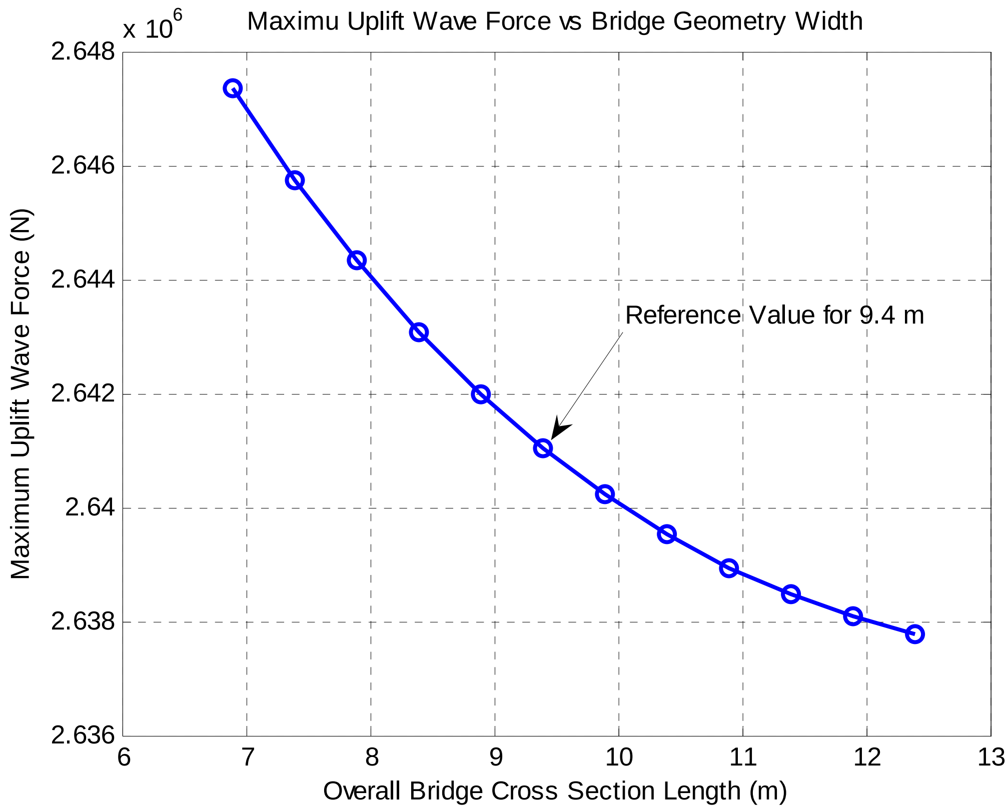

Figure 5.13: Maximum uplift wave forces according to bridge geometry width

As width of the bridge deck cross section increases, the maximum uplift wave force goes down. Maximum uplift force is the integration of wave hydraulic pressure under the bridge deck and girders. The hydraulic pressure changes with time and it could be large, small or even negative. The larger the width of bridge cross section is, the more chances the bridge deck has to have negative or smaller hydraulic pressure under it. This is the reason why the maximum uplift wave force decreases when the width of bridge deck increases.

The coefficient of bridge geometry A_l is defined as the ratio of maximum uplift wave force for deck width index of l/l^* , where l^* is the reference model bridge deck width. In this section for reference model, $l^* = 9.4\,\mathrm{m}$ is considered as the reference length. The coefficients are plotted in Figure 5.14.

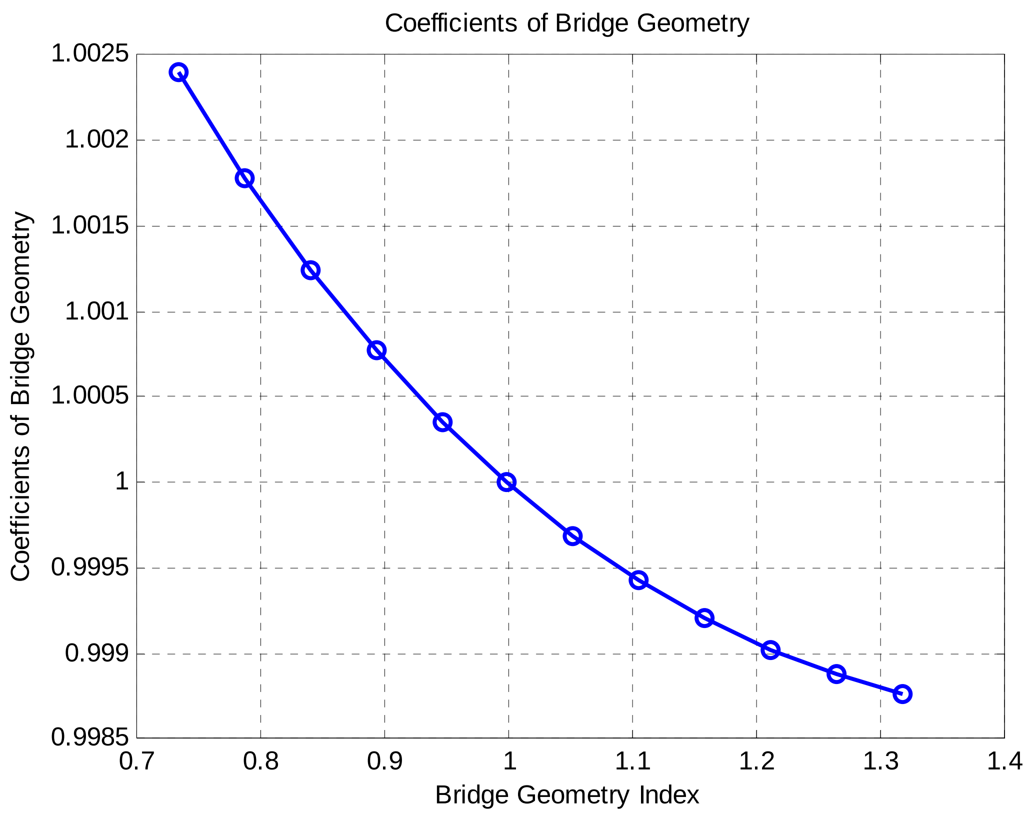

Figure 5.14: Coefficients of bridge geometry for reference model of water depth of 6m

The changes of A_l coefficients are very small due to the changes of geometry index from 0.7 to 1.4 and can be regarded that the bridge geometry length has no effects on the bridge deck maximum uplift wave forces. Comparing to the bridge width, the wave length for water depth of 6m and wave period of 6s are about 5 times larger. The changes of the bridge width in that range above can hardly reduce the force much.

5.6 Maximum Uplift Wave Forces due to Water Depth

Water depth is a very important parameter in transitional and shallow water. It determines not only wave forms, wave mechanics, breaking wave height, wave length, but also all the assumptions and the applicable wave theories. In this section, the objective is to find out how the maximum uplift wave forces change due to different water depth.

The 2D Model component is set up according to the reference model. The bridge deck is 9.4m wide, with six girders separated 1.4m from each other. The wave height and wave period is set to be 2m and 6s. Water depths are chosen from 5.4m to 8.2m.

Calculation results are plotted as Figure 5.15:

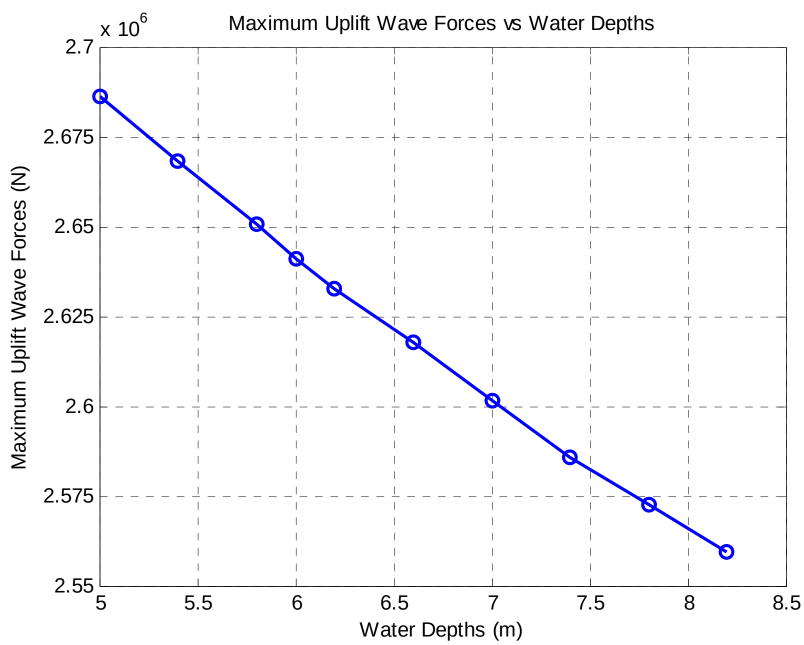

Figure 5.15: Maximum uplift wave forces according to water depth

The coefficient of water depth A_d is defined as the ratio of maximum uplift wave force for water depth index of $D/D*$, where $D*$ is the reference model bridge deck width. For the reference model, $D* = 6\,\text{m}$ is considered as the reference water depth. The coefficients are plotted in Figure 5.16.

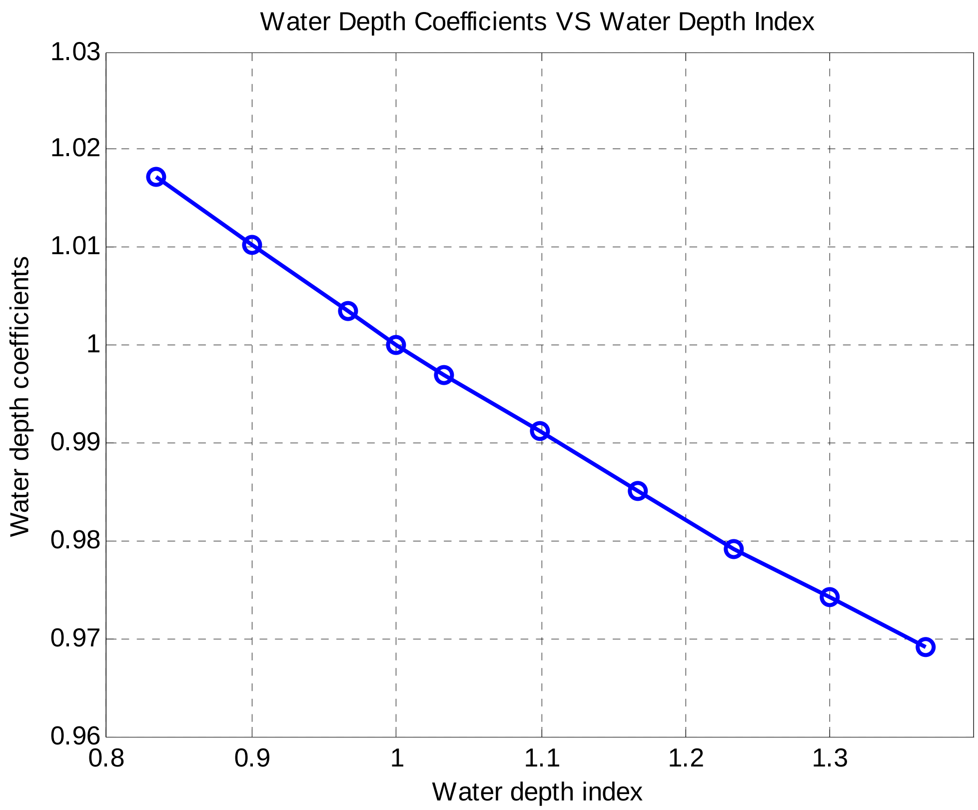

Figure 5.16: Coefficients of water depth for reference model of wave height 2m and wave period 6s

Water depth coefficient decreases 5% when water depth increases 30%. That proves the water depth does play a great role in uplift wave forces. The general relationship and equation between them will be found in the next section.

5.7 General Equations for Maximum Uplift Wave Force for Bridges over Sea

Many bridges along the coastal line have been damaged by waves induced by hurricane. Most of them are not designed to withstand the surge waves. More and more attention is paid on this problem nowadays. In this section, a general equation is going to be given according to the calculation results from the 2D Model to estimate the maximum uplift wave force on the bridge deck over the sea. In this equation, many aspects and parameters are considered, including wave heights, wave periods, water depth, water clearance and bridge deck geometry length.

All of the equations are given based on the reference model solutions from Table 5.1-5.4. All the conclusions and results comparison are from previous sections in this chapter.

5.7.1 Relation between Maximum Uplift Wave Forces and Wave Heights

In Table 5.1-5.4, assuming that wave periods are fixed separately at 2, 3, 4, 5, 6, 7, 8, 9 and 10 seconds, the relationship between the forces and wave heights according to these wave periods are plotted as Figure 5.17:

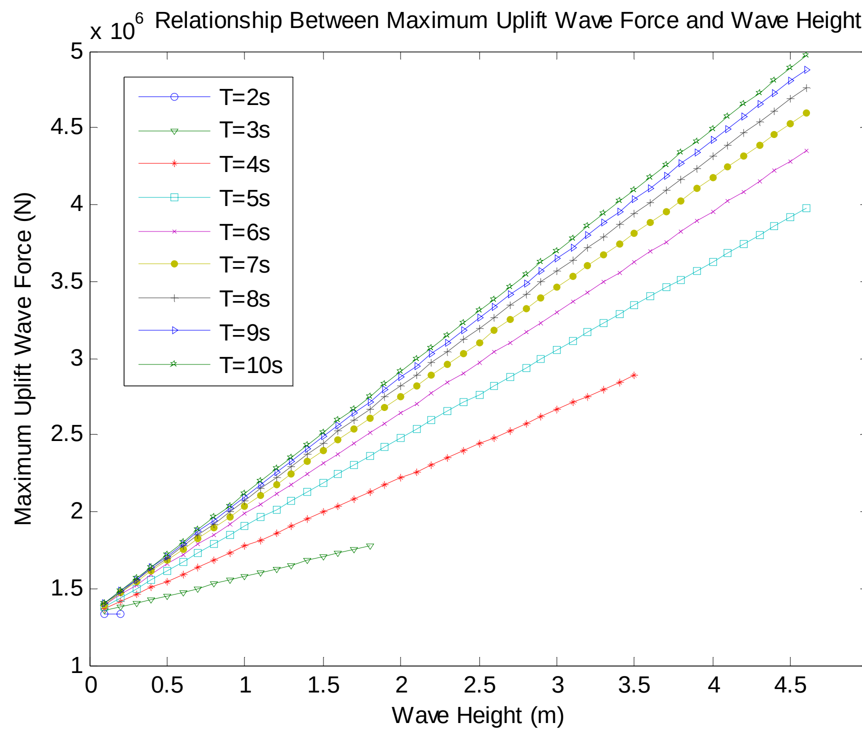

Figure 5.17: Relationship between maximum uplift wave forces and wave heights

In Figure 5.17, it shows that:

- At a specific wave period, the maximum uplift wave forces are linearly related to wave heights. The diffraction wave theory model in this study is based on the linear wave potential theory and the results coincide with this theory.

- The maximum uplift wave forces at different wave periods converge to one point as wave heights decrease to 0. As shown in Figure 5.17, this point is around $1.3\times10^6 N$, which is almost equal to the static buoyancy force $F_B = 1.326\times10^6 N$.

5.7.2 Relation between Maximum Uplift Wave Forces and Wave Periods

Similar to 5.7.1, assuming that wave heights are fixed separately at 0.5, 1.5, 2.5, 3.5 and 4.6 meters, the relationship between the forces and wave periods from Table 5.1 to 5.4 are plotted as Figure 5.18:

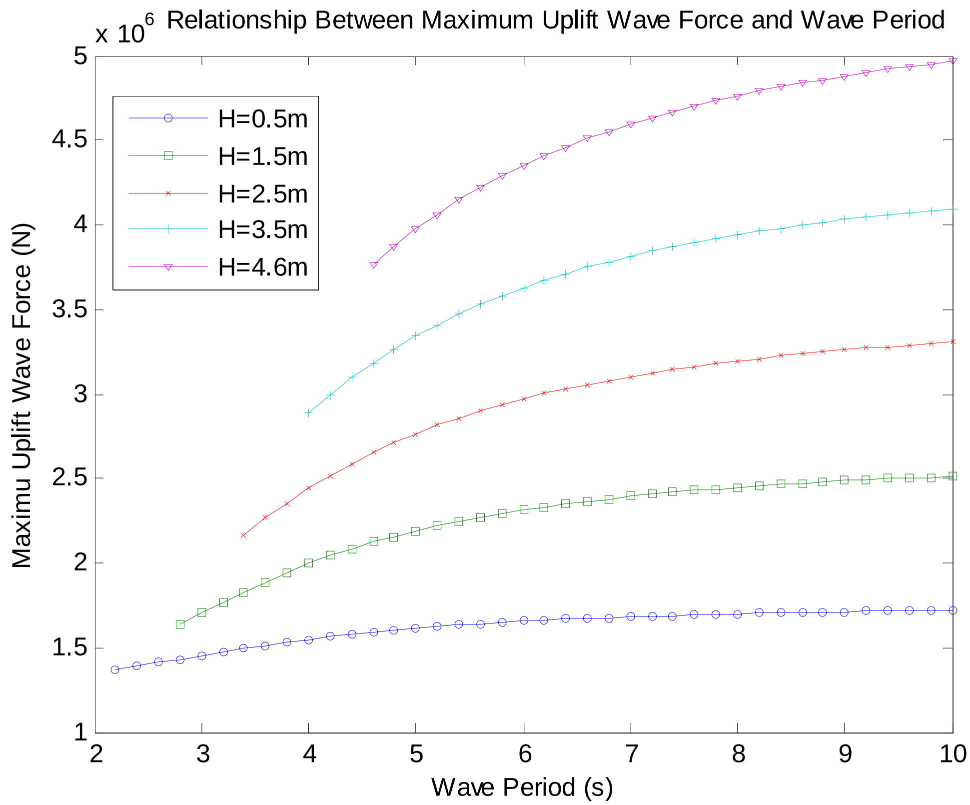

Figure 5.18: Relationship between maximum uplift wave forces and wave periods

In Figure 5.18, it shows that:

- At a specific wave height, the maximum uplift wave forces are nonlinearly related to wave periods. The larger the wave height is, the more nonlinear the forces are related to the wave periods.

- The maximum uplift wave forces at different wave heights converge to one point as wave period decrease to 0. As shown in Figure 5.18, this point is around $1.3\times10^6 N$, which is almost equal to the static buoyancy force $F_B = 1.326\times10^6 N$.

5.7.3 Relation between the Ratio of Force/Wave Height and Wave Periods

From the conclusions of 5.7.1 and 5.7.2, it can be determined that,

- Maximum uplift wave forces are linearly related to wave heights at a specific wave period;

- Maximum uplift wave forces are nonlinear related to wave periods at a specific wave height;

- Maximum uplift wave forces converge to a certain point, which can be regarded as static buoyancy force, as wave heights or wave periods decrease to 0.

At different periods, it has different slopes or ratios of wave forces to wave heights. The relation between these ratios and wave periods are figured out as following Figure 5.19:

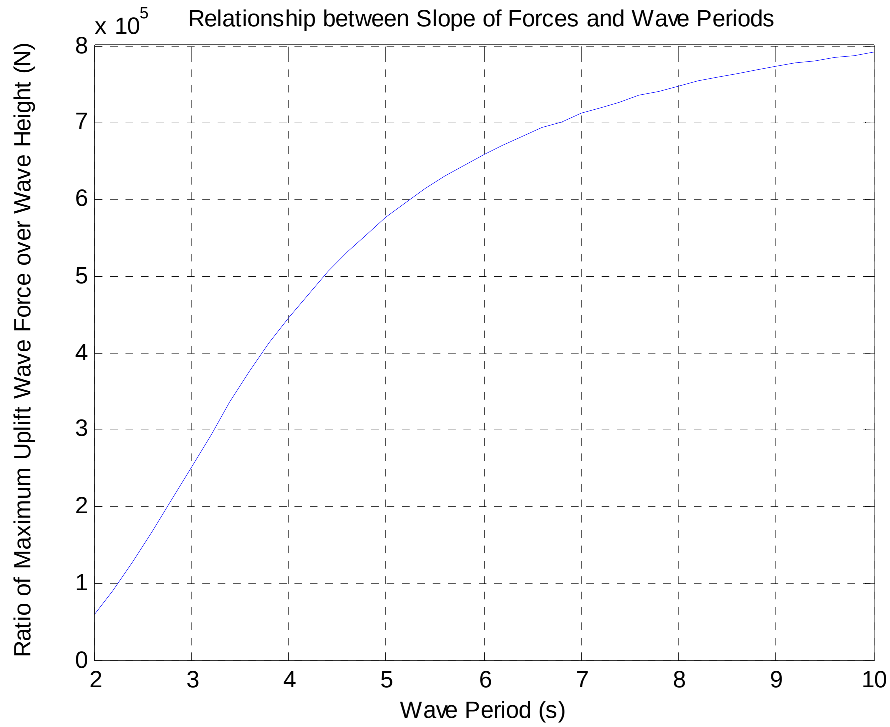

Figure 5.19: Relationship between slope of forces/wave heights and wave periods

From Figure 5.19, it shows that:

- As wave period increases, the slope of forces over wave heights increases;

The ratio or slope of wave force over wave heights means how much the wave forces depend on wave heights. According to the dispersion relationship in shallow water, the wave length is linearly related to wave period as $L = T \cdot \sqrt{gd}$, where

L = wave length;

g = earth gravity acceleration;

d = water depth;

T = wave period

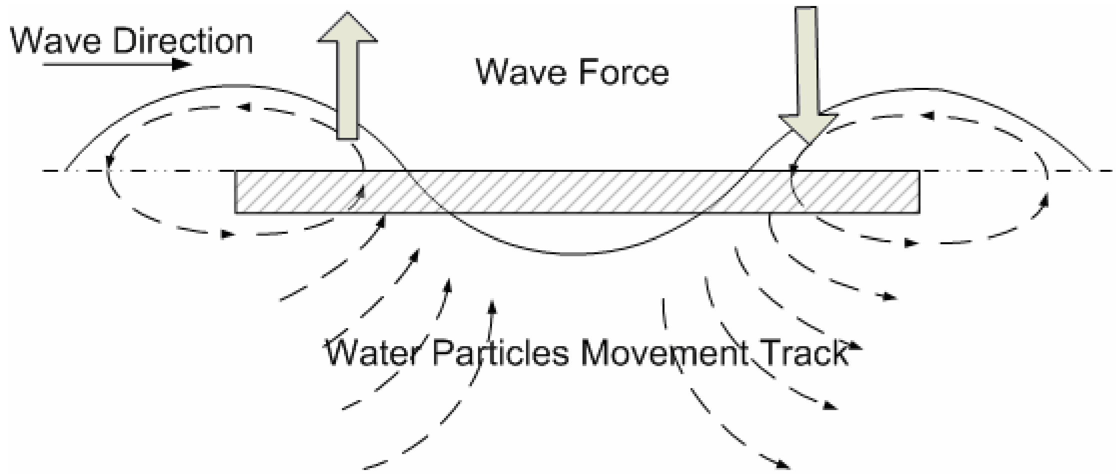

Figure 5.20: General view of bridge in waves

As shown in Figure 5.20, the bridge deck in the waves sustains both uplift and downward wave forces according to the wave mechanism. The maximum uplift wave force depends on how much contacting section area there is when the bridge interacts with the upward going water particles. The more section area the bridge contacts with rising water particles than the falling ones, the bigger the maximum uplift wave force is.

It is difficult to determine the time when the bridge endures the maximum uplift wave force, because it depends on many variables, such as bridge geometry, wave period, wave height, and clearance. But one point is clear that for longer wave lengths, the bridge deck has more chances and more contacting area in the rising water particle flow and thus has larger maximum uplift wave force. And then it can depend more on the wave heights.

As wave period increases, the wave length increases, and the bridge will depend more on wave heights, which is described as the slopes of forces over wave heights.

- As wave period decreases to 0, the slope decreases to 0.

This is for the same reason as point 1. As wave period decreases to very small ones, within the bridge length along the wave direction, there are several periods of wave length. The uplift and downward wave forces counteract each other and the maximum uplift wave force doesn't depend on the wave height very much.

- The slope of wave force over wave height is nonlinearly related to the wave periods; at periods of 2.2-3.4 sec, the slope increases fastest, which means the slope of the plot is the highest.

From the conclusions of point 1 and point 2, we know that, if the wave length is longer than the bridge length, the bridge will have chances to endure the rising water particles interaction only. Therefore, the maximum uplift wave force depends more on wave heights. Otherwise, if the wave length is less than the bridge deck length along the incoming wave direction, there are several cycles of waves within the bridge length and the uplift and downward wave forces counteract each other which makes the maximum uplift wave force less dependent on the wave height.

5.7.4 Estimation Equations According to Wave Heights and Wave Periods

In this section, a simplified approach and equation is going to be given for estimating wave loads on bridge decks. The overall uplift wave force is estimated in terms of the static buoyancy force component and the dynamic uplift wave force component.

$$F_v = F_B + F_D \tag{5.6}$$

where:

F_v = the overall uplift wave force

F_B = the buoyancy force

F_D = Maximum dynamic uplift wave force

For the buoyancy force and the maximum dynamic uplift wave force, according to the conclusions from sections 5.7.1 and 5.7.2:

$$F_B = \rho g l_1 l_2 \cdot h^* \tag{5.7}$$

$$F_D = \rho g l_1 l_2 \cdot c(T^*) \cdot H \tag{5.8}$$

Then substitute Eqs. 5.7 and 5.8 into 5.6 we have

$$F_v = \rho g l_1 l_2 (h^* + c(T^*) \cdot H) \tag{5.9}$$

where:

ρ = density of sea water which is $1.032 \times 10^3 kg/m^3$;

g = gravity acceleration which is $9.81 m/s^2$;

l_1 = length of the bridge in the direction crossing the wave direction;

l_2 = length of the bridge in the wave direction;

$c(T^*) =$ a coefficient which is a function of non-dimension variable T^*;

H = incoming wave height.

h^* = the relative buoyancy height of the cube which has the same volume and same deck surface section area as that of the model bridge including the six girders. It is determined only by the geometry of the bridge and the clearance of the water. In this reference case, $h^* = 0.757m$ as shown in Figure 5.21

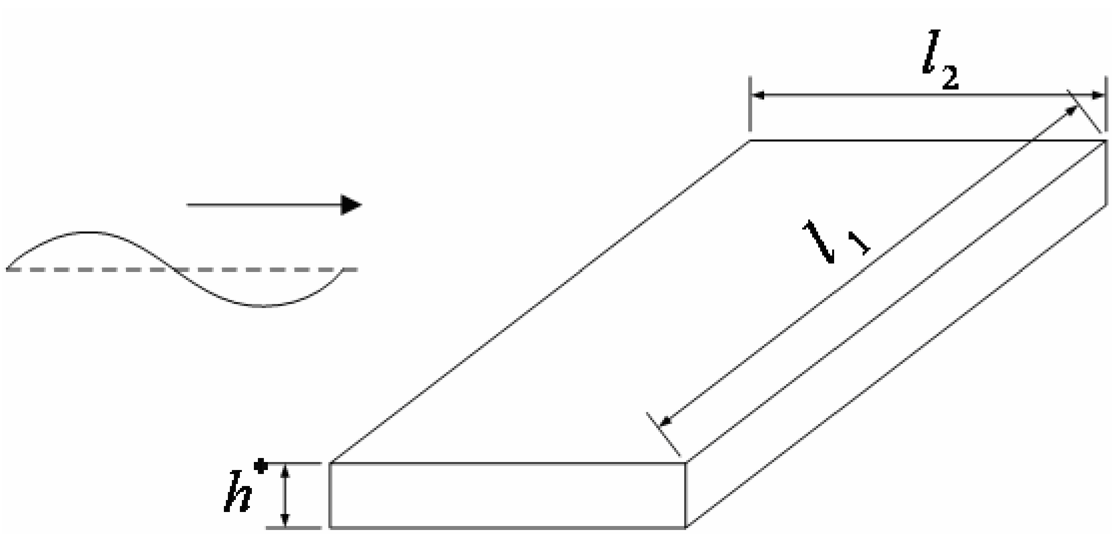

Figure 5.21: A figure showing the relative buoyancy height h^* (The cube in the figure has the same volume as the model bridge)

5.7.5 Simulation of $c(T^*)$

The results from Figure 5.19 are going to be simulated by a simplified equation. But before that, the variables should be dimensionless for the convenient future use of this equation in other cases. Here a variable $T^* = T / T_R$ is introduced, where T is the wave period and T_R is the reference wave period of 6 second.

The estimation equation is given as following:

$$c(T^*) = a_1 + b_1\sqrt{T^*} + \frac{c_1}{T^*} \quad (\text{for } T^* > 0.6) \tag{5.10}$$

$$c(T^*) = a_2 T^* + b_2 \quad (\text{for } 0.5 < T^* \le 0.6) \tag{5.11}$$

$$c(T^*) = a_3 + b_3 T^* + c_3\sqrt{T^*} \quad (\text{for } T^* \le 0.5) \tag{5.12}$$

Where:

T^* = T/T_R, the dimensionless variable.

T_R = the reference wave period of 6 second.

T = wave period.

and the coefficients are

$a_1 = 0.765, b_1 = -0.129, c_1 = -0.277$

$a_2 = 0.677, b_2 = -0.201$

$a_3 = 0.299, b_3 = 1.808, c_3 = -1.506$

The comparison between the results from Figure 5.19 and the estimating results by the Eqs. 5.10-5.12 in the reference example is plotted in the following Figure 5.22.

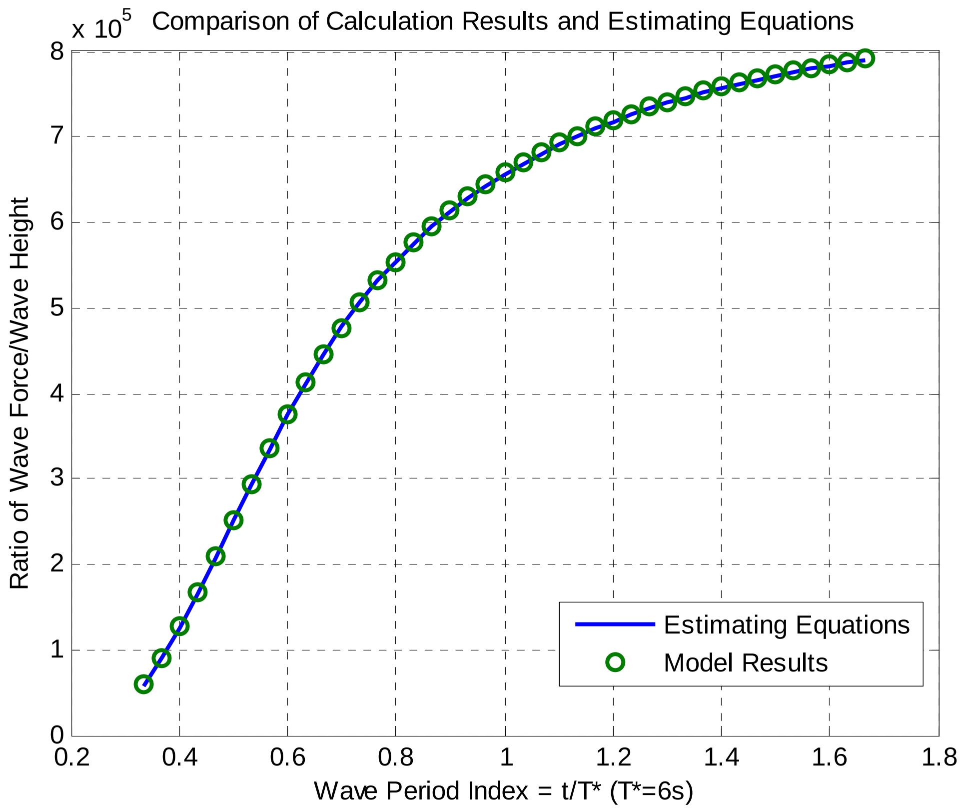

Figure 5.22: Simulation of slope coefficient

Substituting the Eqs. 5.10 5.11 5.12 to Eq. 5.9, we can have the uplift wave forces according to wave heights and wave periods.

By taking wave periods of 2s, 4s, 6s, 8s, 10s for examples, the errors between estimating uplift wave force and calculation results from Table 5.1-5.4 are plotted in the Figure 5.23.

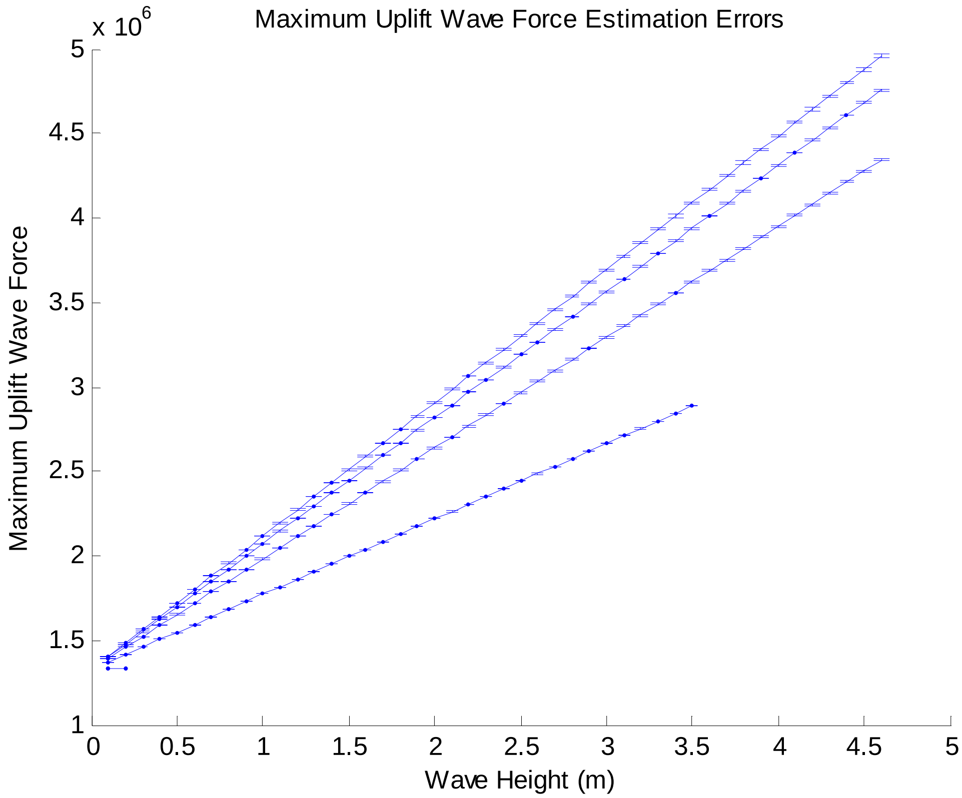

Figure 5.23: Maximum uplift wave force estimation errors for wave periods of 2s, 4s, 6s, 8s and 10s

The overall root mean square error is 0.10%, which can prove that the Eqs. 5.9-5.12 can well estimate the solutions from Table 5.1-5.4.

5.7.6 Modification Coefficient of Water Clearance, Water Depth, Bridge Geometry and Green Water Load

5.7.6.1 Coefficient of water clearance

According to the assumption and validation of coefficient of water clearance in chapter III, the coefficient equation is given as Eqs. 3.33 and 3.34:

$$A_{cl} = 1 - \frac{2\arcsin\frac{2cl}{H}}{\pi}(1-a)$$

where H = wave height

cl = water clearance

a = $\dfrac{\text{girder section area}}{\text{deck section area}}$ as geometry coefficient

5.7.6.2 Coefficient of water depth

The estimation of water depth coefficient comes from section 5.6. According to Figure 5.16, the solutions from wave potential model, the estimation equation and comparison are shown in Figure 5.24.

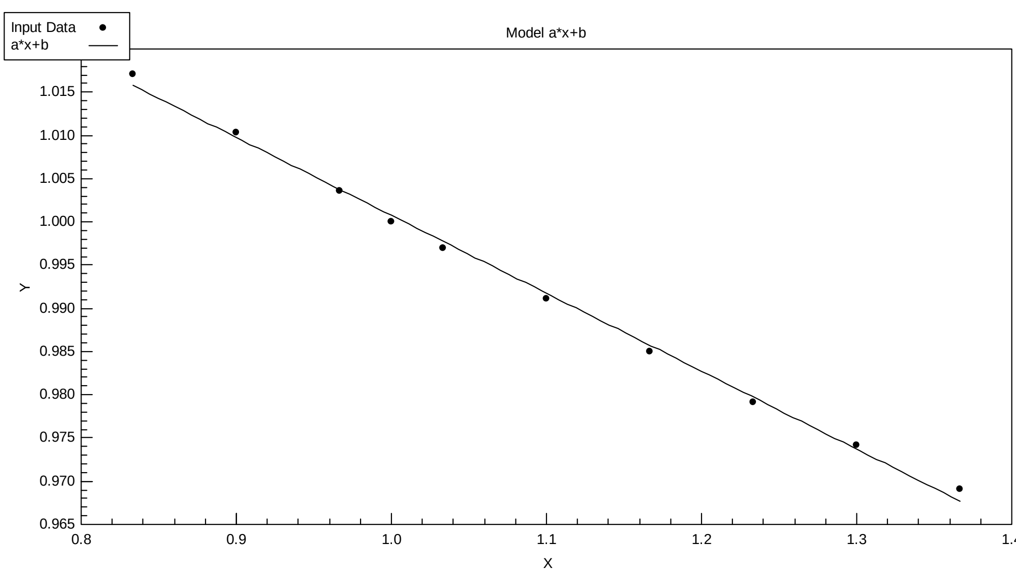

Figure 5.24: Estimation equation for water depth coefficient, $A_d = ax + b$ where

a=-0.090, b=1.091

The estimation of coefficient of water depth is

$$A_d = ax + b \tag{5.13}$$

where a=-0.090, b=1.091

5.7.6.3 Coefficient of bridge geometry A_l and green water deduction A_g

As mentioned in section 5.5, there is very little deduction of maximum uplift wave force as bridge width increase. As a result,

$$A_l = 1 \tag{5.14}$$

Although the overtopping wave can reduce the overall vertical force on the bridge deck, for designing purpose, as mentioned in section 5.4, should be

$$A_g = 1 \tag{5.15}$$

5.7.7 Maximum Uplift Wave Force Estimating Equations

Considering a bridge with six girders located across sea, according to Eqs. 3.33-3.35 and 5.9-5.15, the maximum uplift wave force on the bridge superstructure is:

$$F_v = \rho g l_1 l_2 (h^* + c(T^*) \cdot H) \cdot A_{cl} \cdot A_d \cdot A_l \cdot A_g$$

where

$$c(T^*) = a_1 + b_1\sqrt{T^*} + \frac{c_1}{T^*} \quad (\text{for} \quad T^* > 0.6)$$

$$c(T^*) = a_2 T^* + b_2 \qquad (\text{for} \quad 0.5 < T^* \le 0.6)$$

$$c(T^*) = a_3 + b_3 T^* + c_3\sqrt{T^*} \ (\text{for} \quad T^* \le 0.5)$$

$$A_{cl} = 1 - \frac{2\arcsin\frac{2cl}{H}}{\pi}(1-a)$$

$$A_d = a_5 x + b_6$$

$$A_l = 1$$

$$A_g = 1$$

and

$$\begin{cases} a_1 = 0.765, b_1 = -0.129, c_1 = -0.277 \\ a_2 = 0.677, b_2 = -0.201 \\ a_3 = 0.299, b_3 = 1.808, c_3 = -1.506 \\ a_4 = \dfrac{\text{girder section area}}{\text{deck section area}} \\ a_5 = -0.090, b_5 = 1.091 \end{cases}$$

where T^* = T / T_R, a dimensionless variable;

T_R = the reference wave period of 6 second;

T = the wave period;

H = wave height;

cl = water clearance;

l_1 = length of one bridge deck in the direction across sea;

l_2 = width of the bridge in the wave direction;

g = the gravity acceleration which is $9.81 m/s^2$;

5.8 Maximum Uplift Wave Forces on I-10 Bridge across Escambia Bay in Hurricane Ivan in September, 2004

Time: September 16th, 2004

Location: I-10 Bridge across Escambia Bay in Pensacola, Florida

Wave Parameters and I-10 Bridge Geometry:

I-10 Bridge is 9.4 m wide with six girders, located at 6m above sea bottom

Wave height H=1.78 meters

Wave period T=4.45 seconds

Water depth D=6 meters

Desired: Find out the maximum uplift wave force

Solution:

According to Eq. 5.9, $F_v = \rho g l_1 l_2 (h^* + c(T^*) \cdot H) \cdot A_{cl} \cdot A_d \cdot A_l \cdot A_g$

Table 5.7 Maximum uplift wave force calculation for I-10 Bridge across Escambia Bay in September, 2004

Estimating Equations	Values
$T^* = T / T_R$	0.74
$c(T^*) = a_1 + b_1\sqrt{T^*} + \frac{c_1}{T^*}$	0.2797
$F_v = \rho g l_1 l_2 (h^* + c(T^*) \cdot H)$	2.236×10^6 N
$A_{cl} = A_d = A_l = A_g$	1
$F_v = \rho g l_1 l_2 (h^* + c(T^*) \cdot H) \cdot A_{cl} \cdot A_d \cdot A_l \cdot A_g$	2.236×10^6 N

Solution process and equations are listed in table 5.7.

Comparing with results from case study of Chapter IV, $2.236 \times 10^6\, N$, the error comes to 0.08%.

5.9 Maximum Uplift Wave Forces on US90 Bridge across Biloxi Bay, Mississippi in Hurricane Katrina in August, 2005

Time: August, 2005

Location: US 90 Bridge across Biloxi Bay, Mississippi

Wave Parameters and Bridge Geometry:

US 90 Bridge is 10.2 m wide, 15.85m long with six girders, located at 4.87m above sea bottom

Wave height $H_s = 1.89m$ and $H_{1/250} = 3.402m$

Wave period T=6 seconds

Water depth D=3.62 meters

Desired: Find out the maximum uplift wave force

Solution:

Solution process and equations are listed in table 5.8.

Table 5.8 Maximum uplift wave force calculation for US 90 Bridge across Biloxi Bay, Mississippi in Hurricane Katrina

Estimating Equations	Values
$T^* = T / T_R$	1
$c(T^*) = a_1 + b_1\sqrt{T^*} + \frac{c_1}{T^*}$	0.359
$F_v = \rho g l_1 l_2 (h^* + c(T^*) \cdot H)$	3.512×10^6 N
$A_{cl} = 1 - \frac{2\arcsin\frac{2cl}{H}}{\pi}(1-a)$ where a=0.26	0.61
$F_v = \rho g l_1 l_2 (h^* + c(T^*) \cdot H) \cdot A_{cl} \cdot A_d \cdot A_l \cdot A_g$	2.142×10^6 N = 481.44 Kips

Douglass et al. (2004) calculates the uplift wave force as 440Kips using empirical Eq. 2.2. The span weights 340Kips and can not resist the wave loads. Comparing with Douglass's results, results by the estimating equation in this study are more conservative.

CHAPTER VI

CONCLUSIONS

2D wave velocity potential model (2D Model) is applied to predict the extreme wave loads on bridge decks in hurricane situation. The linear governing Laplace equation and boundary condition equations are converted to Complex Velocity Potential equations and discritized and solved by finite difference method. 2D Model simulates hydraulic pressure in the domain and integrates pressure under structure surface for uplift wave forces in time domain, among which the max value is the maximum uplift wave force; the same is conducted for horizontal wave force.

Computational fluid dynamic software Flow3D, which is using Navier Stoke theory up to 5th, is applied to validate 2D Model's applicability. A simple model is set up and results are compared with those from 2D Model. Flow3D's outflow boundary condition can only determine the fluid vector flowing out the domain but can not determine the fluid vector flowing into the domain. This situation affects the diffraction of wave potential and induces 10% error comparing with 2D Model's prediction. Tirindelli et al. (2002) set up a model of jetty in a flume and measured maximum uplift wave forces on jetty deck. The simulation results from 2D Model are compared with his laboratory data. The predicted maximum uplift wave forces are in great agreement with Tirindelli's measurement which approves the validation of 2D Model and the water clearance coefficient assumption. Horizontal wave forces on the model plate can also be obtained by integrating hydraulic pressure around vertical surface. However, the model is such a thin plate that the hydraulic pressure around the edge may change rapidly. In this case, the calculation results may have much error as well as Tirindelli's measurement.

A case study is conducted for calculating wave forces on I-10 Bridge across Escambia Bay, Florida during Hurricane Ivan in September 2004. To investigate the wave parameters of wave heights and wave periods around bridge sites, Simulating WAves Nearshore model (SWAN) is adopted. Four input parameters are selected from National Oceanic & Atmosphere Administration (NOAA), including significant wave heights, peak wave periods, peak wave directions and sea bottom depths. Three kinds of domains are generated, which are general domain, intermediate domain and sub domain. The predicted significant wave heights are calculated by SWAN and are in excellent agreements with the measurements by Buoy Station 42039 and 42040 nearest to Escambia Bay. The wave force calculation results from 2D Model are referring to monochromatic regular wave force. For application in real sea state, statistic analysis is adopted. Random wave heights are assumed to obey Rayleigh distribution. Therefore, for random waves with significant wave height H_s, the 2D Model result of maximum wave force means significant wave force $F_s = F_{1/3}$. For designing or evaluating purpose, $F_{1/250}$ should be calculated or even $F_{1/1000}$. The final result for the case study concludes that the bridge fail to resist wave loads, the decks are lifted up and washed away.

A new prediction equation of maximum uplift wave forces on bridge decks is developed in terms of wave height, wave period, water depth, bridge width, water clearance and over top water load. To develop the equations, the relationship is investigated between maximum uplift wave force and wave parameters, water clearance, green water effects and bridge width. A group of wave parameters of wave heights and wave periods, excluding those higher than breaking wave heights, is considered as input data for 2D Model.

The relationship between these parameters is investigated:

- At a specific wave period, the maximum uplift wave forces are linearly related to wave heights. The maximum uplift wave forces at different wave periods converge to static buoyancy as wave heights decrease to 0.
- At a specific wave height, the maximum uplift wave forces are nonlinearly related to wave periods. And the larger the wave height is, the more nonlinear the forces are related to the wave periods.
- The water clearance coefficient is assumed to decrease linearly as wave-structure interaction area decrease, which is also proved by Flow3D model simulation.
- Water depth coefficient decreases 5% linearly when water depth increases 30% and the prediction equation for the coefficient is also proposed as a linear function.
- Green water load on bridge plays an important role in the overall vertical force on bridge as wave heights increase. The amplitude of downward wave load could even be equal to 35% of the uplift wave force. However, the phase steps between overtop green water load and uplift wave force under bridge are not consistent with each other. As a result, for designing purpose, maximum uplift wave force is assumed to be not affected by green water load, that is, the coefficient of overtop water load is 1.
- The changes of geometry coefficient are very small due to changes of bridge width. It can be regarded that the bridge geometry length has no effects on the bridge deck maximum uplift wave forces.

According to all the conclusions above, given the wave parameters, water depth, water clearance, the maximum uplift wave force can be calculated out by the proposed prediction equations.

REFERENCES

Airy, G.B., 1845. Tides and waves. Encyc. Metrop., Article 192, pp. 241-396

Bea, R.G.., Xu, T., Stear J., Ramos R., 1999. Wave forces on decks of offshore platforms. Journal of Waterway, Port, Coastal and Ocean Engineering 125(3), 136-144.

Berkhoff, J.C.W., 1972. Computation of combined refraction-diffraction. In: Proceedings of 13th Coastal Eng. Conf., Vancouver. Vol. 1, pp. 471-490.

Blue, F.L., Johnson, J.W., 1949. Diffraction of water waves passing through a breakwater gap. Transactions, American Geophysical Union, Berkeley. Vol. 33, pp. 705-718.

Bunchner, B., 2002. Green water on ship-type offshore structures. Ph.D. Dissertation, Delft University of Technology, The Netherlands.

Buchner, B., Bunnik, T., 2007. Extreme wave effects on deepwater floating structures. In: Proceedings of the 24th Annual Conference on Offshore Technology, Houston. (paper 6814).

Chen, H.S., and Mei, C.C., 1974. Oscillations and wave forces in a manmade harbor in the open sea. In: TR No. 190. Ralph M. Parsons Laboratory, Dept. Civil Engineering, MIT.

Cheong, H. T., Shankar, N. J. and Nallayarasu, S., 1996. Analysis of submerged platform breakwater by eigenfunction expansion method, Ocean Engineering, 23(8), 649-666.

Cox, D.T., Orgeta, J.A., 2002. Laboratory observations of green water overtopping a fixed deck. Ocean Engineering vol.29, pp. 1827-1840.

Demirbilek, Z., Panchang, V.G., 1998. CGWAVE: a coastal surface water wave model of the mild slope equation. In: TR CHL-98-26, USACOE R&D Center, Vicksburg, MS.

Denson, K.H., 1978. Wave forces on causeway-type coastal bridges, water resources research institute, Mississippi State University, Miss State, pp. 1-42

Denson, K.H., 1980. Wave forces on causeway-type coastal bridges: effects of angle of wave incidence and cross-section shape. Water Resources Research Institute, Mississippi State University, Miss State, pp. 1-242.

Douglass, S. L., Hughes, S. A., Rogers, S., and Chen, Q., 2004. The impact of hurricane Ivan on the coastal roads of Florida and Alabama: a preliminary report. Coastal Transportation Engineering Research & Education Center, University of South Alabama, Alabama, pp. 1-19.

El Ghamry, O.S., 1963. Wave forces on a Dock. In: Technical Report HEL-9-1, University of California, Institute of engineering Research, Berkeley.

Fekken, G., Veldman, A.E.P., Buchner, B., 1999. Simulation of green water loadings using the Navier-Stokes equations. In: Seventh International Conference on Numerical Ship Hydrodynamics, Nantes.

Franco, C., Franco, L., 1999. Overtopping formulas for caisson breakwaters with nonbreaking 3D waves. Journal of Waterway, Port, Coastal and Ocean Engineering 125(2), pp. 98-108.

French, J.A., 1970. Wave uplift pressures on horizontal platforms. In: Proceedings of the Civil Engineering in the Oceans Conference. ASCE, vol. I, pp. 187-202.

Greco, M., 2001. A two-dimensional study of green-water loading. Ph.D. Dissertation, Department of Marine Hydrodynamics, Faculty of Marine Technology, Norwegian University of Science and Technology, Trondheim, Norway.

Gudmestad, O.T., Hansen, K., 2000. On some research issues related to requalification of fixed steel jacket structures. In: Proceedings of the Tenth International Offshore and Polar Engineering Conference, vol. 1, pp. 349-357 (ISOPE).

Ijima, T., Ozaki, S., Eguchi, Y. and Kobayashi, A., 1971. Breakwater and quay wall by horizontal plates. In: Proceedings of Coastal Engg. Con., vol. 3, 1537-1556.

Kaplan, P., 1992, Wave impact forces on offshore structures: re-examination and new interpretations. In: Proceedings of the 24th Annual Conference on Offshore Technology, pp. 79-86 (paper 6814).

Kaplan, P., Murray, J.J., & Yu, W.C., 1995. Theoretical analysis of wave impact forces on platform deck structures. In: Offshore Mechanics and Arctic Engineering Conference, Offshore Technology, OMAE Copenhagen, vol. 1A, pp. 189-198.

Li, D., Panchang, V.G., Jin, J., 2005. Development of an online coastal wave prediction system. In: International Solutions to Coastal Disasters Conference, May, 2005.

McConnell, K. J., Allsop, W., Cuomo, G., and Cruickshank, I. C. 2003. New guidance for wave forces on jetties in exposed locations. In: Proceedings of the Sixth Conference on Coastal and Port Engineering Developing Countries (COPEDEC VI), Colombo, Sri Lanka, 20pp

McCowan, J., 1891. On the solitary wave. Philosophical Magazine, London, 5th Series, vol. 36, pp. 430-437.

Mei, C.C., 1978. Numerical methods in water-wave diffraction and radiation. Ann. Rev. Fluid Mech, vol. 10, pp. 393-416.

Morison, J.R., O'Brien, M.P., Johnson, J.W., and Schaaf, S.A., 1950. The force exerted by surface waves on piles. Petrol. Trans., AIME, Vol. 189, pp. 149-189

Nallayarasu, S., Cheong, H.F., Shankar N.J., 1994. Wave induced pressures and forces on a fixed submerged inclined plate. Finite elements in analysis and design vol.18, pp. 289-299.

Nielsen, K.B., 2003. Numerical prediction of green water loads on ships. Ph.D. Dissertation, Department of Mechanical engineering, Technical University of Denmark, Lyngby.

Panchang, V.G.., Pearce, B.R., and Puri, K.K., 1990. Hindcast estimates of extreme wave conditions in the Gulf of Maine. Applied Ocean Research 12(1), pp. 43-49.

Panchang, V.G., Ge, W., Cushman, R.B., Pearce, B.R., 1991. Solution to the mild slope wave problem by iteration. Applied Ocean Research 13(4), 187-199.

Panchang, V.G., 2005. A modeling strategy for incorporating the effect of floating structures on waves in a coastal region. In: Report submitted to the Office of Naval Research, Arlington, VA.

Panchang, V.G., Jeong C., Li, D. 2008. Wave climatology in coastal Maine for aquaculture and other application. Estuaries and Coasts, vol.31, pp. 289-299.

Penny, W.G., Price, A.T., 1944. Diffraction of water waves by breakwaters. Misc. Weapons Development Technical History 26, Artificial Harbors, Sec. 3D.

Putnam, J.A., and Arthur, R.S., 1948. Diffraction of water waves by breakwaters. Transactions, American Geophysical Union, Berkeley, Vol. 29, pp. 481-490.

Rahman, M., Satish, M.G., and Xiang, Y., 1992. Wave diffraction due to large offshore structures: a boundary element analysis. Ocean Engineering 19(3), pp. 271-287.

Ryu, Y., and Chang, K.A., 2008. Green water void fraction due to breaking wave impinging and overtopping. Experiments in Fluids. Vol. 45, no. 5, pp. 883-898.

Sheppard, D.M., Renna, R., 2004. Preliminary forensic investigation of damage at the I-10 bridge over Escambia bay during hurricane Ivan. Ocean Engineering Associates, Inc., Gainesville, Florida.

Shih, R.W.K., Anastasiou, K., 1992. A laboratory study of the wave-induced vertical loading on platform decks. In: Proceedings of ICE, Water Maritime and Energy 96(1), pp. 19-33.

Stansberg, C.T., Karlsen, S.I., 2001. Green sea and water impact on FPSO in steep random waves. In: Practical Design of Ships and Other Floating Structures (PRADS 2001), Shanghai, China, pp. 593-601.

Tirindelli, M., Cuomo, G.., Allsop, W., McConnell, K., 2002. Exposed jetties: inconsistencies and gaps in design methods for wave-induced forces. In: Proceedings of the International Conference on Coastal Engineering. ASCE, vol. 2, pp. 1684-1696.

Tsay, T.K., Zhu, W., and Liu, P.L.F., 1989. A finite element model for wave refraction diffraction, reflection, and dissipation. Appl. Oc. Res., vol. 11, pp. 8-33.

Wan, D.C., Wu, G.X., 1999. The numerical simulation of the green water effect. In: Proceedings of 14th International Workshop on Water Waves and Floating Bodies. National Academic Press, pp. 163-176.

Wang, H., 1970. Water wave pressure on horizontal plate. Journal of the Hydraulics Division 96(10), pp. 1997-2017.

Weggel, J.R., 1972. Maximum breaker height. Journal of the Waterways, Harbors and Coastal Engineering Division. Vol. 98, No. WW4, pp. 529-548

Wiegel, R.L., 1962. Diffraction of waves by semi-infinite breakwater. Journal Hydraulics Division, ASCE, January, pp. 27-44.

Yueh, C.Y., and Kuo, Y.Y., 1993. The study of wave pressure and uplift force on a submerged plate. Ocean Engineering 20(3), pp. 263-280.

VITA

Bo Meng was born in Yantai, China. He received his B.S. in Ocean and Naval Structural Design and Architecture from Tianjin University in 2001 and his M.S. in Ocean and Naval Structural Design and Architecture from Tianjin University in 2004. He entered the Ocean Engineering Program, Civil Engineering Department of Texas A&M University in January, 2004 and received his Ph.D. in Ocean Engineering in December, 2008.

He can be reached at:

Department of Maritime System Engineering

C/o Dr. Jun Jin

TAMUG

Galveston, TX 77550